

Untwisted and Twisted Rényi Negativities: Toward a Rényi Proxy for Logarithmic Negativity in Fermionic Systems

Fo-Hong Wang^{1, 2} and Xiao Yan Xu^{1, 2, 3, *}

¹Key Laboratory of Artificial Structures and Quantum Control (Ministry of Education), School of Physics and Astronomy, Shanghai Jiao Tong University, Shanghai 200240, China

²Tsung-Dao Lee Institute, Shanghai Jiao Tong University, Shanghai 201210, China

³Hefei National Laboratory, Hefei 230088, China

(Dated: August 14, 2025)

Entanglement entropy is a fundamental measure of quantum entanglement for pure states, but for large-scale many-body systems, Rényi entanglement entropy is much more computationally accessible. For mixed states, logarithmic negativity (LN) serves as a widely used entanglement measure, but its direct computation is often intractable, leaving Rényi negativity (RN) as the practical alternative. In fermionic systems, RN is further classified into untwisted and twisted types, depending on the definition of the fermionic partial transpose. However, which of these serves as the true Rényi proxy for LN has remained unclear—until now. In this work, we address this question by developing a robust quantum Monte Carlo (QMC) method to compute both untwisted and twisted RNs, focusing on the rank-4 twisted RN, where non-trivial behavior emerges. We identify and overcome two major challenges: the singularity of the Green’s function matrix and the exponentially large variance of RN estimators. Our method is demonstrated in the Hubbard model and the spinless t - V model, revealing critical distinctions between untwisted and twisted RNs, as well as between rank-2 and high-rank RNs. Remarkably, we find that the twisted Rényi negativity ratio (RNR) adheres to the area law and decreases monotonically with temperature, in contrast to the untwisted RNR but consistent with prior studies of bosonic systems. This study not only establishes the twisted RNR as a more pertinent Rényi proxy for LN in fermionic systems but also provides comprehensive technical details for the stable and efficient computation of high-rank RNs. Our work lays the foundation for future studies of mixed-state entanglement in large-scale fermionic many-body systems.

I. INTRODUCTION

Quantum entanglement in many-body systems aids in identifying exotic phases and quantum criticality [1–3]. Among the various entanglement measures [4, 5], the entanglement entropy (EE) has garnered significant interest over recent decades [6–16, 18, 90]. EE is a fundamental measure of quantum entanglement for pure states, but for large-scale many-body systems, Rényi entanglement entropy (REE) is much more computationally accessible. Although EE is effective for identifying bipartite entanglement for pure states, it is not a reliable measure for mixed-state entanglement due to its inability to distinguish quantum entanglement from classical correlations. Instead, the logarithmic negativity (LN) [19–22], designed based on positive partial transpose criterion for the inseparability of density matrices [23, 24], can effectively detect quantum correlations in mixed states. The definition of LN hinges on the partial transpose of density matrices. For fermionic systems, additional considerations are necessary to respect their anticommuting statistical properties. A modified definition, known as the fermionic partial transpose (FPT), was proposed [25–27]. There are two types of FPT, characterized by different boundary conditions in the spacetime picture but yielding the same LN: the *untwisted* and *twisted* FPTs [28].

Although being a computable entanglement measure without invoking any optimization, LN is still hard to compute in interacting many-body systems. For bosonic cases, certain tensor network techniques including tree tensor networks [29] and matrix product states/operators [30, 31] were utilized to represent the partially transposed density matrix (PTDM) and thus obtain LN. There also exists early study using traditional density matrix renormalization group [32]. However, while the matrix product states/operators approach is universal, it is highly demanding in computational resources [30, 31, 33]. The moments of PTDM (referred to as the Rényi negativity (RN)), originally defined via the replica trick in the context of conformal field theory [29, 34, 35], are easier to compute using various many-body algorithms, including tensor network [33] and Monte Carlo [36–39]. There are also feasible experimental protocols for measuring RN in artificial quantum systems [40–43]. Although the RN has no direct relation to either entanglement or correlation, both equilibrium [36–39] and non-equilibrium [33, 44, 45] studies indicate that its deviation from Rényi entropy (moments of the full density matrices) of the same moment rank, called Rényi negativity ratio (RNR), measures either entanglement or correlation.

Computing the LN or RN in interacting fermionic systems is even more difficult due to the appearance of extra phases beyond conventional partial transpose [25–27]. In particular, it is challenging to implement the FPT for matrix product states. When the regions of interest

* xiaoyanxu@sjtu.edu.cn

comprise only a few points in total, one can first perform tomography of the reduced density matrix (e.g., using correlation functions to represent each of its elements [46, 47]), and then apply a partial transpose. However, for large regions, the size of the reduced density matrices increases exponentially. For general system sizes, since the FPT of fermionic Gaussian states remains Gaussian, it enables the calculation of fermionic RN and LN through the Green's function or covariance matrix for free-fermion systems [25, 48–50]. The two definitions of FPTs, namely, the untwisted and twisted FPTs, yield the same LN but different RNs in general. Recently, in previous work [51], we demonstrated that the untwisted RN of interacting systems can be feasibly calculated within the framework of determinantal quantum Monte Carlo (DQMC), provided the models are sign-problem-free. We computed the rank-2 untwisted RN for two representative models in the realm of strongly-correlated systems, namely, the Hubbard model and the t - V model.

For interacting fermionic systems with large system sizes, employing DQMC to compute exponential observables, such as REE and RN, encounters an inaccurate sampling issue due to the exponentially large invariance. Since Grover's pioneering work [14], many efforts have been devoted to calculating the REE of interacting fermionic systems via DQMC. However, for large system sizes, Grover's original method becomes less accurate, prompting the development of several incremental algorithms to address this issue. There are two main approaches to designing incremental algorithms. One approach involves intermediate processes without physical meaning [16–18, 52–55, 90]. The other approach is grounded in the concept of annealing, where each incremental process is assigned a physical interpretation, such as temperature [56–61]. Fermionic RN also suffers from this inaccurate sampling problem as the system size increases. In previous work [51], we developed an incremental algorithm for rank-2 untwisted RN and unveiled its behavior across a finite-temperature phase transition point.

In addition to the rank-2 untwisted RN examined in Ref. [51], higher-order moments of the PTDM, including both untwisted and twisted RNs of arbitrary ranks, warrant further investigation. Given that the untwisted PTDM is generally non-Hermitian and only the twisted RN can be analytically continued to LN by definition [28], twisted RN is more analogous to the RN in bosonic systems [29, 34, 35, 38]. Indeed, the rank-2 twisted RN is trivially the rank-2 Rényi entropy [28], making rank 3 the smallest non-trivial rank, analogous to the conventional bosonic RN [38]. This highlights the need to explore the computation of high-rank RNs (i.e., ranks greater than 2) for fermionic systems, a largely unexplored area that is the focus of this paper.

In this work, we address two primary challenges in computing high-rank RNs of Gibbs states using DQMC: (i) the numerical instability associated with inverting the partially transposed Green's function, and (ii) the expo-

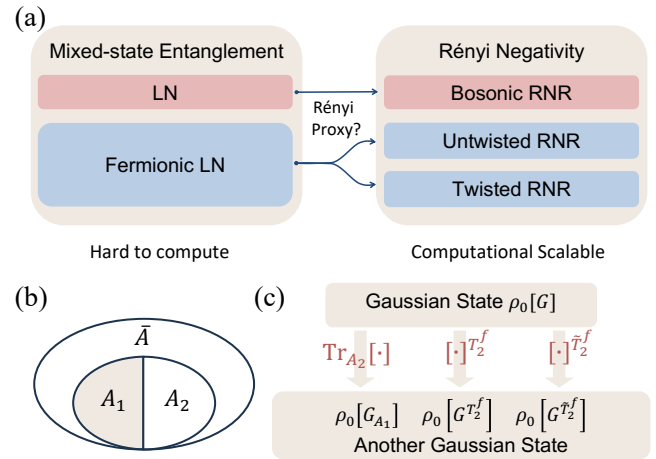


FIG. 1. (a) Overview of various negativity definitions, whose mathematical expressions can be found in Sec. III. While LN and its fermionic analog are computationally challenging, RNRs are scalable with QMC algorithms. This work seeks to identify a Rényi proxy for LN in fermionic systems. (b) Tripartition geometry: system $A = A_1 \cup A_2$ is embedded in environment \bar{A} , and we examine entanglement between subsystems A_1 and A_2 . (c) Foundation underlying DQMC algorithms for REE and RNRs. Operations $\text{Tr}_{A_2}[\cdot]$ (partial trace), $[\cdot]^{T_2^f}$ (untwisted FPT) and $[\cdot]^{\tilde{T}_2^f}$ (twisted FPT) transform Gaussian states with modified Green's functions.

nentially large variance in Monte Carlo sampling. We present a comprehensive technical analysis of the numerical instability and introduce stable update schemes for the incremental measurement of RNs. These algorithms are applied to analyze the RNs in the Hubbard model and spinless t - V model. We demonstrate the distinctions between untwisted and twisted RNs, as well as the variations among RNs of different ranks. Based on the numerical results, we discuss which version of RN, untwisted or twisted, is more appropriate as a Rényi proxy for LN. This work provides robust technical support for the stable QMC computation of exponential observables with analogous mathematical structures, including Rényi entropy and REE.

The remainder of this paper is organized as follows. In Sec. II, we set the stage by reviewing the FPT of both general states and Gaussian states, subsequently transitioning to interacting fermionic states within the framework of DQMC. Various definitions of Rényi negativities and their Monte Carlo estimators, termed as Grover determinants, are introduced in Sec. III. Readers less versed in technical details may wish to bypass Secs. IV and V. Sec. IV addresses the first key challenge in calculating high-rank RNs using DQMC: the numerical instability arising from inverting partially transposed Green's functions. In Sec. V, we tackle the second challenge, namely the inaccurate sampling issue, and present a fast update scheme sufficiently stable for incremental measurement of RNs. Sec. VI exhibits and discusses the simulation re-

sults for the Hubbard chain and the spinless t - V model. Finally, we encapsulate our work and provide a perspective on potential future avenues in Sec. VII.

II. FERMIONIC PARTIAL TRANSPOSE: FROM GAUSSIAN STATES TO INTERACTING FERMIONS

In this section, we review the definition of FPT in the Fock space and how it acts on Gaussian states. Subsequently, leveraging the FPT of Gaussian states, we develop a formulation for the FPT of interacting fermionic Gibbs states within the framework of DQMC.

In this paper, we employ two types of fermionic operators. For systems that conserve particle number and do not include pairing terms in the Hamiltonian, the formalism is fully captured using the complex fermion basis, or Dirac basis. This is characterized by the creation and annihilation operators c_j^\dagger, c_j ($j = 1, 2, \dots, N$, where N denotes the number of modes, such as the number of sites for spinless fermions), which adhere to the anti-commutation relations $\{c_j, c_{j'}^\dagger\} = \delta_{jj'}$. In more general scenarios, it is necessary to work in the Majorana basis¹ with the Majorana operators defined as:

$$\gamma_j^{(1)} = \gamma_{2j-1} = c_j + c_j^\dagger, \gamma_j^{(2)} = \gamma_{2j} = i(c_j^\dagger - c_j). \quad (1)$$

Given that it is more convenient to present and derive certain formulas in the Majorana basis, we will primarily utilize this basis in this section. If necessary for potential applications, we will reduce some results to the Dirac basis.

A. Fermionic partial transpose

We begin by revisiting the definition of FPT within the Fock space, where each basis state $|n\rangle$ is represented by a bit string $n = (n_1 n_2 \dots n_N)$ that encodes the occupation numbers of each mode. Along the way, we establish several intriguing general trace properties of both the untwisted and twisted PTDM, some of which will be corroborated by numerical simulations in the subsequent sections.

Under a bipartite geometry ($A = A_1 \cup A_2$, see Fig. 1(b) for illustration), where the modes are divided into two parts, A_1 with N_1 modes and A_2 with N_2 modes ($N_1 + N_2 = N$), the partial transpose of a density matrix ρ with respect to the subsystem A_2 is defined as [21]

$$(|n_{A_1}, n_{A_2}\rangle \langle \bar{n}_{A_1}, \bar{n}_{A_2}|)^{T_2} = |n_{A_1}, \bar{n}_{A_2}\rangle \langle \bar{n}_{A_1}, n_{A_2}|, \quad (2)$$

where n_{A_b} denotes the (sub-)bit string of length N_b comprising the occupation numbers of the modes within subsystem A_b (with $b = 1, 2$ denoting distinct subsystem blocks). A more suitable definition for fermions, which respects the fermionic anti-commutation statistics and preserves fermionic parity, was proposed [25, 48]:

$$(|n_{A_1}, n_{A_2}\rangle \langle \bar{n}_{A_1}, \bar{n}_{A_2}|)^{T_2^f} = (-1)^{\phi(n, \bar{n})} |n_{A_1}, \bar{n}_{A_2}\rangle \langle \bar{n}_{A_1}, n_{A_2}|, \quad (3)$$

where

$$\phi(n, \bar{n}) = \frac{[(\tau_2 + \bar{\tau}_2) \bmod 2]}{2} + (\tau_1 + \bar{\tau}_1)(\tau_2 + \bar{\tau}_2), \quad (4)$$

with $\tau_b = \sum_{j \in A_b} n_j$ being the norm of the bit string n_{A_b} ($b = 1, 2$). This is referred to as the *untwisted* FPT [28]. In general, the untwisted FPT of a density matrix is pseudo-Hermitian. The untwisted PTDM satisfies $\rho^{T_2^f\dagger} = X_2 \rho^{T_2^f} X_2$, where $X_2 = (-1)^{\sum_{j \in A_2} c_j^\dagger c_j}$ is the disorder operator acting on the subsystem A_2 . In contrast, the *twisted* PTDM, defined as $\rho^{\tilde{T}_2^f} \equiv \rho^{T_2^f} X_2$, is Hermitian [28]. In the Fock space, the twisted FPT is similarly given by Eq. (3) but the extra phase is modified to $\tilde{\phi}(n, \bar{n}) = \phi(n, \bar{n}) + \tau_2$.

Utilizing the definitions in Eqs. (3) and (4), we have proven some intriguing trace properties of the PTDM (see Appendix A for detailed proofs). Firstly, the moment of untwisted PTDM is expressed as

$$\begin{aligned} \text{Tr} \left[\left(\rho^{T_2^f} \right)^r \right] &= \sum_{n^1, n^2, \dots, n^r} \\ &\langle n_{A_1}^1, n_{A_2}^3 | \rho | n^2 \rangle \dots \langle n_{A_1}^i, n_{A_2}^{i+2} | \rho | n^{i+1} \rangle \dots \langle n_{A_1}^r, n_{A_2}^2 | \rho | n^1 \rangle \\ &\times (-1)^{\phi(n^1, n^2)} \dots (-1)^{\phi(n^i, n^{i+1})} \dots (-1)^{\phi(n^r, n^1)}. \end{aligned} \quad (5)$$

In particular, for $r = 1$, we find that $\text{Tr}[\rho^{T_2^f}] = \text{Tr}[\rho]$, while for $r = 2$, we have

$$\text{Tr} \left[\left(\rho^{T_2^f} \right)^2 \right] = \text{Tr}(\rho X_2 \rho X_2). \quad (6)$$

The second relation concerns the twisted moments:

$$\begin{aligned} \text{Tr} \left[\left(\rho^{\tilde{T}_2^f} \right)^r \right] &= \text{Tr} \left[\left(\rho^{T_2^f} X_2 \right)^r \right] = \sum_{n^1, n^2, \dots, n^r} \\ &\langle n_{A_1}^1, n_{A_2}^3 | \rho | n^2 \rangle \langle n_{A_1}^2, n_{A_2}^4 | \rho | n^3 \rangle \dots \langle n_{A_1}^r, n_{A_2}^2 | \rho | n^1 \rangle \\ &\times (-1)^{\tilde{\phi}(n^1, n^2)} (-1)^{\tilde{\phi}(n^2, n^3)} \dots (-1)^{\tilde{\phi}(n^r, n^1)}. \end{aligned} \quad (7)$$

In particular, in the case of $r = 2$ we have $\text{Tr}[\rho^{T_2^f} \rho^{T_2^f\dagger}] = \text{Tr}[\rho^2]$. Finally, for a density matrix with a well-defined parity (as required by the parity superselection rule [64, 65]), the parity constrain on Eqs. (5) and (7) leads to further simplification. On the one hand, we prove that

$$\text{Tr} \left[\left(\rho^{\tilde{T}_2^f} \right)^{4r} \right] = \text{Tr} \left[\left(\rho^{T_2^f} \right)^{4r} \right], r \in \mathbb{Z}. \quad (8)$$

¹ Alternatively, one can employ the Nambu vector $\Psi \equiv \{c_1, \dots, c_N, c_1^\dagger, \dots, c_N^\dagger\}$ [62, 63].

On the other hand, the phase chain in the third line of Eq. (5) can also be simplified to

$$\begin{aligned} & (-1)^{\phi(n^1, n^2)} \cdots (-1)^{\phi(n^i, n^{i+1})} \cdots (-1)^{\phi(n^r, n^1)} \\ & = (-1)^{\sum_{i=1}^r (\tau_2^i) + \sum_{i=1}^r (\tau_2^i \tau_2^{(i+1) \bmod r})}. \end{aligned} \quad (9)$$

These relations are applicable to arbitrary fermionic states and are not restricted to Gaussian states (the last two relations hold for states with well-defined parity).

B. Gaussian states

Free fermionic systems, characterized by quadratic Hamiltonians \hat{H}_0 , are typically found in *Gaussian states* when in equilibrium. These states include the thermal Gibbs states, expressed as $\rho_T = e^{-\beta \hat{H}_0} / \text{Tr}[e^{-\beta \hat{H}_0}]$, at finite temperature $T = 1/\beta$. Additionally, the ground states can be derived by taking the zero-temperature limit, given by $\rho_{\text{GS}} = \lim_{T \rightarrow 0} \rho_T$ ². Formally, the Gaussian states are defined as the exponential of quadratic forms:

$$\rho_0 = \frac{1}{Z} \exp \left(\frac{1}{4} \sum_{k,l} W_{kl} \gamma_k \gamma_l \right) = \frac{1}{Z} \exp \left(\frac{1}{4} \boldsymbol{\gamma}^T W \boldsymbol{\gamma} \right). \quad (10)$$

In this expression, the matrix W defining the Gaussian state is antisymmetric due to the anti-commutation relations between Majorana operators. For Hermitian systems, W is also purely imaginary and can be expressed as $W = iW_0$ with W_0 a real antisymmetric matrix. Hereafter, we consider a general case where W could be non-Hermitian. The normalization factor Z can be determined in terms of the eigenvalues of the W matrix and is given by $\det[\sqrt{I + e^W}]^{1/2}$ up to a sign ambiguity [67]. The (fermionic) partial transpose of pure Gaussian states can be expressed within the overlap matrix framework, enabling analytical calculations and highly efficient numerical evaluations of LN [68, 69]. However, for general mixed Gaussian states, the Green's function method to be introduced is more applicable.

One fundamental attribute of Gaussian states is that the covariance matrix, defined as $\Gamma_{ij} = \frac{1}{2} \text{Tr}(\rho_0[\gamma_i, \gamma_j])$, fully characterizes a Gaussian state. The covariance matrix Γ is related to the matrix W via

$$\Gamma = -\tanh \left(\frac{W}{2} \right) \text{ and } W = \ln [(I + \Gamma)^{-1} (I - \Gamma)]. \quad (11)$$

² Indeed, every pure Gaussian state can be viewed as the ground state of some quadratic Hamiltonian. Furthermore, under an appropriate basis transformation, it can be reformulated into a BCS-like form [66].

Ref. [51] presents a proof utilizing the trace formula [67] which applies to cases where $Z = \sqrt{\det(I + e^W)}$ without sign ambiguity, a condition typically met when W is Hermitian. A more comprehensive proof employs the product form of Gaussian states [70–72] (see Appendix B for detailed exposition). All high-order correlations can be derived using Wick's theorem, indicating that the entirety of information pertaining to these Gaussian states is encapsulated within Γ . It is convenient to represent Gaussian states in a functional form as $\rho_0[\Gamma]$, where Γ determines W via Eq. (11), and subsequently, W determines ρ_0 through Eq. (10).

In addition to considering temperature, a mixed Gaussian state can also be obtained by tracing out certain degrees of freedom from a pure Gaussian state. The partial trace of a Gaussian state remains a Gaussian state [73–75]. Remarkably, the FPT of a Gaussian state is also a Gaussian state [25], and it can be efficiently calculated through the “partial transpose” of its covariance matrix. For instance, with respect to subsystem A_2 , this is given by

$$\Gamma^{T_2^f} = \begin{pmatrix} \Gamma_{11} & i\Gamma_{12} \\ i\Gamma_{21} & -\Gamma_{22} \end{pmatrix}, \quad (12)$$

where $\Gamma_{b,b'}$ denotes the matrix block of Γ , with rows corresponding to the A_b region and columns corresponding to the $A_{b'}$ region. This notation will be consistently used throughout the paper. Using the functional form of Gaussian states, the untwisted PTDM can be expressed as $\rho_0^{T_2^f}[\Gamma] = \rho_0[\Gamma^{T_2^f}]$. This fact was proved by utilizing Wick's theorem [51, 76]. The twisted PTDM, defined as $\rho_0^{\tilde{T}_2^f} \equiv \rho_0^{T_2^f} X_2$, is also a Gaussian state [28], owing to the product rule of Gaussian states [72] (see Appendix C for further details). By employing Eqs. (C4) and (11), we can express the covariance matrix of $\rho_0^{\tilde{T}_2^f}$ in terms of the blocks of $\Gamma^{T_2^f}$ [28]:

$$\Gamma^{\tilde{T}_2^f} = \begin{pmatrix} \Gamma_{11} - \Gamma_{12} \Gamma_{22}^{-1} \Gamma_{21} & i\Gamma_{12} \Gamma_{22}^{-1} \\ -i\Gamma_{22}^{-1} \Gamma_{21} & -\Gamma_{22}^{-1} \end{pmatrix}. \quad (13)$$

It is important to note that $\rho_0^{\tilde{T}_2^f}$ may be not normalized, but $\Gamma^{\tilde{T}_2^f}$ actually corresponds to the normalized Gaussian state $\rho_0^{\tilde{T}_2^f} / \mathcal{Z}_{\tilde{T}_2^f}$ with $\mathcal{Z}_{\tilde{T}_2^f} \equiv \text{Tr}[\rho_0^{T_2^f} X_2] = \pm \sqrt{\det(\Gamma_{22})}$ [28].

For particle-number-conserving fermionic systems, their Gaussian states can be expressed in terms of Dirac operators and are completely characterized by the Green's function $G_{ij} = \text{Tr}(\rho_0 c_i c_j^\dagger)$, as given by [74]

$$\rho_0[G] = \det G \exp [\mathbf{c}^\dagger \ln (G^{-1} - I) \mathbf{c}]. \quad (14)$$

Its FPT is given by the same functional form $\rho_0[\cdot]$, but with the input of partially transposed Green's function,

$$G^{T_2^f} = \begin{pmatrix} G_{11} & iG_{12} \\ iG_{21} & I_2 - G_{22} \end{pmatrix}, \quad (15)$$

which satisfies $\rho_0^{T_2^f}[G] = \rho_0[G^{T_2^f}]$. By applying the product rule formulated in Eq. (C5b), we obtain $[(G^{T_2^f})^{-1} - I] = [(G^{T_2^f})^{-1} - I]U_2$ with $U_2 \equiv I_1 \oplus (-I_2)$, where I_b is the diagonal block of the identity matrix I , corresponding to rows and columns in region A_b . Consequently, the twisted partially transposed Green's function is derived as follows:

$$\begin{aligned} G^{T_2^f} &= \begin{pmatrix} I_1 & 2G_{12}^{T_2^f} \\ 0 & 2G_{22}^{T_2^f} - I_2 \end{pmatrix}^{-1} G^{T_2^f} \\ &= \begin{pmatrix} I_1 & -2iG_{12}(I_2 - 2G_{22})^{-1} \\ 0 & (I_2 - 2G_{22})^{-1} \end{pmatrix} G^{T_2^f}, \end{aligned} \quad (16)$$

which is related to the twisted PTDM via $\text{Tr}(\rho_0^{T_2^f} c_i c_j^\dagger) = \mathcal{Z}_{T_2^f} G_{ij}^{T_2^f}$ with $\mathcal{Z}_{T_2^f} = \det(I_2 - 2G_{22})$. The determinants of the untwisted and twisted Green's functions are directly related by $\det[\mathcal{Z}_{T_2^f} G^{T_2^f}] = \det[G^{T_2^f}]$. We note that the Gaussian-preserving property of untwisted and twisted FPTs is also shared by partial trace, as illustrated collectively in Fig. 1(c).

C. Interacting fermions

Before we start, we emphasize that the use of a hat, such as in \hat{H} , denotes an operator, while the same symbol without a hat represents its corresponding matrix representation. In the Majorana basis, the operator is expressed as $\hat{H} \equiv \frac{1}{4}\gamma^\dagger H \gamma$, whereas in the Dirac basis, it is given by $\hat{H} \equiv \mathbf{c}^\dagger H \mathbf{c}$. Note that the matrix representations of the same operator differ in different bases, even though the same symbols are used.

The Gibbs states of interacting fermionic systems with a Hamiltonian $\hat{H} = \hat{H}_0 + \hat{H}_I$, where \hat{H}_I includes a quartic term, are inherently non-Gaussian. However, by successively employing the Trotter-Suzuki decomposition and Hubbard-Stratonovich (HS) transformations, we can systematically decouple the interaction terms into quadratic forms. This process leads to the expression: $e^{-\Delta_\tau \hat{H}} = \sum_s \alpha[s] e^{\hat{K}} e^{\hat{V}[s]} e^{\hat{K}} + O(\Delta_\tau^3)$ where $\hat{K} \equiv -\Delta_\tau \hat{H}_0/2$ simply incorporates the prefactor, while the quadratic interaction term $\hat{V}[s]$ along with the coupling coefficient $\alpha[s]$ depend on the HS auxiliary fields s . For an interacting Gibbs state at inverse temperature $\beta = L_\tau \Delta_\tau$, the partition function is given by

$$Z = \text{Tr} \left[e^{-\beta \hat{H}} \right] = \sum_{\{s_l\}} \text{Tr} \left[\prod_{l=1}^{L_\tau} \left(\alpha[s_l] e^{\hat{K}_l} e^{\hat{V}[s_l]} e^{\hat{K}_l} \right) \right]. \quad (17)$$

In what follows, we adopt a shorthand notation to represent the complete set of all spacetime-dependent auxiliary fields, $\mathbf{s} \equiv \{s_l | l = 1, \dots, L_\tau\}$. The partition function is thus a summation over the weights of all possible \mathbf{s} -configurations, given by $Z = \sum_{\mathbf{s}} w_{\mathbf{s}}$.

The density matrix $\rho = e^{-\beta \hat{H}}/Z$ can be expressed as a sum of Gaussian states by utilizing the product rules for Gaussian states (refer to Appendix C for details). Indeed, for each \mathbf{s} -configuration, the operators within the square bracket in the final expression of Eq. (17) combine to form a single Gaussian state, represented as $e^{\hat{W}_{\mathbf{s}}} = e^{\frac{1}{4}\gamma^\dagger W_{\mathbf{s}}\gamma} \equiv \prod_l e^{\hat{h}_l[\mathbf{s}]}$. Each $e^{\hat{h}_l[\mathbf{s}]}$ is further decomposed into a product of three Gaussian states, $e^{\hat{h}_l[\mathbf{s}]} \equiv e^{\hat{K}_l} e^{\hat{V}_l[\mathbf{s}]} e^{\hat{K}_l}$. Incorporating normalization factors, the density matrix can be expressed as

$$\rho = \sum_{\mathbf{s}} p_{\mathbf{s}} \rho_{\mathbf{s}} \text{ with } \rho_{\mathbf{s}} = \det[I + e^{W_{\mathbf{s}}}]^{-1/2} e^{\frac{1}{4}\gamma^\dagger W_{\mathbf{s}}\gamma}, \quad (18)$$

where $p_{\mathbf{s}} = w_{\mathbf{s}}/Z$ is the probability of \mathbf{s} -configuration. Due to the linearity of the FPT, we can partially transpose the Gaussian states corresponding to different \mathbf{s} -configurations independently, and then sum them to obtain

$$\rho^{T_2^f} = \sum_{\mathbf{s}} p_{\mathbf{s}} \rho_{\mathbf{s}}^{T_2^f} = \sum_{\mathbf{s}} p_{\mathbf{s}} \rho_0 \left[\Gamma_{\mathbf{s}}^{T_2^f} \right], \quad (19)$$

where $\Gamma_{\mathbf{s}} = \frac{1}{2}\text{Tr}(\rho_{\mathbf{s}}[\gamma_i, \gamma_j])$ represents the covariance matrix of the Gaussian state for configuration \mathbf{s} , and $\Gamma_{\mathbf{s}}^{T_2^f}$ is obtained from Eq. (12), with explicit dependence on the auxiliary fields \mathbf{s} . Finally, the twisted PTDM is then given by

$$\rho^{T_2^f} = \sum_{\mathbf{s}} p_{\mathbf{s}} \rho_{\mathbf{s}}^{T_2^f} X_2 = \sum_{\mathbf{s}} p_{\mathbf{s}} \mathcal{Z}_{T_2^f, \mathbf{s}} \rho_0 \left[\Gamma_{\mathbf{s}}^{T_2^f} \right], \quad (20)$$

where $\mathcal{Z}_{T_2^f, \mathbf{s}} = \pm \sqrt{\det(\Gamma_{\mathbf{s}, 22})}$ is a normalization factor and $\Gamma_{\mathbf{s}}^{T_2^f}$ is obtained from Eq. (13), again explicitly dependent on the auxiliary fields \mathbf{s} .

If the weight in Eq. (18) is consistently real and positive, the summation can be efficiently evaluated using Monte Carlo sampling over the configuration space of \mathbf{s} . For simplicity, we have disregarded the sign ambiguity of the normalization factor in Eq. (18). When the sign is determined by symmetry arguments, Majorana QMC [77] can be employed for calculations. In cases where sign problems arise, one may turn to Pfaffian QMC [78] as an alternative approach. By focusing exclusively on particle-number-conserving systems, we can express the equations in terms of Dirac operators. Specifically, we have $e^{\hat{W}_{\mathbf{s}}} = e^{\mathbf{c}^\dagger W_{\mathbf{s}} \mathbf{c}} \equiv \prod_l e^{\hat{h}_l[\mathbf{s}]}$, which transforms Eq. (18) into the following form [14]:

$$\rho = \sum_{\mathbf{s}} p_{\mathbf{s}} \rho_{\mathbf{s}} \text{ with } \rho_{\mathbf{s}} = \det[G_{\mathbf{s}}] e^{\mathbf{c}^\dagger \ln[G_{\mathbf{s}}^{-1} - I] \mathbf{c}}, \quad (21)$$

which aligns with the framework of the celebrated DQMC [79–82]. After performing the untwisted and twisted FPTs, we derive the following expressions:

$$\rho^{T_2^f} = \sum_{\mathbf{s}} p_{\mathbf{s}} \rho_{\mathbf{s}}^{T_2^f} = \sum_{\mathbf{s}} p_{\mathbf{s}} \rho_0 \left[G_{\mathbf{s}}^{T_2^f} \right], \quad (22)$$

and

$$\rho^{\tilde{T}_2^f} = \sum_{\mathbf{s}} p_{\mathbf{s}} \rho_{\mathbf{s}}^{T_2^f} X_2 = \sum_{\mathbf{s}} p_{\mathbf{s}} \mathcal{Z}_{\tilde{T}_2^f, \mathbf{s}} \rho_0 \left[G_{\mathbf{s}}^{\tilde{T}_2^f} \right], \quad (23)$$

where $\mathcal{Z}_{\tilde{T}_2^f, \mathbf{s}} = \det(I_2 - 2G_{\mathbf{s}, 22})$, and the matrices $G_{\mathbf{s}}^{\tilde{T}_2^f}$ and $G_{\mathbf{s}}^{T_2^f}$ are given by Eqs. (15) and (16), respectively.

The Green's function $G_{\mathbf{s}}$ appearing above is given by $G_{\mathbf{s}, ij} \equiv \text{Tr}[\rho_{\mathbf{s}} c_i c_j^\dagger] = (I + e^{W_{\mathbf{s}}})^{-1}$. We can extend it to a more general construct, specifically the equal-time Green's function for the total system governed by \hat{H} . This function is defined as $G_{ij}(\tau) \equiv \text{Tr}[e^{-\beta \hat{H}} c_i(\tau) c_j^\dagger(\tau)]$, evaluated at a particular imaginary time $\tau \in [0, \beta]$. For a Hermitian \hat{H} , the value of G remains invariant across different τ . However, since $\hat{W}_{\mathbf{s}}$ is typically non-Hermitian, translation symmetry along the imaginary-time direction is not preserved for a specific \mathbf{s} . We define intermediate imaginary-time evolution operators by decomposing $e^{\hat{W}_{\mathbf{s}}}$ as follows:

$$e^{\hat{W}_{\mathbf{s}}} \equiv \prod_{l=1}^{L_{\tau}} e^{\hat{h}_l[\mathbf{s}]} \equiv \hat{B}_{\mathbf{s}}(\beta, 0) = \hat{B}_{\mathbf{s}}(\beta, \tau) \hat{B}_{\mathbf{s}}(\tau, 0), \quad (24)$$

where $\hat{B}_{\mathbf{s}}(\tau_1 = l_1 \Delta_{\tau}, \tau_2 = l_2 \Delta_{\tau}) = \prod_{l=l_1}^{l_2+1} e^{\hat{h}_l[\mathbf{s}]}$ can be interpreted as un-normalized intermediate Gaussian states. Consequently, we have [82]

$$\begin{aligned} G_{\mathbf{s}, ij}(\tau, \tau) &= \frac{\text{Tr} \left[\hat{B}_{\mathbf{s}}(\beta, \tau) c_i c_j^\dagger \hat{B}_{\mathbf{s}}(\tau, 0) \right]}{\text{Tr} \left[\hat{B}_{\mathbf{s}}(\beta, 0) \right]} \\ &= (I + B_{\mathbf{s}}(\tau, 0) B_{\mathbf{s}}(\beta, \tau))^{-1}, \end{aligned} \quad (25)$$

where $B_{\mathbf{s}}(\tau_1 = l_1 \Delta_{\tau}, \tau_2 = l_2 \Delta_{\tau}) = \prod_{l=l_1}^{l_2+1} e^{K_l} e^{V_l[\mathbf{s}]} e^{K_l}$. The imaginary-time translation symmetry is restored after summing over all \mathbf{s} -configurations. By averaging these \mathbf{s} -dependent Green's functions over different τ , we obtain the overall Green's function $G = \frac{1}{L_{\tau}} \sum_{\mathbf{s}, \tau} p_{\mathbf{s}} G_{\mathbf{s}}(\tau, \tau)$. All equal-time measurements follow a similar sampling process, which also applies to the RN introduced in the next section.

III. RÉNYI NEGATIVITY (RATIO), GROVER MATRIX AND GROVER DETERMINANT

In this section, we introduce variations of the LN, namely, the untwisted and twisted RNs, and next section will discuss methods for stably calculating their sampled value for a specific \mathbf{s} -configuration.

Based on the bosonic and fermionic partial transposes (see Eqs. (2) and (3)), the LN is defined as

$$\mathcal{E} = \ln \text{Tr} \sqrt{\rho^{T_2^f \dagger} \rho^{T_2^f}}. \quad (26)$$

This quantity has been shown to be an entanglement monotone for both bosonic [21] and fermionic systems [27]. It is noteworthy that since $\rho^{T_2^f \dagger} \rho^{T_2^f} =$

$\rho^{\tilde{T}_2^f \dagger} \rho^{\tilde{T}_2^f} = (\rho^{\tilde{T}_2^f})^2$, both untwisted and twisted FPTs yield the same LN. However, due to challenges associated with evaluating the trace norm in both analytical and numerical contexts, some researchers have turned to a variation of LN, known as the RN or negativity moments [28, 34, 35, 38]. The untwisted and twisted RN are defined as follows:

$$\mathcal{E}_r = \frac{1}{1-r} \ln \text{Tr} \left[\left(\rho^{T_2^f} \right)^r \right] \text{ and } \tilde{\mathcal{E}}_r = \frac{1}{1-r} \ln \text{Tr} \left[\left(\rho^{\tilde{T}_2^f} \right)^r \right], \quad (27)$$

respectively. Here, we define the RNs in a way analogous to the Rényi entropy, incorporating the prefactor $1/(1-r)$ to ensure a positive value. The twisted RN is analytically continued to the LN via $\mathcal{E} = \lim_{r \rightarrow 1/2} (1-2r)\tilde{\mathcal{E}}_{2r}$ [28]. It is important to note that untwisted and twisted FPTs of the same rank can yield different values of RN. Specifically, while $\mathcal{E}_2 = -\ln \text{Tr}[(\rho X_2)^2]$ using Eq. (6), $\tilde{\mathcal{E}}_2 = -\ln \text{Tr}[\rho^2]$ is trivially related to the Rényi entropy. Therefore, there is generally a greater interest in high-rank RN, which is the primary focus of this work. As discussed in the introduction, the deviation of RN from the Rényi entropy of the same rank may provide meaningful insights related to either entanglement or correlation. We define this deviation as the Rényi negativity ratio (RNR):

$$R_r = \frac{1}{1-r} \ln \frac{\text{Tr} \left[\left(\rho^{T_2^f} \right)^r \right]}{\text{Tr} \left[(\rho)^r \right]} = \mathcal{E}_r - S_r^{\text{th}}, \quad (28)$$

where the thermal Rényi entropy is denoted by $S_r^{\text{th}} = \ln \text{Tr}[\rho^r]/(1-r)$. The twisted RNR is similarly defined as $\tilde{R}_r = \tilde{\mathcal{E}}_r - S_r^{\text{th}}$.

By substituting the decomposition forms from Eqs. (22) and (23) into the definition of rank- r RN in Eq. (27), we obtain

$$e^{(1-r)\mathcal{E}_r} = \text{Tr} \left[\left(\rho^{T_2^f} \right)^r \right] = \sum_{\mathbf{s}^{(1)} \dots \mathbf{s}^{(r)}} \left(\prod_{i=1}^r p_{\mathbf{s}^{(i)}} \right) \det g_{r, \bar{\mathbf{s}}}, \quad (29a)$$

and

$$\begin{aligned} e^{(1-r)\tilde{\mathcal{E}}_r} &= \text{Tr} \left[\left(\rho^{\tilde{T}_2^f} \right)^r \right] \\ &= \sum_{\mathbf{s}^{(1)} \dots \mathbf{s}^{(r)}} \left(\prod_{i=1}^r p_{\mathbf{s}^{(i)}} \right) \left(\prod_{i=1}^r \mathcal{Z}_{\tilde{T}_2^f, \mathbf{s}^{(i)}} \right) \det \tilde{g}_{r, \bar{\mathbf{s}}}, \end{aligned} \quad (29b)$$

where $\mathcal{Z}_{\tilde{T}_2^f, \mathbf{s}} = \det(I_2 - 2G_{\mathbf{s}, 22})$, and $\bar{\mathbf{s}}$ is a shorthand notation for the replica collection $\mathbf{s}^{(1)} \dots \mathbf{s}^{(r)}$. The rank- r Grover matrices are defined as

$$g_{r, \bar{\mathbf{s}}} \equiv \left[\prod_{i=r}^1 G_{\mathbf{s}^{(i)}}^{T_2^f} \right] \left[I + \prod_{i=r}^1 \left(\left(G_{\mathbf{s}^{(i)}}^{T_2^f} \right)^{-1} - I \right) \right], \quad (30a)$$

and

$$\tilde{g}_{r, \bar{\mathbf{s}}} \equiv \left[\prod_{i=r}^1 G_{\mathbf{s}^{(i)}}^{\tilde{T}_2^f} \right] \left[I + \prod_{i=r}^1 \left(\left(G_{\mathbf{s}^{(i)}}^{\tilde{T}_2^f} \right)^{-1} - I \right) \right]. \quad (30b)$$

The untwisted and twisted Green's functions, $G_{\mathbf{s}}^{T_2^f}$ and $G_{\mathbf{s}}^{\tilde{T}_2^f}$, are provided in Eqs. (15) and (16), respectively. The determinants of Grover matrices are referred to as the *Grover determinants*. The term “Grover” is used because these formulas are analogous to Grover's formulas for calculating REE [14]. The twisted Grover determinant can be combined with the normalization factors via $\det[\mathcal{Z}_{\tilde{T}_2^f} G^{\tilde{T}_2^f}] = \det[G^{\tilde{T}_2^f}]$ (see the discussion below Eq. (16)). This allows the calculation of twisted RN using untwisted Green's function, as given by the formula:

$$e^{(1-r)\tilde{\mathcal{E}}_r} = \sum_{\mathbf{s}^{(1)} \dots \mathbf{s}^{(r)}} \left(\prod_{i=1}^r p_{\mathbf{s}^{(i)}} \right) \det \tilde{g}_{r,\mathbf{s}}, \quad (31)$$

where a modified Grover matrix is defined as:

$$\tilde{g}_{r,\mathbf{s}} \equiv \left[\prod_{i=r}^1 G_{\mathbf{s}^{(i)}}^{T_2^f} \right] \left[I + \prod_{i=r}^1 \left[\left(\left(G_{\mathbf{s}^{(i)}}^{T_2^f} \right)^{-1} - I \right) U_2 \right] \right], \quad (32)$$

which satisfies $\det \tilde{g}_{r,\mathbf{s}} = \left(\prod_{i=1}^r \mathcal{Z}_{\tilde{T}_2^f, \mathbf{s}^{(i)}} \right) \det \tilde{g}_{r,\mathbf{s}}$. Eq. (31) is advantageous over Eq. (29b) when the matrix block $(I_2 - 2G_{22})$ in Eq. (16) becomes singular. This singularity leads to a nearly zero value for $\mathcal{Z}_{\tilde{T}_2^f}$ and results in an unstable $G^{\tilde{T}_2^f}$.

IV. NUMERICALLY STABLE CALCULATION OF RANK- r GROVER DETERMINANTS

In this section, we address the first challenge in computing high-rank RNs via DQMC: the instability arising from inverting partially transposed Green's functions, which appears necessary in Eqs. (30) and (32).

The direct computation of high-rank Grover determinants is plagued by numerical instability due to the singular nature of the partially transposed Green's functions, which itself stems from the singularity of the Green's function G . For free-fermion systems, where the HS transformation and Monte Carlo sampling are unnecessary, we have $G_{\mathbf{s}^{(i)}}^{T_2^f/\tilde{T}_2^f} = G^{T_2^f/\tilde{T}_2^f}$ for all $i = 1, 2, \dots, r$. Therefore, stable formulas for RNs can be derived without invoking the inversion of Green's functions:

$$e^{(1-r)\mathcal{E}_r} = \det \left[\left(G^{T_2^f} \right)^r + \left(I - G^{T_2^f} \right)^r \right], \quad (33a)$$

$$e^{(1-r)\tilde{\mathcal{E}}_r} = \mathcal{Z}_{\tilde{T}_2^f}^r \det \left[\left(G^{\tilde{T}_2^f} \right)^r + \left(I - G^{\tilde{T}_2^f} \right)^r \right]. \quad (33b)$$

In these expressions, one can diagonalize the matrices $G^{T_2^f}$ and $G^{\tilde{T}_2^f}$, allowing the untwisted and twisted RNs to be computed from their eigenvalues, respectively. In interacting systems, rank-2 Grover determinants maintain stability. For instance, the untwisted Grover determinant is expressed as $\det g_{2,\mathbf{s}} = \det[G_{\mathbf{s}^{(1)}}^{T_2^f} G_{\mathbf{s}^{(2)}}^{T_2^f} + (I -$

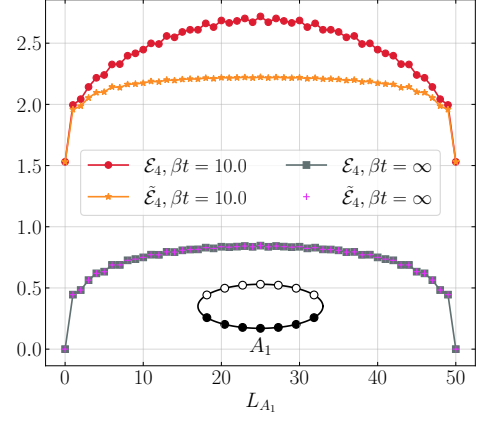


FIG. 2. The variations of untwisted and twisted rank-4 RNs of a free-fermion chain with $\mu/t = 0.5$ are shown as functions of subsystem length L_{A_1} for two temperatures (finite-temperature and ground-state). The chain length is $L_A = 50$ and the inset illustrates the bipartite geometry. All the points are calculated using Eq. (33), except for the ground-state $\tilde{\mathcal{E}}_4$ at $L_{A_1} = L_A/2$. At this specific point, the matrix block $(I_2 - 2G_{22})$ in Eq. (16) becomes singular and we utilize Eq. (39) instead.

$G_{\mathbf{s}^{(1)}}^{T_2^f}) (I - G_{\mathbf{s}^{(2)}}^{T_2^f})]$. However, as the rank increases beyond 2, it becomes unavoidable to deal with the inverse of the partially transposed Green's functions, leading to potential numerical difficulties.

Given that Eq. (33) provides standard results suitable for benchmarking, we demonstrate the issue of numerical instability of Grover determinants in the context of free fermions. The Hamiltonian under consideration, $\hat{H}_0 = -t \sum_{i=1}^N (c_i^\dagger c_{i+1} + \text{H.c.}) - \mu \sum_i c_i^\dagger c_i$, describes a simple tight-binding periodic chain. Utilizing Eq. (33), we calculate the rank-4 untwisted and twisted RNs as functions of subsystem length L_{A_1} , as depicted in Fig. 2. At finite temperatures, the untwisted negativity differs from the twisted negativity, whereas they coincide when considering ground state averages. These observations align with our theoretical proof of Eq. (8). At finite temperatures, Fock states with varying total particle numbers mix to form a Gibbs state, which lacks a well-defined parity. In contrast, the ground state, along with all other eigenstates of \hat{H}_0 , possesses a well-defined parity due to the parity symmetry preserved by the Hamiltonian.

In the following discussion, we seek stable approaches to compute the Grover determinants without relying on Eq. (33), as this formula is impractical for interacting systems, where the matrices $G_{\mathbf{s}^{(i)}}^{T_2^f/\tilde{T}_2^f}$ for different i do not commute. We will begin by demonstrating the singularity of the partially transposed Green's function matrices and then introduce two solutions to stabilize the computation.

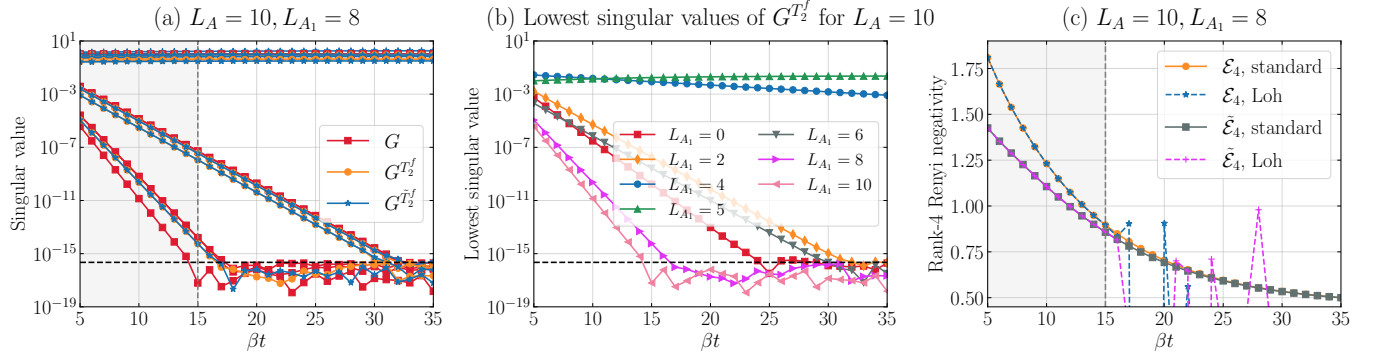


FIG. 3. The numerical instability of high-rank Grover determinants and its stabilization in the high-temperature regime, demonstrated in the context of a $L_A = 10$ free-fermion chain with $\mu/t = 0.5$. The bipartition geometry is consistent with that shown in Fig. 2. (a) All the singular values of matrices G (red squares), $G^{T_2^f}$ (orange circles), and $G^{\tilde{T}_2^f}$ (blue stars) are plotted against the dimensionless inverse temperature βt , and for the latter two matrices, the subsystem length L_{A_1} is 8. As β increases, several singular values of the three matrices decrease exponentially. The matrix inversion becomes unstable when the smallest singular value approaches machine precision, indicated by the black dashed horizontal line, which is approximately 2.22×10^{-16} for double-precision floating-point numbers. (b) The lowest singular values of $G^{T_2^f}$ are shown as functions of inverse temperature β for various subsystem lengths L_{A_1} . (c) The rank-4 RNs, calculated using both the standard formula in Eq. (33) (origin circles and grey squares) and Loh's stable inversion formula in Eq. (37) (blue stars and purple plus signs), are plotted as functions of βt . Loh's stable inversion breaks down beyond $\beta t = 15$, as indicated by the grey dashed vertical line, which aligns with (a). Within the gray-filled region, the stable inverse formula in Eq. (37) for Grover determinants remains effective.

A. Singularity of the Green's function matrix

If one naively performs the calculation following the formula, say, for the untwisted case,

$$\det g_{r,\bar{s}} = \det \left[\prod_{i=r}^1 G_{\bar{s}^{(i)}}^{T_2^f} \left[I + \prod_{i=r}^1 \left(\left(G_{\bar{s}^{(i)}}^{T_2^f} \right)^{-1} - I \right) \right] \right], \quad (34)$$

a nonsense, exponentially large value would result. The issue arises from the unstable inverse of the partially transposed Green's functions. In Fig. 3(a), we plot the singular values of G , $G^{T_2^f}$, and $G^{\tilde{T}_2^f}$ against the inverse temperature β . While generally less severe, the partially transposed Green's functions ($G^{T_2^f}$ and $G^{\tilde{T}_2^f}$) indeed inherit singularities from G . The degree of singularity exhibits an evident dependence on temperature. Specifically, as the temperature decreases, the smallest few singular values of $G^{T_2^f}/\tilde{T}_2^f$ decrease exponentially. When the smallest singular value approaches machine precision (below the so-called “breakdown temperature”), the matrix inversion becomes numerically unstable.

Additionally, the degree of instability is strongly influenced by the specific bipartite geometry. In fact, Fig. 3(a) only exhibits a particularly unstable case for $L_A = 10$ (namely, $L_{A_1} = 8$). In Fig. 3(b), we present the lowest singular values of $G^{T_2^f}$ for various subsystem lengths L_{A_1} , revealing that the breakdown temperature varies significantly with L_{A_1} . For most values of L_{A_1} , the lowest singular values exponentially decay with increasing β . Remarkably, exactly at the equal-bipartition point ($L_{A_1} = L_A/2 = 5$), the lowest singular value is insensitive

to temperature, allowing $G^{T_2^f}$ to be considered as a non-singular matrix. This permits the direct evaluation of Grover determinants using Eq. (34) for equal-bipartition geometry, at very low temperatures and even in ground-state calculations. A general conclusion is that, as L_{A_1} approaches the equal-bipartition point, the lowest singular value of $G^{T_2^f}/\tilde{T}_2^f$ decreases more slowly as β increases.

These observations—namely, that $G^{T_2^f}/\tilde{T}_2^f$ exhibits increasingly singular with decreasing temperature and as the geometry deviates from equal bipartition—remain valid for two-dimensional free systems and for interacting systems after HS transformation, based on practical experience. It is unsurprising that the overall singularity is significantly affected by the model under consideration and its specific parameters. In the context of interacting systems, within the framework of DQMC, additional factors such as the HS transformation employed and the specific auxiliary-field configuration also play crucial roles. We conclude that the severity of the singularity is contingent upon three factors: (i) the model and the HS transformation employed, (ii) the bipartition geometry, and (iii) the temperature.

B. Solution 1: Loh's stable inversion formula and regularization of Green's functions

Our first solution insists on working with the inversion of the partially transposed Green's functions and aims at stabilizing the Grover determinant calculation in Eq. (34). We first show that, prior to the break-

down point where the lowest singular values are close to machine precision, the Grover determinant can still be computed stably using a stabilization scheme based on matrix decomposition [83, 84]. Subsequently, we introduce a regularization scheme [85] for the partially transposed Green's functions to extend the stable calculation to lower temperatures.

The stable formula bears a close resemblance to the methodologies employed for the stable computation of weights in DQMC (refer to Appendix F for a brief overview of numerical stabilization in DQMC). Indeed, the term $(G_{\mathbf{s}}^{T_2^f})^{-1} - I$ is reminiscent of the matrix $B_{\mathbf{s}}(\beta, 0) = (G_{\mathbf{s}}^{-1} - I)$ in Eq. (24), and they should exhibit similar mathematical behavior, characterized by the presence of exponentially large and small scales, leading to an exponentially large condition number [83, 84]. For convenience, we denote $\mathbb{B}_i \equiv (G_{\mathbf{s}^{(i)}}^{T_2^f})^{-1} - I$, and sometimes use $\mathbb{B}_{\mathbf{s}^{(i)}}$ to emphasize its dependence on $\mathbf{s}^{(i)}$. However, a more challenging situation arises here since \mathbb{B}_i is not known from a priori (unlike $B(\beta, 0)$), which can be calculated using the decoupled Hamiltonians e^{K_1} and $e^{V_1[\mathbf{s}]}$. \mathbb{B}_i must be determined by inverting $G_{\mathbf{s}^{(i)}}^{T_2^f}$. After obtaining \mathbb{B}_i , we perform UDV decomposition³ on \mathbb{B}_i , and then utilize stable multiplication and inversion formulas to separate large and small scales in the matrices as much as possible. Analogous to the $B(\tau, \tau')$ matrices in Eq. (24), we define

$$\mathbb{B}(i, i') \equiv \prod_{j=i}^{i'+1} \mathbb{B}_j = \mathbb{B}_i \mathbb{B}_{i-1} \cdots \mathbb{B}_{i'+1}, \quad (35)$$

where $0 \leq i' \leq i \leq r$. It also satisfies $\mathbb{B}(i, i) = I$. After performing matrix decomposition $\mathbb{B}(r, 0) = UDV$, we have⁴

$$\mathbb{G} \equiv [I + \mathbb{B}(r, 0)]^{-1} = [D_+^{-1}U^\dagger + D_-V]^{-1} D_+^{-1}U^\dagger, \quad (36)$$

where $D_+ = \max(D, 1)$ and $D_- = \min(D, 1)$. Subsequently, we obtain the stable formula for the Grover determinant:

$$\begin{aligned} \ln \det g_{r, \mathbf{s}} &= \sum_{i=1}^r \ln \det G_{\mathbf{s}^{(i)}}^{T_2^f} + \ln \det U + \ln \det D_+ \\ &\quad + \ln \det (D_+^{-1}U^\dagger + D_-V). \end{aligned} \quad (37)$$

A similar formula can be obtained for the twisted case. As depicted in Fig. 3(b), when the temperature is relatively moderate and within the grey-shaded region, the

stabilized formula (Eq. (37)) works well, yielding results consistent with those obtained from Eq. (33). However, as the temperature decreases further, Eq. (37) fails to benchmark against Eq. (33). This breakdown occurs at a temperature around $\beta t = 15$, where the lowest singular value of $G^{T_2^f}$ or $G^{\tilde{T}_2^f}$ approaches machine precision, as illustrated in Fig. 3(a).

In summary, we have demonstrated that the singularity of partially transposed Green's functions leads to numerical instability in calculating high-rank Grover determinants. The workaround proposed in Eq. (37) borrows the idea of numerical stabilization in DQMC [83, 84] and was also mentioned in Ref. [55] for computing high-rank REE. However, this formula is only effective when the smallest singular value of the partially transposed Green's functions is not close to machine precision. This obstacle prevents us from stably calculating high-rank RNs for generic bipartition at very low temperatures, including the zero-temperature or ground-state RNs, which corresponds to the projective QMC algorithm [86–88].

To stabilize the computation of high-rank ground-state REE, Assaad *et al.* proposed a regularization scheme for the Green's function matrices [85]. Before reducing the Green's function matrix to a subsystem, they regularized the matrix by adding a small positive constant Λ to the zero eigenvalues and subtracting Λ from other eigenvalues. Since they used the naive formula (similar to Eq. (34)) to calculate high-rank REE, the regularization parameter Λ should be large enough to stabilize the calculation. Additionally, the physical results should be tested to ensure they converge as Λ decrease ($\Lambda \sim 10^{-5}$ is a good choice for the Kane-Mele Hubbard model they studied [85]). Motivated by these findings, we propose a new regularization scheme for partially transposed Green's function matrices, which can harbor complex eigenvalues. Instead of adding Λ to the matrices' zero eigenvalues, we incorporate Λ into their (nearly) vanishing singular values. Since Eq. (37) remains numerically stable when the smallest singular value is not near machine precision, a very small Λ (approximately 10^{-13}) suffices to stabilize the calculation. It is anticipated that the physical results should not be significantly affected by such a small Λ . Indeed, as shown in Fig. 4, we applied this regularization scheme to the same free-fermion chain as in Fig. 3 and found that the results closely match those obtained from Eq. (33) across all temperatures. For interacting systems, this method is sufficiently accurate when the systematic error introduced by Λ is negligible compared to the statistical error from Monte Carlo sampling.

C. Solution 2: Drut's reconstruction of the Grover matrix

The second solution is quite elegant and simple. Drut and Porter found a way to reconstruct high-rank Grover matrices in the context of REE, such that one can avoid

³ Specifically, it can either be a SVD decomposition, or a QR decomposition followed by extracting the diagonal elements of R as D. See Appendix F for details.

⁴ One could also split the \mathbb{B} chain into two UDV decompositions and then use the corresponding formula for a stable inverse of the form, say, $(I + UDVUDV)^{-1}$. This approach is used in the incremental algorithm (see Appendix E).

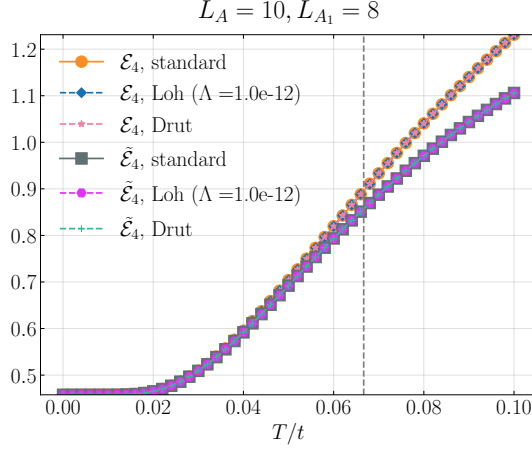


FIG. 4. The rank-4 RNs of the same free-fermion chain studied in Fig. 3(c) are calculated using the standard formula in Eq. (33), Loh's stable inversion formula in Eq. (37) with regularized $G^{T_2^f}$ and $G^{\tilde{T}_2^f}$, and Drut's formula in Eqs. (38) and (39). These results are plotted as functions of temperature T/t . The grey dashed vertical line indicates the breakdown temperature of Loh's formula without regularization (see Fig. 3).

the inversion of reduced Green's function matrices [89]. Let us write the corresponding formulas for RNs. First we consider the untwisted case:

$$\det g_{r,\bar{s}} = \det \mathcal{G}_{1 \rightarrow r, \bar{s}}^{T_2^f} \det K_{r,\bar{s}} = \det T_{r,\bar{s}}, \quad (38a)$$

where $\mathcal{G}_{1 \rightarrow r, \bar{s}}^{T_2^f} = \text{diag}[G_{\mathbf{s}^{(1)}}^{T_2^f}, \dots, G_{\mathbf{s}^{(r)}}^{T_2^f}]$ is a block-diagonal matrix with $G_{\mathbf{s}^{(i)}}^{T_2^f}$ as the i -th block, $K_{r,\bar{s}}$ is given by

$$K_{r,\bar{s}} \equiv \begin{pmatrix} I & 0 & \cdots & 0 & \mathbb{B}_{\mathbf{s}^{(r)}} \\ -\mathbb{B}_{\mathbf{s}^{(1)}} & I & \cdots & 0 & 0 \\ 0 & -\mathbb{B}_{\mathbf{s}^{(2)}} & \ddots & 0 & 0 \\ \vdots & \vdots & \ddots & \vdots & \vdots \\ 0 & 0 & \cdots & -\mathbb{B}_{\mathbf{s}^{(r-1)}} & I \end{pmatrix}, \quad (38b)$$

and thus $T_{r,\bar{s}}$ is given by

$$T_{r,\bar{s}} \equiv K_{r,\bar{s}} \mathcal{G}_{1 \rightarrow r, \bar{s}}^{T_2^f} = \begin{pmatrix} G_{\mathbf{s}^{(1)}}^{T_2^f} & 0 & \cdots & 0 & I - G_{\mathbf{s}^{(r)}}^{T_2^f} \\ G_{\mathbf{s}^{(1)}}^{T_2^f} - I & G_{\mathbf{s}^{(2)}}^{T_2^f} & \cdots & 0 & 0 \\ \vdots & \vdots & \ddots & \vdots & \vdots \\ 0 & 0 & \cdots & G_{\mathbf{s}^{(r-1)}}^{T_2^f} & 0 \\ 0 & 0 & \cdots & G_{\mathbf{s}^{(r-1)}}^{T_2^f} - I & G_{\mathbf{s}^{(r)}}^{T_2^f} \end{pmatrix}. \quad (38c)$$

To calculate the twisted Grover determinants, one can similarly define $\tilde{T}_{r,\bar{s}}$, satisfying $\det \tilde{g}_{r,\bar{s}} = \det \tilde{T}_{r,\bar{s}}$, by replacing $G_{\mathbf{s}^{(i)}}^{T_2^f}$ with $G_{\mathbf{s}^{(i)}}^{\tilde{T}_2^f}$ in Eq. (38c). Additionally, the determinant of the modified Grover matrix $\tilde{g}_{r,\bar{s}}$ defined

in Eq. (32) can also be reconstructed following a similar procedure. One can show that

$$\det \tilde{g}_{r,\bar{s}} = \det \mathcal{G}_{r \rightarrow 1, \bar{s}}^{T_2^f} \det \tilde{K}_{r,\bar{s}} = \det \tilde{T}_{r,\bar{s}}, \quad (39a)$$

where $\mathcal{G}_{r \rightarrow 1, \bar{s}}^{T_2^f} = \text{diag}[G_{\mathbf{s}^{(1)}}^{T_2^f}, \dots, G_{\mathbf{s}^{(1)}}^{T_2^f}]$, $\tilde{K}_{r,\bar{s}}$ is given by

$$\tilde{K}_{r,\bar{s}} = \begin{pmatrix} I & -\mathbb{B}_{\mathbf{s}^{(r)}} U_2 & \cdots & 0 & 0 \\ 0 & I & \cdots & 0 & 0 \\ \vdots & \vdots & \ddots & \vdots & \vdots \\ 0 & 0 & \cdots & I & -\mathbb{B}_{\mathbf{s}^{(2)}} U_2 \\ \mathbb{B}_{\mathbf{s}^{(1)}} U_2 & 0 & \cdots & 0 & I \end{pmatrix}, \quad (39b)$$

and

$$\begin{aligned} \tilde{T}_{r,\bar{s}} &\equiv \mathcal{G}_{r \rightarrow 1, \bar{s}}^{T_2^f} \tilde{K}_{r,\bar{s}} \\ &= \begin{pmatrix} G_{\mathbf{s}^{(r)}}^{T_2^f} & (G_{\mathbf{s}^{(r-1)}}^{T_2^f} - I) U_2 & \cdots & 0 \\ 0 & G_{\mathbf{s}^{(r-1)}}^{T_2^f} & \cdots & 0 \\ \vdots & \vdots & \ddots & \vdots \\ (I - G_{\mathbf{s}^{(1)}}^{T_2^f}) U_2 & 0 & \cdots & G_{\mathbf{s}^{(1)}}^{T_2^f} \end{pmatrix}. \end{aligned} \quad (39c)$$

Here, the matrix U_2 is defined above Eq. (16). Using Eqs. (38) and (39), we revisit the computation of RNs in Fig. 4. The results are consistent with those obtained from both Eq. (33) and Eq. (37) with regularized Green's function matrices for all temperatures.

V. INCREMENTAL ALGORITHM FOR RANK- r RÉNYI NEGATIVITY

As system size L or temperature increases, the RN in general become larger, and the associated Grover determinant becomes exponentially small, which causes the second challenge in calculating high-rank RN. This challenge is well-documented in the literature on various quantum Monte Carlo methods aimed at calculating REE, and several incremental algorithms have been proposed to address this issue [16–18, 52–55, 90].

In this section, we develop numerically stable incremental algorithms for calculating both untwisted and twisted RNs. For each variant, we first establish the theoretical framework of the incremental algorithm, then propose specific, computationally stable update scheme. Finally, we demonstrate that the RNR can be efficiently computed within a single QMC run, eliminating the need for separate calculations of RN and thermal Rényi entropy S_r^{th} .

A. Incremental algorithm for untwisted Rényi negativity

Let us first rewrite the DQMC formula for untwisted RN in Eq. (29a),

$$e^{(1-r)\mathcal{E}_r} = \frac{\sum_{\mathbf{s}^{(1)} \dots \mathbf{s}^{(r)}} W_{\mathbf{s}^{(1)} \dots \mathbf{s}^{(r)}} \det g_{r,\bar{\mathbf{s}}}}{\sum_{\mathbf{s}^{(1)} \dots \mathbf{s}^{(r)}} W_{\mathbf{s}^{(1)} \dots \mathbf{s}^{(r)}}}, \quad (40)$$

where $W_{\mathbf{s}^{(1)} \dots \mathbf{s}^{(r)}} = \prod_{i=1}^r w_{\mathbf{s}^{(i)}}$ represents the joint DQMC weight in the combined configuration space $\{\mathbf{s}^{(1)} \dots \mathbf{s}^{(r)}\}$. We refer to $\mathbf{s}^{(i)}$ as the configuration at the i -th replica. When \mathcal{E}_r is large, the Grover determinant, $\det g_r$, is typically exponentially small. The appearance of sampling spikes leads to the infinite variance problem [91], significantly affecting the evaluation of \mathcal{E}_r through Eq. (40). Further studies on REE unveiled that the distribution of the Grover determinant defined by the reduced Green's function is non-Gaussian, whereas the logarithm and the N_{inc} -th root of the Grover determinant follow a Gaussian distribution [90]. These findings motivate a similar incremental algorithm for untwisted RN,

$$e^{(1-r)\mathcal{E}_r} = \frac{Z_{N_{\text{inc}}}}{Z_{N_{\text{inc}}-1}} \dots \frac{Z_{k+1}}{Z_k} \dots \frac{Z_1}{Z_0}, \quad (41)$$

with the partition function defined as

$$Z_k = \sum_{\mathbf{s}^{(1)} \dots \mathbf{s}^{(r)}} W_{\mathbf{s}^{(1)} \dots \mathbf{s}^{(r)}} (\det g_{r,\bar{\mathbf{s}}})^{\frac{k}{N_{\text{inc}}}}. \quad (42)$$

Each intermediate incremental process (denoted by k) is an average of an ensemble existing in the replicated configuration space:

$$\begin{aligned} \frac{Z_{k+1}}{Z_k} &= \frac{\sum_{\mathbf{s}^{(1)} \dots \mathbf{s}^{(r)}} W_{\mathbf{s}^{(1)} \dots \mathbf{s}^{(r)}}^{(k)} (\det g_{r,\bar{\mathbf{s}}})^{\frac{1}{N_{\text{inc}}}}}{\sum_{\mathbf{s}^{(1)} \dots \mathbf{s}^{(r)}} W_{\mathbf{s}^{(1)} \dots \mathbf{s}^{(r)}}^{(k)}} \\ &= \left\langle (\det g_{r,\bar{\mathbf{s}}})^{\frac{1}{N_{\text{inc}}}} \right\rangle_{W^{(k)}}, \end{aligned} \quad (43)$$

where $W_{\mathbf{s}^{(1)} \dots \mathbf{s}^{(r)}}^{(k)} = W_{\mathbf{s}^{(1)} \dots \mathbf{s}^{(r)}} (\det g_{r,\bar{\mathbf{s}}})^{\frac{k}{N_{\text{inc}}}}$. For a sign-problem-free Monte Carlo sampling of each factor, it is essential to prove that $\det g_{r,\bar{\mathbf{s}}}$ is real and positive for any rank r . In previous work [51], we proved that for two classes of sign-problem-free models, represented by the Hubbard model and t - V model, the Grover determinant of any rank is indeed real and positive. We also provide the proof in Appendix D.

B. Local update scheme for untwisted Rényi negativity

As illustrated in Fig. 5, we sequentially update the \mathbf{s} -configurations, starting from the first replica $\mathbf{s}^{(1)}$ and proceeding to the last replica $\mathbf{s}^{(r)}$. Within each replica, updates occur from the first spacetime coordinate to the

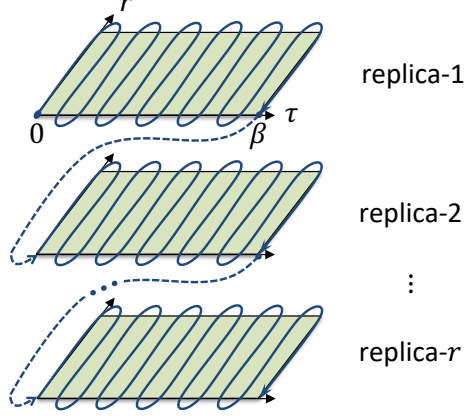


FIG. 5. Illustration of the (forward) local sweep in each incremental process of the incremental algorithm for rank- r RN.

last. When updating the auxiliary field at a specific spacetime coordinate in replica- i , the acceptance ratio is given by

$$R_i^{(k)} \equiv \frac{W_{\mathbf{s}^{(1)} \dots \mathbf{s}^{(i)} \dots \mathbf{s}^{(r)}}^{(k)}}{W_{\mathbf{s}^{(1)} \dots \mathbf{s}^{(i)} \dots \mathbf{s}^{(r)}}^{(k)}} = \frac{w_{\mathbf{s}^{(i)'}}}{w_{\mathbf{s}^{(i)}}} \left(\frac{\det g_{r,\bar{\mathbf{s}}'}}{\det g_{r,\bar{\mathbf{s}}}} \right)^{k/N_{\text{inc}}}. \quad (44)$$

In practice, each calculation task associated with the intermediate factor labeled by k is assigned to a single CPU, allowing these factors to be computed in parallel. One essential task for every CPU is to compute the ratio of Grover determinants before and after the update, $\det g_{r,\bar{\mathbf{s}}'}/\det g_{r,\bar{\mathbf{s}}}$. The only difference between the CPUs lies in the root order of the Grover determinant ratio when evaluating the total ratio $R_i^{(k)}$.

To design a fast update scheme for Monte Carlo sampling, the initial step is to select one or a few central matrices to update, which will be referred to as the update objects in the following discussion. A practical Monte Carlo sampling scheme involves both the update formula and the stabilization formula for these update objects. In normal DQMC, the update object is the Green's function matrix $G_{s,ij}$ in Eq. (25). The inverse determinant ratio $(\det [G_{\mathbf{s}^{(i)}'}]/\det [G_{\mathbf{s}^{(i)}'}])$ corresponds to the “quantum part” of ratio $w_{\mathbf{s}^{(i)'}}/w_{\mathbf{s}^{(i)}}$, excluding the ratio of the coupling coefficients $\alpha[\mathbf{s}^{(i)}] = \prod_l \alpha[s_l^{(i)}]$ (see Eq. (17)). A straightforward update scheme for an incremental algorithm could involve splitting the total ratio $R_i^{(k)}$ into three components, $R_i^{(k)} = r_1(r_2 r_3)^{k/N_{\text{inc}}}$, where

$$\begin{aligned} r_1 &= \frac{w_{\mathbf{s}^{(i)'}}}{w_{\mathbf{s}^{(i)}}}, \quad r_2 = \frac{\det G_{\mathbf{s}^{(i)'}}^{T_2^f}}{\det G_{\mathbf{s}^{(i)}}^{T_2^f}}, \\ r_3 &= \frac{\det [I + \mathbb{B}_r \dots \mathbb{B}_i' \dots \mathbb{B}_1]}{\det [I + \mathbb{B}_r \dots \mathbb{B}_i \dots \mathbb{B}_1]}. \end{aligned} \quad (45)$$

It is important to note that as one sweeps through the local auxiliary fields back and forth, the Grover deter-

minant in the weight should be fixed at a specific imaginary time to ensure the weight is well-defined [17, 18, 54, 55, 90]. This point is typically set to $\tau = 0$ in finite-temperature DQMC, so all instances of $G_{\mathbf{s}^{(i)}}^{T_2^f}$ appearing in r_2 and r_3 in Eq. (45), including those inside \mathbb{B}_i , are actually $G_{\mathbf{s}^{(i)}}^{T_2^f}(0, 0)$.

The calculation of r_1 follows standard DQMC procedures. In the following discussion, we introduce an update scheme for calculating the remaining part of the ratio which demonstrates sufficient numerical stability for the spinless t - V model. We also discuss two alternative schemes with simpler update objects but lower numerical stability in Appendix E. For convenience, Table I summarizes the dimensions of all key matrices across these schemes.

Dimension	Intermediate matrices
$N \times m$	$U, \mathcal{U}, \mathcal{U}'$
$m \times N$	$V, \mathcal{V}, \mathbb{V}, \mathcal{V}^a, \mathcal{V}^b, \mathcal{V}^c$
$m \times m$	I_m, D

TABLE I. Table for the dimensions of the intermediate matrices in the key steps in the update schemes. m is the number of non-zero entries in the deviation matrix Δ , see the explanation below Eq. (46).

Before introducing the actual update object employed in this scheme, we must first derive an essential formula for the local update of the partially transposed Green's function matrix. Since the $G_{\mathbf{s}^{(i)}}^{T_2^f}$ in Eq. (45) originates from the equal-time Green's function at $\tau = 0$, we begin with the update formula for $G_{\mathbf{s}^{(i)}}(0, 0)$ at time τ^5

$$G_{\mathbf{s}^{(i)'}}(0, 0) = G_{\mathbf{s}^{(i)}}(0, 0) + G_{\mathbf{s}^{(i)}}(0, \tau) U (I_m + VU)^{-1} V(\tau, 0). \quad (46)$$

Here is an explanation of the above formula. We first define the deviation matrix between the interaction matrix after and before the update, $\Delta \equiv e^{-V[\mathbf{s}^{(i)}]} e^{V[\mathbf{s}^{(i)'}]}$ $- I$, and restrict ourselves to consider only $N \times N$ diagonal Δ with m non-zeros entries. For instance, $m = 1$ for the Hubbard model, and $m = 2$ for the t - V model. Next, we define projection matrices $P_{N \times m}$ and $P_{m \times N}$, which are cropped from the identity matrix $I = I_N$, with columns or rows corresponding to the non-zero entries of Δ . The matrices in the above formula can then be expressed as $\Delta = P_{N \times m} D P_{m \times N}$, $U \equiv P_{N \times m} D$, $V \equiv P_{m \times N} (I - G_{\mathbf{s}^{(i)}}(\tau, \tau))$, and $V(\tau, 0) \equiv P_{m \times N} G_{\mathbf{s}^{(i)}}(\tau, 0)$. For simplicity, we abbreviate the subscript $\mathbf{s}^{(i)}$ in these intermediate matrices, but it is essential to remember that they depend on the \mathbf{s} -configuration in the current replica before the update. The update formula for $G_{\mathbf{s}^{(i)'}}^{T_2^f}$

⁵ Technically, due to the symmetric Trotter decomposition, the Green's functions in the update formula have undergone partial propagation, i.e., $G(\tau, \tau) \rightarrow e^{-K} G(\tau, \tau) e^K$, $G(\tau, 0) \rightarrow e^{-K} G(\tau, 0)$, and $G(0, \tau) \rightarrow G(0, \tau) e^K$.

can be derived by applying Eq. (15) to Eq. (46):

$$\begin{aligned} G_{\mathbf{s}^{(i)'}}^{T_2^f} &= G_{\mathbf{s}^{(i)}}^{T_2^f} (I + \mathcal{U} \mathcal{V}) = G_{\mathbf{s}^{(i)}}^{T_2^f} + \mathcal{U} \mathcal{V}, \\ \mathcal{U} &\equiv \begin{pmatrix} (G_{\mathbf{s}^{(i)}}(0, \tau))_{A_1 N} \\ i (G_{\mathbf{s}^{(i)}}(0, \tau))_{A_2 N} \end{pmatrix} P_{N \times m} \equiv G_{\mathbf{s}^{(i)}}^{T_2^f} \mathcal{U}, \\ \mathcal{V} &\equiv D (I_m + VU)^{-1} (V_{m A_1}(\tau, 0) \ i V_{m A_2}(\tau, 0)). \end{aligned} \quad (47)$$

We assume that the linear indices of the system's degrees of freedom are divided into two continuous subsystems A_1 and A_2 , allowing for convenient expression of the block form of \mathcal{U} and \mathcal{V} . This approach is easily generalizable to any bipartition, and for different bipartition geometries, the formula above is the only aspect that changes.

Building upon the established update formula, we now define our primary update object for replica- i ,

$$\begin{aligned} \mathbb{F}_i &= \left[G_{\mathbf{s}^{(i)}}^{T_2^f} \mathbb{B}_{\mathbf{i}}^{-1} G_{\mathbf{s}^{(i-1)}}^{T_2^f} \mathbb{B}_{i-1} + G_{\mathbf{s}^{(i)}}^{T_2^f} \mathbb{B}_i G_{\mathbf{s}^{(i-1)}}^{T_2^f} \mathbb{B}_{i-1} \right]^{-1} \\ &= \left[G_{\mathbf{s}^{(i)}}^{T_2^f} \mathbb{F}_{\mathbf{i}}^{-1} + I - G_{\mathbf{s}^{(i-1)}}^{T_2^f} \right]^{-1}, \end{aligned} \quad (48)$$

where $\mathbb{B}_{\mathbf{i}} \equiv \mathbb{B}(i-1, 0) \mathbb{B}(r, i) = \mathbb{B}_{i-1} \cdots \mathbb{B}_1 \mathbb{B}_r \cdots \mathbb{B}_{i+1}$ and

$$\begin{aligned} \mathbb{F}_{\mathbf{i}}^{-1} &\equiv \left(\mathbb{B}_{\mathbf{i}}^{-1} - I \right) G_{\mathbf{s}^{(i-1)}}^{T_2^f} \mathbb{B}_{i-1} \\ &= \mathbb{B}_{i+1}^{-1} \cdots \mathbb{B}_r^{-1} \mathbb{B}_1^{-1} \cdots \mathbb{B}_{i-2}^{-1} G_{\mathbf{s}^{(i-1)}}^{T_2^f} - \left(I - G_{\mathbf{s}^{(i-1)}}^{T_2^f} \right). \end{aligned} \quad (49)$$

It can be verified that the update ratio of $\det \mathbb{F}_i^{-1}$ is equivalent to the update ratio of $\det g_{r, \bar{s}}$, since

$$\begin{aligned} \det \mathbb{F}_i^{-1} &= \det \left[G_{\mathbf{s}^{(i)}}^{T_2^f} \right] \det \left[\mathbb{B}_{\mathbf{i}}^{-1} + \mathbb{B}_i \right] \det \left[G_{\mathbf{s}^{(i-1)}}^{T_2^f} \mathbb{B}_{i-1} \right] \\ &= \det \left[G_{\mathbf{s}^{(i)}}^{T_2^f} \right] \det [I + \mathbb{B}(i, 0) \mathbb{B}(r, i)] \\ &\quad \times \det \left[\mathbb{B}_{\mathbf{i}}^{-1} \right] \det \left[G_{\mathbf{s}^{(i-1)}}^{T_2^f} \mathbb{B}_{i-1} \right], \end{aligned} \quad (50)$$

where the third line is independent of $\mathbf{s}^{(i)}$ and cancels out when considering the update ratio. This definition is based on two basic ideas. First, instead of using \mathbb{B}_i , we use its inverse, \mathbb{B}_i^{-1} , which provides better stability during numerical calculations. Second, we explicitly incorporate matrices from neighboring replicas, $G_{\mathbf{s}^{(i-1)}}^{T_2^f}$ and \mathbb{B}_{i-1} , into the definition of \mathbb{F}_i . We note that for high-rank Grover determinants, using the property $\det AB = \det A \det B$, the matrices $G_{\mathbf{s}^{(j)}}^{T_2^f}$ and \mathbb{B}_j can be combined for at most two different $j \in [1, r]$, as the matrices are non-commutative. When $r = 2$, \mathbb{F}_i reduces to the inverse of the total Grover matrix:

$$\mathbb{F}_i^{-1} = G_{\mathbf{s}^{(i)}}^{T_2^f} G_{\mathbf{s}^{(i-1)}}^{T_2^f} + \left(I - G_{\mathbf{s}^{(i)}}^{T_2^f} \right) \left(I - G_{\mathbf{s}^{(i-1)}}^{T_2^f} \right) = g_{2, \bar{s}} \quad (51)$$

Updating the inverse of the rank-2 Grover matrix is stable and commonly used in practice, as evidenced by previous studies on the incremental algorithm for rank-2 REE [17, 18, 90].

Updating \mathbb{F}_i in Eq. (48) follows from Eq. (47):

$$\mathbb{F}'_i = \mathbb{F}_i \left(I - \mathcal{U} (I_m + \mathcal{V}^c \mathcal{U})^{-1} \mathcal{V}^c \right), \quad (52)$$

with the ratio given by

$$r_2 r_3 = \frac{\det g_{r,\bar{s}'}}{\det g_{r,\bar{s}}} = \frac{\det \mathbb{F}'_i}{\det \mathbb{F}'_i} = \det (I_m + \mathcal{V}^c \mathcal{U}), \quad (53)$$

where $\mathcal{V}^c \equiv \mathcal{V} \mathbb{F}_i^{-1} \mathbb{F}_i$. However, the numerical stabilization of \mathbb{F}_i is more tedious and does not simply reuse the numerical stabilization routines from DQMC (listed in Appendix F). Nevertheless, the core principle of numerical stabilization remains the same: perform matrix decomposition and separate small and large scales as much as possible. A detailed discussion and code implementation are provided in Appendix G. Finally, the measurement of $\det g_{r,\bar{s}}$ is given by:

$$\ln \det g_{r,\bar{s}} = -\ln \det \mathbb{F}_i + \sum_{j \neq i, i-1} \ln \det \left[I - G_{\mathbf{s}^{(j)}}^{T_2^f} \right], \quad (54)$$

as derived from Eq. (50).

C. Incremental algorithm for twisted Rényi negativity

The incremental algorithm for rank- r twisted RN can be implemented in a similar manner. We start with Eq. (31) and define the following partition function:

$$\tilde{Z}_k = \sum_{\mathbf{s}^{(1)} \dots \mathbf{s}^{(r)}} W_{\mathbf{s}^{(1)} \dots \mathbf{s}^{(r)}} \left(\det \tilde{g}_{r,\bar{s}} \right)^{\frac{k}{N_{\text{inc}}}}, \quad (55)$$

which results in an incremental expression for rank- r twisted RN:

$$e^{(1-r)\tilde{\mathcal{E}}_r} = \frac{\tilde{Z}_{N_{\text{inc}}}}{\tilde{Z}_{N_{\text{inc}}-1}} \dots \frac{\tilde{Z}_{k+1}}{\tilde{Z}_k} \dots \frac{\tilde{Z}_1}{\tilde{Z}_0}. \quad (56)$$

Each intermediate factor's calculation is assigned to an incremental process (denoted by k), with

$$\begin{aligned} \frac{\tilde{Z}_{k+1}}{\tilde{Z}_k} &= \frac{\sum_{\mathbf{s}^{(1)} \dots \mathbf{s}^{(r)}} \tilde{W}_{\mathbf{s}^{(1)} \dots \mathbf{s}^{(r)}}^{(k)} \left(\det \tilde{g}_{r,\bar{s}} \right)^{\frac{1}{N_{\text{inc}}}}}{\sum_{\mathbf{s}^{(1)} \dots \mathbf{s}^{(r)}} \tilde{W}_{\mathbf{s}^{(1)} \dots \mathbf{s}^{(r)}}^{(k)}} \\ &= \left\langle \left(\det \tilde{g}_{r,\bar{s}} \right)^{\frac{1}{N_{\text{inc}}}} \right\rangle_{\tilde{W}^{(k)}}, \end{aligned} \quad (57)$$

where $\tilde{W}_{\mathbf{s}^{(1)} \dots \mathbf{s}^{(r)}}^{(k)} = W_{\mathbf{s}^{(1)} \dots \mathbf{s}^{(r)}} \left(\det \tilde{g}_{r,\bar{s}} \right)^{\frac{k}{N_{\text{inc}}}}$. As demonstrated in Appendix D, analogous to the untwisted case, the twisted Grover determinant exhibits real and non-negative properties ($\det \tilde{g}_{r,\bar{s}} \geq 0$) for two classes of sign-problem-free models. However, the normalization factor $\mathcal{Z}_{\tilde{T}_2^f, \mathbf{s}^{(i)}}$ can be negative for certain ranks and subsystem sizes. In particular, for the first class of models, such

as the Hubbard model, the normalization factor $\mathcal{Z}_{\tilde{T}_2^f, \mathbf{s}^{(i)}}$ is proportional to $(-1)^{N_{A_2}}$, where N_{A_2} represents the number of sites in subsystem A_2 (see Eq. (D7)). Consequently, for odd ranks and odd values of N_{A_2} , the twisted RN is ill-defined (see Fig. 6 for an example with $r = 3$). In what follows, we will focus exclusively on cases where both the modified Grover determinant $\det \tilde{g}_{r,\bar{s}}$ and the weight $\tilde{W}_{\mathbf{s}^{(1)} \dots \mathbf{s}^{(r)}}^{(k)}$ are sign-problem-free.

D. Local update scheme for twisted Rényi negativity

Consider an update occurring in replica- i . The update ratio is given by

$$\tilde{R}_i^{(k)} \equiv \frac{\tilde{W}_{\mathbf{s}^{(1)} \dots \mathbf{s}^{(i)} \dots \mathbf{s}^{(r)}}^{(k)}}{\tilde{W}_{\mathbf{s}^{(1)} \dots \mathbf{s}^{(i-1)} \dots \mathbf{s}^{(r)}}^{(k)}} = r_1 (r_2 \tilde{r}_3)^{\frac{k}{N_{\text{inc}}}}, \quad (58)$$

where r_1 and r_2 are defined in Eq. (45), and

$$\tilde{r}_3 = \frac{\det \left[I + \tilde{\mathbb{B}}_r \dots \tilde{\mathbb{B}}_i' \dots \tilde{\mathbb{B}}_1 \right]}{\det \left[I + \tilde{\mathbb{B}}_r \dots \tilde{\mathbb{B}}_i \dots \tilde{\mathbb{B}}_1 \right]}. \quad (59)$$

Here, $\tilde{\mathbb{B}}_i = \mathbb{B}_i U_2 = [(G^{T_2^f})^{-1} - I] U_2$. Similar to the untwisted case in Sec. V B, we implement a scheme to directly calculate $r_2 \tilde{r}_3$, offering numerical stability. The primary adjustment involves incorporating U_2 into the update object and intermediate matrices. Eqs. (48) and (49) are thus replaced by

$$\tilde{\mathbb{F}}_i = \left[G_{\mathbf{s}^{(i)}}^{T_2^f} \tilde{\mathbb{F}}_i^{-1} + U_2 \left(I - G_{\mathbf{s}^{(i-1)}}^{T_2^f} \right) U_2 \right]^{-1} \quad (60)$$

and

$$\tilde{\mathbb{F}}_i^{-1} = \left(\tilde{\mathbb{F}}_i^{-1} - U_2 \right) \left(I - G_{\mathbf{s}^{(i-1)}}^{T_2^f} \right) U_2, \quad (61)$$

respectively. The update formula for Eq. (60) and the calculation of the ratio $r_2 \tilde{r}_3$ are analogous to Eqs. (52) and (53), provided that one replaces \mathbb{F}_i and $\tilde{\mathbb{F}}_i$ therein with \mathbb{F}_i^{-1} and $\tilde{\mathbb{F}}_i^{-1}$, respectively. The numerical stabilization of $\tilde{\mathbb{F}}_i$ is also similar, as discussed in Appendix G. Finally, the measurement of $\det \tilde{g}_r$ is given by

$$\ln \det \tilde{g}_r = -\ln \det \tilde{\mathbb{F}}_i^{-1} + \sum_{j \neq i, i-1} \ln \det \left[\left(I - G_{\mathbf{s}^{(j)}}^{T_2^f} \right) U_2 \right]. \quad (62)$$

E. Incremental algorithm for Rényi negativity ratio

The rank- r RNR defined in Eq. (28) can be efficiently calculated using an incremental algorithm in a

single simulation, rather than computing RN and thermal Rényi entropy separately. This approach offers an additional computational advantage: since RNR is intrinsically smaller than the corresponding RN of the same rank, fewer incremental processes are required for small statistical errors. When dividing two exponential observables, the result remains an exponential observable, yielding the following expression for untwisted RNR:

$$\begin{aligned} e^{(1-r)R_r} &= \frac{e^{(1-r)\mathcal{E}_r}}{e^{(1-r)S_r^{\text{th}}}} = \frac{\sum_{\mathbf{s}^{(1)} \dots \mathbf{s}^{(r)}} W_{\mathbf{s}^{(1)} \dots \mathbf{s}^{(r)}} \det g_{r,\bar{\mathbf{s}}}}{\sum_{\mathbf{s}^{(1)} \dots \mathbf{s}^{(r)}} W_{\mathbf{s}^{(1)} \dots \mathbf{s}^{(r)}} \det g_{r,\bar{\mathbf{s}}}^{\text{th}}} \\ &= \frac{\sum_{\mathbf{s}^{(1)} \dots \mathbf{s}^{(r)}} W_{\mathbf{s}^{(1)} \dots \mathbf{s}^{(r)}} \det g_{r,\bar{\mathbf{s}}}^{\text{th}} (\det g_{r,\bar{\mathbf{s}}} / \det g_{r,\bar{\mathbf{s}}}^{\text{th}})}{\sum_{\mathbf{s}^{(1)} \dots \mathbf{s}^{(r)}} W_{\mathbf{s}^{(1)} \dots \mathbf{s}^{(r)}} \det g_{r,\bar{\mathbf{s}}}^{\text{th}}} \\ &= \frac{Z_{N_{\text{inc}}}}{Z_{N_{\text{inc}}-1}} \dots \frac{Z_{k+1}}{Z_k} \dots \frac{Z_1}{Z_0}, \end{aligned} \quad (63)$$

where the partition function is defined as

$$Z_k = \sum_{\mathbf{s}^{(1)} \dots \mathbf{s}^{(r)}} W_{\mathbf{s}^{(1)} \dots \mathbf{s}^{(r)}} \det g_{r,\bar{\mathbf{s}}}^{\text{th}} (\det g_{r,\bar{\mathbf{s}}} / \det g_{r,\bar{\mathbf{s}}}^{\text{th}})^{k/N_{\text{inc}}}. \quad (64)$$

Here, we use $g_{r,\bar{\mathbf{s}}}^{\text{th}}$ to denote the Grover determinant corresponding to the rank- r Rényi entropy, i.e., by setting $A_1 = A$ and $G^{T_2^f} = G$ in Eq. (34). In each incremental CPU, the Monte-Carlo involves the following factor:

$$\frac{Z_{k+1}}{Z_k} = \frac{\sum_{\mathbf{s}^{(1)} \dots \mathbf{s}^{(r)}} W_{\mathbf{s}^{(1)} \dots \mathbf{s}^{(r)}}^{(k)} (\det g_{r,\bar{\mathbf{s}}} / \det g_{r,\bar{\mathbf{s}}}^{\text{th}})^{1/N_{\text{inc}}}}{\sum_{\mathbf{s}^{(1)} \dots \mathbf{s}^{(r)}} W_{\mathbf{s}^{(1)} \dots \mathbf{s}^{(r)}}^{(k)}}, \quad (65)$$

where the total weight is given by

$$W_{\mathbf{s}^{(1)} \dots \mathbf{s}^{(r)}}^{(k)} = W_{\mathbf{s}^{(1)} \dots \mathbf{s}^{(r)}} (\det g_{r,\bar{\mathbf{s}}}^{\text{th}})^{1-k/N_{\text{inc}}} (\det g_{r,\bar{\mathbf{s}}}^{\text{th}})^{k/N_{\text{inc}}}. \quad (66)$$

In practice, it is essential to perform the same procedures for $\det g_{r,\bar{\mathbf{s}}}^{\text{th}}$ as for $\det g_{r,\bar{\mathbf{s}}}$, including both updates and stabilization. When evaluating the update ratio, particular attention is required to properly account for the distinct root orders specified in the preceding equations. These formulas address only the untwisted case; similar principles apply to the twisted case.

VI. MODEL SIMULATION: BENCHMARKS AND RESULTS

A. Quantum-classical crossover in the Hubbard chain

As a first example, we apply the methods in Sec. IV within the framework of normal DQMC (without using incremental algorithm) to a half-filled Hubbard chain, whose Hamiltonian is expressed as

$$\hat{H} = -t \sum_{i,\sigma=\uparrow,\downarrow} (c_{i,\sigma}^\dagger c_{i+1,\sigma} + \text{H.c.}) + \frac{U}{2} \sum_i (\hat{n}_i - 1)^2, \quad (67)$$

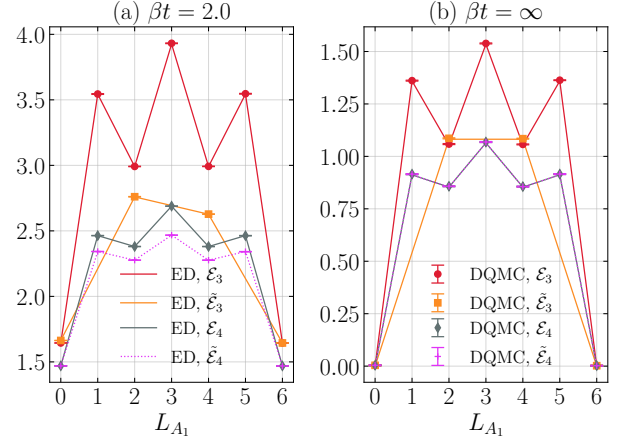


FIG. 6. The variations of high-rank RNs as functions of subsystem length L_{A_1} for a half-filled Hubbard chain with $U/t = 1$ and $L_A = 6$ is calculated using both DQMC and exact diagonalization (ED). The bipartition geometry follows the inset of Fig. 2. For the untwisted RNs, the ED and DQMC results are obtained using Eq. (3) and Eq. (38), respectively. Analogous formulas are applied for the calculation of the twisted RNs. We note that for $\beta t = 2.0$, the DQMC data can alternatively be calculated directly from Eq. (37). Additionally, in the zero-temperature limit ($\beta t = \infty$), employing Eq. (37) with slightly regularized $G^{T_2^f}$ and $G^{\tilde{T}_2^f}$ matrices ($\Lambda = 10^{-13}$) yields results that are consistent within the error bars. For odd L_{A_1} , $\tilde{\mathcal{E}}_3$ is ill-defined and not shown, as $\text{Tr}[(\rho^{\tilde{T}_2^f})^3]$ is negative (see Eq. (D7) and the related discussion on the sign problem of the Grover determinants).

where $\hat{n}_i = c_{i\uparrow}^\dagger c_{i\uparrow} + c_{i\downarrow}^\dagger c_{i\downarrow}$. As shown in Fig. 6, both the untwisted and twisted RNs have been successfully validated against the exact diagonalization (ED) results at both finite and zero temperatures. The singularity of the partially transposed Green's functions depends on the model and the HS transformation. For the Hubbard model with $U/t = 1.0$, practical experience indicates that Eq. (37) remains stable up to approximately $\beta t = 20.0$. At lower temperatures, unstable large values of the Grover determinant may appear randomly, depending on the specific \mathbf{s} -configuration. However, either approach—using Eq. (37) with a regularized $G^{T_2^f}$ or using Eq. (38a)—yields the same accurate results within the error bars. For the former approach, a regularization parameter of $\Lambda = 10^{-13}$ suffices to achieve the desired accuracy⁶. We also note that, similarly to the free-fermion results in Fig. 2, the ground-state values of untwisted and twisted rank-4 RNs, exhibited in Fig. 6(b), are exactly identical, which aligns with the analytical result in Eq. (8).

⁶ While the real part of Monte-Carlo average $\langle \det g_r \rangle$ is sufficiently accurate, there may be an unexpected non-zero imaginary part on the order of 10^{-6} to 10^{-8} , which should be disregarded.

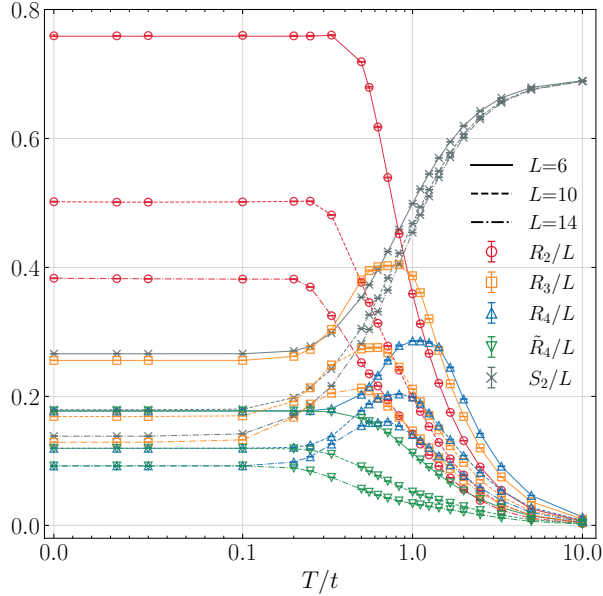


FIG. 7. The quantum-classical crossover in the Hubbard chain is illustrated by the diminishing rank-2 untwisted and rank-4 twisted RNRs (R_2 and \tilde{R}_4 , respectively) as temperature rises, while the rank-2 REE S_2 tends towards a volume law. In contrast, the rank-3 and rank-4 untwisted RNRs (R_3 and R_4 , respectively) exhibit a local maximum at intermediate temperatures. The subsystem length is set to $L_{A_1} = L/2$. Error bars are smaller than the symbol size. The solid lines for $L = 6$ are derived from ED calculations. For larger L , the dashed and dash-dot lines simply connect the DQMC data points.

Next, we investigate the finite-temperature dependence of the RNRs in the Hubbard chain. In this paper, we further reveal that the rank-4 twisted RNR exhibits behavior similar to the rank-2 untwisted RNR studied in Ref. [51]. Fig. 7 shows the rescaled behaviors of rank-2 REE (S_2/L), rank-2 to rank-4 untwisted RNRs ($R_{2,3,4}/L$), and rank-4 twisted RNR (\tilde{R}_4/L) as functions of temperature. The monotonic decrease of both R_2/L and \tilde{R}_4/L with increasing temperature highlights the quantum-classical crossover in the Hubbard chain [48, 51]. This finding not only provides a physical interpretation for the definition of RNR but also illustrates why the RNR may serve as a more reliable indicator of mixed-state entanglement compared to the REE, which tends to follow a volume law as temperature rises. Remarkably, R_3 and R_4 exhibit a local maximum at intermediate temperatures, contrasting with the monotonic decrease observed for R_2 and \tilde{R}_4 . These results highlight the nuanced definition of untwisted RNR and suggest that certain ranks may not serve as reliable indicators of entanglement.

B. Finite-temperature phase transition in the spinless t - V model

Now we apply our incremental algorithm for arbitrary-rank RNRs (detailed in Sec. V) to the half-filled spinless t - V model on a square lattice with periodic boundary conditions, as illustrated in Fig. 8(a) [92–94],

$$H = -t \sum_{\langle i,j \rangle} (c_i^\dagger c_j + c_j^\dagger c_i) + V \sum_{\langle i,j \rangle} \left(n_i - \frac{1}{2} \right) \left(n_j - \frac{1}{2} \right), \quad (68)$$

where both the hopping t and the interaction V involve only nearest neighbors. This model has been proved to be sign-problem-free model [77, 95–98], and its Grover determinants of various ranks are also sign-problem-free [51]. When a finite coupling V is present, this model exhibits a charge density wave (CDW) ground state and undergoes a transition from the CDW phase to a metallic phase at a finite temperature, as illustrated in Fig. 8(b). The critical behavior of this transition is governed by the 2D Ising universality class [93, 99]. Here, we concentrate on a specific coupling strength of $V/t = 2$, where the critical temperature has been estimated to be $T_c/t \approx 1.0$ [93]. This temperature falls within the range where the singularity of the partially transposed Green's function can be handled stably, thus ensuring the feasibility of our simulation.

As depicted in Fig. 8(c), the untwisted RNRs of different ranks exhibit similar behavior as temperature increases. Remarkably, the area-law coefficient of rank- r untwisted RNR displays a peak at the replicated critical temperature $T = rT_c$ for various system sizes. This phenomenon arises from the replica trick, $\rho^r \sim e^{-rH/T}$, which effectively elevates the phase transition temperature to r times its original value. The logarithmic divergence of R_r/L with respect to the linear size L , as unveiled in Ref. [51] for rank 2, is also observed for higher ranks. This result qualitatively aligns with findings from studies on the RNR of bosonic systems near finite-temperature transition points [38, 39, 100, 101], in that singular behaviors for both bosons and fermions are observed at rT_c . However, the quantitative behavior of the singularity differs significantly. In the 2D transverse field Ising model, which features a finite-temperature transition also belonging to the 2D Ising universality class, the RNR monotonically decreases, and the singularity was identified in its temperature derivative [38, 101]. In contrast, in the present fermionic case, the singularity of untwisted RNR is clearly observed directly, without the need for a derivative. Furthermore, perhaps the most intriguing observation in Fig. 8(c) is that the rank-4 twisted RNR \tilde{R}_4 more closely resembles the bosonic case: it monotonically decreases and obeys the area-law within error bars [38, 39].

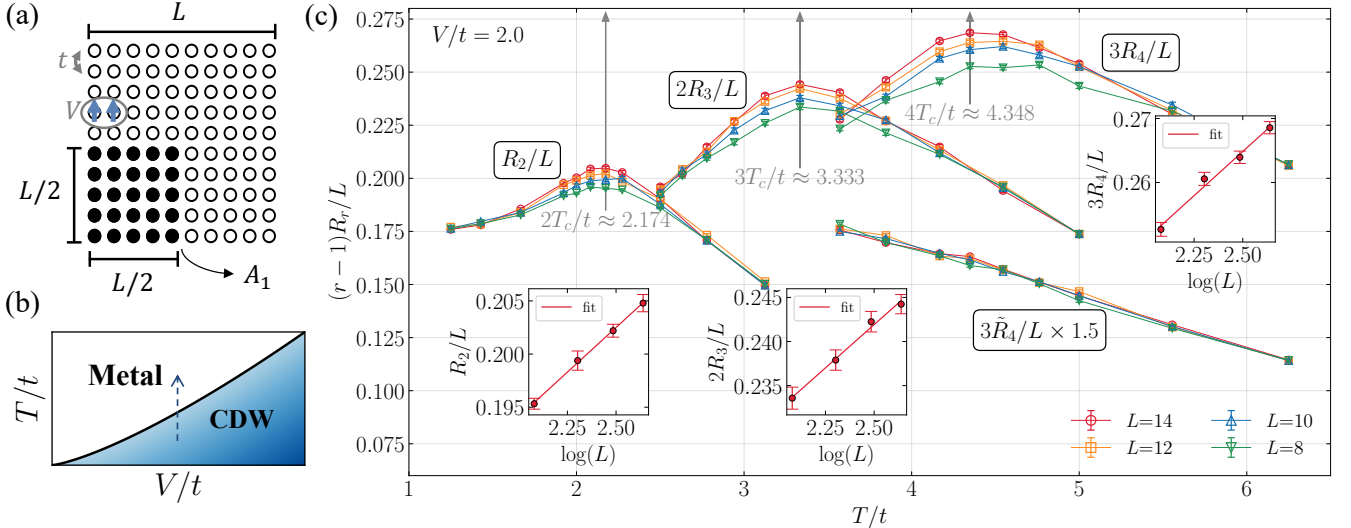


FIG. 8. The behavior of different RNRs across the finite-temperature transition point of the spinless t - V model. (a) Illustration of the spinless t - V model on a square lattice and our chosen bipartite geometry. The model includes hopping and interaction terms between nearest neighboring sites. We select the subsystem A_1 as the lower-left corner of the lattice, with a boundary length L shared with A_2 . (b) Illustration of the phase diagram for the t - V model. The blue dashed arrow indicates our parameter path in (c). (c) The temperature dependence of the area-law coefficients for rank-2, 3, and 4 untwisted RNRs, as well as the rank-4 twisted RNR, is illustrated. To facilitate a direct comparison of values across different ranks and enhance the clarity of the plot, we present $(r-1)R_r = -\ln\{\text{Tr}[(\rho^{T_2^f})^r]/\text{Tr}[\rho^r]\}$ instead. Additionally, the twisted RNR is scaled by a factor of 1.6 for improved visualization. The gray arrows indicate the finite-temperature transition points identified by the untwisted RNRs at various ranks, with insets displaying the finite-size scaling of their respective area-law coefficients.

TABLE II. Comparison between untwisted and twisted rank- r RNRs as Rényi proxies for LN. The second row summarizes temperature dependence in the Hubbard chain [see Fig. 7]. Subsequent rows labeled “spinless t - V model” summarize behaviors across the finite-temperature transition in the 2D Ising universality class at T_c [see Fig. 8]. The symbols \uparrow and \downarrow indicate that the RNR monotonically increases and decreases, respectively, with increasing temperature.

Scope	Untwisted RNR		Twisted RNR
Relation to LN by definition	Do not relate to LN explicitly		Analytically continued to LN: $\mathcal{E} = \lim_{r \rightarrow 1/2} (1-2r)\mathcal{E}_{2r}$
Hubbard chain	Variation as T	$r = 2: \downarrow$ $r = 3, 4: \text{non-monotonic}$	$r = 4: \downarrow$
Spinless t - V model	Variation as T across T_c Finite-size scaling across T_c	$\uparrow \rightarrow \text{Maximum at } rT_c \rightarrow \downarrow$ area-law \rightarrow beyond-area-law \rightarrow area-law	\downarrow area-law

C. Discussion on Rényi proxy

The above findings offer insights into the nature of untwisted and twisted RNRs, neither of which has been rigorously established as an entanglement measure. Table II summarizes the key differences in definition and temperature dependence between untwisted and twisted RNRs. The primary concern with untwisted RNR stems from the non-Hermitian nature of the untwisted PTDM $\rho^{T_2^f}$, whose moments lack a clear connection to the LN. In contrast, the twisted RNR is arguably more physically meaningful, as the twisted PTDM $\rho^{\tilde{T}_2^f}$ is Hermitian, and even-rank twisted RNs can be analytically continued to the LN (see the discussion below Eq. (27)).

The bosonic RNR, defined using the conventional partial transpose [34, 37, 38], shares this analytical continuation feature with twisted RNR, and their behaviors across the 2D Ising transition are indeed consistent. Moreover, the rank-3 and -4 untwisted RNRs in the Hubbard chain exhibit unphysical temperature dependence. Collectively, both definitional considerations and numerical evidence support the view that twisted RNR serves as a more appropriate Rényi proxy for LN, analogous to how REE relates to EE.

VII. CONCLUSIONS AND OUTLOOK

In summary, to facilitate the calculation of high-rank RNs in interacting fermionic systems using DQMC, we have (i) identified stable formulas for calculating high-rank Grover determinants and (ii) developed stable update schemes for incremental algorithms for untwisted and twisted RNs of arbitrary rank. We applied these methods to study the Hubbard model and spinless t - V model, and presented the temperature-dependent behavior of high-rank RNRs, thereby expanding upon the previous results presented in Ref. [51]. We found that high-rank RNRs, whether untwisted or twisted, can exhibit significantly different behavior compared to the rank-2 untwisted RNR [51]. Specifically, rank-3 and -4 untwisted RNRs fail to accurately represent the quantum-classical crossover in the Hubbard chain. Furthermore, the rank-4 twisted RNR displays behavior distinct from untwisted RNRs in the spinless t - V model, with the former adhering to the area law while the latter exhibits beyond-area-law scaling around the critical points. These results illuminate the nature of untwisted and twisted RNRs. Due to drawbacks in its definition, the untwisted RNR exhibits unusual non-monotonic behaviors in certain cases, whereas the twisted RNR may serve as a more suitable Rényi proxy for LN.

Several potential avenues exist for future research. First and foremost, the nature of untwisted and twisted RNRs remains to be fully elucidated. Although lacking a clear connection to the LN, the untwisted RNR also captures the singularity at the critical point and displays intriguing beyond-area-law behavior in its vicinity. A theoretical investigation of the rank-2 untwisted RN, $\mathcal{E}_2 = -\ln \text{Tr}[\rho X_2 \rho X_2]$, may provide a productive starting point. Secondly, more case studies are needed to examine whether the twisted RNR faithfully captures mixed-state

entanglement. Our stable formulas for Grover determinants (e.g., Eqs. (37) and (38)) enable calculation of high-rank RNs for 1D interacting fermionic models across various bipartitions using direct sampling DQMC, thereby facilitating examination of theoretical predictions. For instance, one could compare the scaling of twisted RN with L_{A_1} for the Hubbard chain at finite temperature against conformal field theory predictions [48]. Additionally, our stable incremental algorithms enable investigation of high-temperature behavior of high-rank RN(R)s in 2D interacting fermionic models, provided they remain free from the sign problem. Finally, to extend these calculations to lower temperatures, a valuable technical advancement would be the development of an incremental algorithm, based on Drut's formula for high-rank Grover determinants, that completely avoids inverting the Green's function matrix, thereby enhancing computational stability. Complementary to this, examining the validity of Green's function regularization within the incremental algorithm, particularly the systematic error it introduces, would offer another promising direction for low-temperature investigations.

ACKNOWLEDGMENTS

This work was supported by the National Key R&D Program of China (Grant No. 2022YFA1402702, No. 2021YFA1401400), the National Natural Science Foundation of China (Grants No. 12447103, No. 12274289), the Innovation Program for Quantum Science and Technology (under Grant No. 2021ZD0301902), Yangyang Development Fund, and startup funds from SJTU. F.-H. W. is supported by T.D. Lee scholarship. The computations in this paper were run on the Siyuan-1 and π 2.0 clusters supported by the Center for High Performance Computing at Shanghai Jiao Tong University.

[1] G. Vidal, J. I. Latorre, E. Rico, and A. Kitaev, Entanglement in quantum critical phenomena, *Physical Review Letters* **90**, 227902 (2003).

[2] L. Amico, R. Fazio, A. Osterloh, and V. Vedral, Entanglement in many-body systems, *Reviews of Modern Physics* **80**, 517 (2008).

[3] N. Laflorencie, Quantum entanglement in condensed matter systems, *Physics Reports* **646**, 1 (2016).

[4] M. B. Plenio and S. Virmani, An introduction to entanglement measures, *Quantum Information & Computation* **7**, 1 (2007).

[5] R. Horodecki, P. Horodecki, M. Horodecki, and K. Horodecki, Quantum entanglement, *Reviews of Modern Physics* **81**, 865 (2009).

[6] P. Calabrese and J. Cardy, Entanglement entropy and quantum field theory, *Journal of Statistical Mechanics: Theory and Experiment* **2004**, P06002 (2004).

[7] D. Gioev and I. Klich, Entanglement entropy of fermions in any dimension and the Widom conjecture, *Physical Review Letters* **96**, 100503 (2006).

[8] A. Kitaev and J. Preskill, Topological entanglement entropy, *Physical Review Letters* **96**, 110404 (2006).

[9] M. Levin and X.-G. Wen, Detecting topological order in a ground state wave function, *Physical Review Letters* **96**, 110405 (2006).

[10] E. Fradkin and J. E. Moore, Entanglement entropy of 2D conformal quantum critical points: Hearing the shape of a quantum drum, *Physical Review Letters* **97**, 050404 (2006).

[11] M. M. Wolf, F. Verstraete, M. B. Hastings, and J. I. Cirac, Area laws in quantum systems: Mutual information and correlations, *Physical Review Letters* **100**, 070502 (2008).

[12] P. Calabrese, J. Cardy, and B. Doyon, Entanglement entropy in extended quantum systems, *Journal of Physics A: Mathematical and Theoretical* **42**, 500301 (2009).

[13] M. B. Hastings, I. González, A. B. Kallin, and R. G. Melko, Measuring Rényi entanglement entropy in quantum Monte Carlo simulations, *Physical Review Letters* **104**, 157201 (2010).

[14] T. Grover, Entanglement of interacting fermions in quantum Monte Carlo calculations, *Physical Review Letters* **111**, 130402 (2013).

[15] M. A. Metlitski and T. Grover, Entanglement Entropy of Systems with Spontaneously Broken Continuous Symmetry (2015), arXiv:1112.5166 [cond-mat, physics:hep-th, physics:quant-ph].

[16] J. Zhao, Y.-C. Wang, Z. Yan, M. Cheng, and Z. Y. Meng, Scaling of entanglement entropy at deconfined quantum criticality, *Physical Review Letters* **128**, 010601 (2022).

[17] Y. D. Liao, G. Pan, W. Jiang, Y. Qi, and Z. Y. Meng, The teaching from entanglement: 2D SU(2) antiferromagnet to valence bond solid deconfined quantum critical points are not conformal (2023), arXiv:2302.11742 [cond-mat, physics:math-ph, physics:physics, physics:quant-ph].

[18] J. D'Emidio, R. Orús, N. Laflorencie, and F. De Juan, Universal features of entanglement entropy in the honeycomb Hubbard model, *Physical Review Letters* **132**, 076502 (2024).

[19] K. Życzkowski, P. Horodecki, A. Sanpera, and M. Lewenstein, Volume of the set of separable states, *Physical Review A* **58**, 883 (1998).

[20] J. Eisert and M. B. Plenio, A comparison of entanglement measures, *Journal of Modern Optics* **46**, 145 (1999).

[21] G. Vidal and R. F. Werner, Computable measure of entanglement, *Physical Review A* **65**, 032314 (2002).

[22] M. B. Plenio, Logarithmic negativity: A full entanglement monotone that is not convex, *Physical Review Letters* **95**, 090503 (2005).

[23] A. Peres, Separability criterion for density matrices, *Physical Review Letters* **77**, 1413 (1996).

[24] M. Horodecki, P. Horodecki, and R. Horodecki, Separability of mixed states: Necessary and sufficient conditions, *Physics Letters A* **223**, 1 (1996).

[25] H. Shapourian, K. Shiozaki, and S. Ryu, Partial time-reversal transformation and entanglement negativity in fermionic systems, *Physical Review B* **95**, 165101 (2017).

[26] K. Shiozaki, H. Shapourian, K. Gomi, and S. Ryu, Many-body topological invariants for fermionic short-range entangled topological phases protected by antiunitary symmetries, *Physical Review B* **98**, 035151 (2018).

[27] H. Shapourian and S. Ryu, Entanglement negativity of fermions: Monotonicity, separability criterion, and classification of few-mode states, *Physical Review A* **99**, 022310 (2019).

[28] H. Shapourian, P. Ruggiero, S. Ryu, and P. Calabrese, Twisted and untwisted negativity spectrum of free fermions, *SciPost Physics* **7**, 037 (2019).

[29] P. Calabrese, L. Tagliacozzo, and E. Tonni, Entanglement negativity in the critical Ising chain, *Journal of Statistical Mechanics: Theory and Experiment* **2013**, P05002 (2013).

[30] P. Ruggiero, V. Alba, and P. Calabrese, Entanglement negativity in random spin chains, *Physical Review B* **94**, 035152 (2016).

[31] M. Gruber and V. Eisler, Time evolution of entanglement negativity across a defect, *Journal of Physics A: Mathematical and Theoretical* **53**, 205301 (2020).

[32] H. Wichterich, J. Molina-Vilaplana, and S. Bose, Scaling of entanglement between separated blocks in spin chains at criticality, *Physical Review A* **80**, 010304 (2009).

[33] E. Wybo, M. Knap, and F. Pollmann, Entanglement dynamics of a many-body localized system coupled to a bath, *Physical Review B* **102**, 064304 (2020).

[34] P. Calabrese, J. Cardy, and E. Tonni, Entanglement negativity in quantum field theory, *Physical Review Letters* **109**, 130502 (2012).

[35] P. Calabrese, J. Cardy, and E. Tonni, Entanglement negativity in extended systems: A field theoretical approach, *Journal of Statistical Mechanics: Theory and Experiment* **2013**, P02008 (2013).

[36] V. Alba, Entanglement negativity and conformal field theory: A Monte Carlo study, *Journal of Statistical Mechanics: Theory and Experiment* **2013**, P05013 (2013).

[37] C.-M. Chung, V. Alba, L. Bonnes, P. Chen, and A. M. Läuchli, Entanglement negativity via the replica trick: A quantum Monte Carlo approach, *Physical Review B* **90**, 064401 (2014).

[38] K.-H. Wu, T.-C. Lu, C.-M. Chung, Y.-J. Kao, and T. Grover, Entanglement Renyi negativity across a finite temperature transition: A Monte Carlo study, *Physical Review Letters* **125**, 140603 (2020).

[39] Y.-M. Ding, Y. Tang, Z. Wang, Z. Wang, B.-B. Mao, and Z. Yan, Tracking the variation of entanglement Rényi negativity: A quantum Monte Carlo study, *Physical Review B* **111**, L241108 (2025), arXiv:2409.10273 [cond-mat, physics:quant-ph].

[40] J. Gray, L. Banchi, A. Bayat, and S. Bose, Machine-Learning-Assisted Many-Body Entanglement Measurement, *Physical Review Letters* **121**, 150503 (2018).

[41] E. Cornfeld, E. Sela, and M. Goldstein, Measuring fermionic entanglement: Entropy, negativity, and spin structure, *Physical Review A* **99**, 062309 (2019).

[42] A. Elben, R. Kueng, H.-Y. R. Huang, R. van Bijnen, C. Kokail, M. Dalmonte, P. Calabrese, B. Kraus, J. Preskill, P. Zoller, and B. Vermersch, Mixed-State Entanglement from Local Randomized Measurements, *Physical Review Letters* **125**, 200501 (2020).

[43] A. Neven, J. Carrasco, V. Vitale, C. Kokail, A. Elben, M. Dalmonte, P. Calabrese, P. Zoller, B. Vermersch, R. Kueng, and B. Kraus, Symmetry-resolved entanglement detection using partial transpose moments, *npj Quantum Information* **7**, 1 (2021).

[44] A. Coser, E. Tonni, and P. Calabrese, Entanglement negativity after a global quantum quench, *Journal of Statistical Mechanics: Theory and Experiment* **2014**, P12017 (2014).

[45] S. Murciano, V. Alba, and P. Calabrese, Quench Dynamics of Rényi Negativities and the Quasiparticle Picture, in *Entanglement in Spin Chains: From Theory to Quantum Technology Applications*, edited by A. Bayat, S. Bose, and H. Johannesson (Springer International Publishing, Cham, 2022) pp. 397–424.

[46] G. Perez and W. Witczak-Krempa, Entanglement negativity between separated regions in quantum critical systems, *Phys. Rev. Res.* **6**, 023125 (2024), arXiv:2310.15273 [cond-mat.str-el].

[47] T.-T. Wang, M. Song, L. Lyu, W. Witczak-Krempa, and Z. Y. Meng, Entanglement microscopy and tomography in many-body systems, *Nature Communications* **16**, 96 (2025).

[48] H. Shapourian and S. Ryu, Finite-temperature entan-

lement negativity of free fermions, *Journal of Statistical Mechanics: Theory and Experiment* **2019**, 043106 (2019).

[49] V. Alba and F. Carollo, Logarithmic negativity in out-of-equilibrium open free-fermion chains: An exactly solvable case, *SciPost Physics* **15**, 124 (2023), arXiv:2205.02139 [cond-mat, physics:hep-th, physics:quant-ph].

[50] W. Choi, M. Knap, and F. Pollmann, Finite-temperature entanglement negativity of fermionic symmetry-protected topological phases and quantum critical points in one dimension, *Physical Review B* **109**, 115132 (2024).

[51] F.-H. Wang and X. Y. Xu, Entanglement Rényi negativity of interacting fermions from quantum Monte Carlo simulations, *Nature Communications* **16**, 2637 (2025), arXiv:2312.14155.

[52] J. D’Emidio, Entanglement Entropy from Nonequilibrium Work, *Physical Review Letters* **124**, 110602 (2020).

[53] J. Zhao, B.-B. Chen, Y.-C. Wang, Z. Yan, M. Cheng, and Z. Y. Meng, Measuring Rényi entanglement entropy with high efficiency and precision in quantum Monte Carlo simulations, *npj Quantum Materials* **7**, 69 (2022).

[54] G. Pan, Y. Da Liao, W. Jiang, J. D’Emidio, Y. Qi, and Z. Y. Meng, Stable computation of entanglement entropy for 2D interacting fermion systems, *Physical Review B* **108**, L081123 (2023).

[55] X. Zhang, G. Pan, B.-B. Chen, K. Sun, and Z. Y. Meng, Integral algorithm of exponential observables for interacting fermions in quantum Monte Carlo simulations, *Physical Review B* **109**, 205147 (2024), arXiv:2311.03448 [cond-mat, physics:quant-ph].

[56] R. M. Neal, Annealed importance sampling, *Statistics and Computing* **11**, 125 (2001).

[57] L. Pollet, C. Kollath, K. Van Houcke, and M. Troyer, Temperature changes when adiabatically ramping up an optical lattice, *New Journal of Physics* **10**, 065001 (2008).

[58] V. Alba, Out-of-equilibrium protocol for Rényi entropies via the Jarzynski equality, *Physical Review E* **95**, 062132 (2017).

[59] A. Bulgarelli and M. Panero, Entanglement entropy from non-equilibrium Monte Carlo simulations, *JHEP* **06**, 030.

[60] Z. Dai and X. Y. Xu, Residual entropy from the temperature incremental Monte Carlo method, *Physical Review B* **111**, L081108 (2025), arXiv:2402.17827 [cond-mat].

[61] Y.-M. Ding, J.-S. Sun, N. Ma, G. Pan, C. Cheng, and Z. Yan, Reweighting-annealing method for evaluating the partition function via quantum Monte Carlo calculations, *Physical Review B* **110**, 165152 (2024), arXiv:2403.08642 [cond-mat, physics:quant-ph].

[62] S. R. P. G. Ripka, J.-P. Blaizot, and G. Ripka, *Quantum Theory of Finite Systems* (MIT Press, 1986).

[63] P. S. de Torres-Solanot, *A Time-Dependent Gaussian Variational Description of Lattice Gauge Theories*, Master’s thesis (2017).

[64] G. C. Wick, A. S. Wightman, and E. P. Wigner, The Intrinsic Parity of Elementary Particles, *Physical Review* **88**, 101 (1952).

[65] Y. Aharonov and L. Susskind, Charge Superselection Rule, *Physical Review* **155**, 1428 (1967).

[66] C. V. Kraus, *A Quantum Information Perspective of Fermionic Quantum Many-Body Systems*, Ph.D. thesis (2009).

[67] I. Klich, A note on the full counting statistics of paired fermions, *Journal of Statistical Mechanics: Theory and Experiment* **2014**, P11006 (2014).

[68] P.-Y. Chang and X. Wen, Entanglement negativity in free-fermion systems: An overlap matrix approach, *Physical Review B* **93**, 195140 (2016).

[69] J. Q. Fang and X. Y. Xu, Fermionic Partial Transpose in the Overlap Matrix Framework for Entanglement Negativity (2025), arXiv:2503.07742 [quant-ph].

[70] S. Bravyi, Lagrangian representation for fermionic linear optics, *Quant. Inf. Comput.* **5**, 216 (2005).

[71] S. Bravyi, Classical capacity of fermionic product channels (2005), arXiv:quant-ph/0507282.

[72] M. Fagotti and P. Calabrese, Entanglement entropy of two disjoint blocks in XY chains, *Journal of Statistical Mechanics: Theory and Experiment* **2010**, P04016 (2010).

[73] I. Peschel, Calculation of reduced density matrices from correlation functions, *Journal of Physics A: Mathematical and General* **36**, L205 (2003).

[74] S.-A. Cheong and C. L. Henley, Many-body density matrices for free fermions, *Physical Review B* **69**, 075111 (2004).

[75] I. Peschel and V. Eisler, Reduced density matrices and entanglement entropy in free lattice models, *Journal of Physics A: Mathematical and Theoretical* **42**, 504003 (2009).

[76] V. Eisler and Z. Zimborás, On the partial transpose of fermionic Gaussian states, *New Journal of Physics* **17**, 053048 (2015).

[77] Z.-X. Li, Y.-F. Jiang, and H. Yao, Solving the fermion sign problem in quantum Monte Carlo simulations by Majorana representation, *Physical Review B* **91**, 241117 (2015).

[78] Z.-Y. Han, Z.-Q. Wan, and H. Yao, Pfaffian quantum Monte Carlo: Solution to Majorana sign ambiguity and applications (2024), arXiv:2408.10311 [cond-mat, physics:physics, physics:quant-ph].

[79] R. Blankenbecler, D. J. Scalapino, and R. L. Sugar, Monte Carlo calculations of coupled boson-fermion systems. I, *Physical Review D* **24**, 2278 (1981).

[80] D. J. Scalapino and R. L. Sugar, Monte Carlo calculations of coupled boson-fermion systems. II, *Physical Review B* **24**, 4295 (1981).

[81] J. E. Hirsch, Two-dimensional Hubbard model: Numerical simulation study, *Physical Review B* **31**, 4403 (1985).

[82] F. Assaad and H. Evertz, World-line and Determinantal Quantum Monte Carlo Methods for Spins, Phonons and Electrons, in *Computational Many-Particle Physics*, Lecture Notes in Physics, edited by H. Fehske, R. Schneider, and A. Weiße (Springer, Berlin, Heidelberg, 2008) pp. 277–356.

[83] E. Y. Loh, J. E. Gubernatis, R. T. Scalettar, R. L. Sugar, and S. R. White, Stable Matrix-Multiplication Algorithms for Low-Temperature Numerical Simulations of Fermions, in *Interacting Electrons in Reduced Dimensions*, edited by D. Baeriswyl and D. K. Campbell (Springer US, Boston, MA, 1989) pp. 55–60.

[84] C. Bauer, Fast and stable determinant quantum Monte Carlo, *SciPost Physics Core* **2**, 011 (2020).

[85] F. F. Assaad, T. C. Lang, and F. Parisen Toldin, Entanglement spectra of interacting fermions in quantum Monte Carlo simulations, *Physical Review B* **89**, 125121 (2014).

[86] G. Sugiyama and S. E. Koonin, Auxiliary field Monte-Carlo for quantum many-body ground states, *Annals of Physics* **168**, 1 (1986).

[87] S. Sorella, S. Baroni, R. Car, and M. Parrinello, A novel technique for the simulation of interacting fermion systems, *Europhysics Letters (EPL)* **8**, 663 (1989).

[88] S. Sorella, A. Parola, M. Parrinello, and E. Tosatti, NUMERICAL STUDY OF THE 2D HUBBARD MODEL AT HALF FILLING, *International Journal of Modern Physics B* **3**, 1875 (1989).

[89] J. E. Drut and W. J. Porter, Entanglement, noise, and the cumulant expansion, *Physical Review E* **93**, 043301 (2016).

[90] Y. D. Liao, Universal term of entanglement entropy in the π -flux Hubbard model, *npj Quantum Information* **11**, 64 (2025), arXiv:2307.10602 [cond-mat].

[91] H. Shi and S. Zhang, Infinite variance in fermion quantum Monte Carlo calculations, *Physical Review E* **93**, 033303 (2016).

[92] D. J. Scalapino, R. L. Sugar, and W. D. Toussaint, Monte Carlo study of a two-dimensional spin-polarized fermion lattice gas, *Physical Review B* **29**, 5253 (1984).

[93] J. E. Gubernatis, D. J. Scalapino, R. L. Sugar, and W. D. Toussaint, Two-dimensional spin-polarized fermion lattice gases, *Physical Review B* **32**, 103 (1985).

[94] L. Wang and M. Troyer, Renyi entanglement entropy of interacting fermions calculated using the continuous-time quantum Monte Carlo method, *Physical Review Letters* **113**, 110401 (2014).

[95] E. F. Huffman and S. Chandrasekharan, Solution to sign problems in half-filled spin-polarized electronic systems, *Physical Review B* **89**, 111101 (2014).

[96] L. Wang, Y.-H. Liu, M. Iazzi, M. Troyer, and G. Harcos, Split orthogonal group: A guiding principle for sign-problem-free fermionic simulations, *Physical Review Letters* **115**, 250601 (2015).

[97] Z. C. Wei, C. Wu, Y. Li, S. Zhang, and T. Xiang, Majorana positivity and the fermion sign problem of quantum Monte Carlo simulations, *Physical Review Letters* **116**, 250601 (2016).

[98] Z.-X. Li, Y.-F. Jiang, and H. Yao, Majorana-time-reversal symmetries: A fundamental principle for sign-problem-free quantum Monte Carlo simulations, *Physical Review Letters* **117**, 267002 (2016).

[99] S. Hesselmann and S. Wessel, Thermal Ising transitions in the vicinity of two-dimensional quantum critical points, *Physical Review B* **93**, 155157 (2016).

[100] T.-C. Lu and T. Grover, Singularity in entanglement negativity across finite-temperature phase transitions, *Physical Review B* **99**, 075157 (2019).

[101] T.-C. Lu and T. Grover, Structure of quantum entanglement at a finite temperature critical point, *Physical Review Research* **2**, 043345 (2020).

[102] R. A. Horn and C. R. Johnson, *Matrix Analysis* (Cambridge University Press, Cambridge, 1985).

Appendix A: Proof of the trace properties of the partially transposed density matrices

Consider the r -moment of the twisted PTDM $\rho^{\tilde{T}_2^f}$:

$$\begin{aligned}
 \text{Tr} \left[\left(\rho^{\tilde{T}_2^f} \right)^r \right] &= \text{Tr} \left[\rho^{\tilde{T}_2^f} X_2 \right] \\
 &= \sum_{n^1, \bar{n}^1, n^2, \bar{n}^2, \dots, n^r, \bar{n}^r} \langle n^1 | \rho | \bar{n}^1 \rangle \cdots \langle n^r | \rho | \bar{n}^r \rangle (-1)^{\phi(n^1, \bar{n}^1)} \cdots (-1)^{\phi(n^r, \bar{n}^r)} \\
 &\quad \times \sum_{n^0} \langle n^0 | n_{A_1}^1, \bar{n}_{A_2}^1 \rangle \langle \bar{n}_{A_1}^1, n_{A_2}^1 | X_2 | n_{A_1}^2, \bar{n}_{A_2}^2 \rangle \langle \bar{n}_{A_1}^2, n_{A_2}^2 | X_2 \cdots X_2 | n_{A_1}^r, \bar{n}_{A_2}^r \rangle \langle \bar{n}_{A_1}^r, n_{A_2}^r | X_2 | n^0 \rangle \\
 &= \sum_{n^1, n^2, \dots, n^r} \langle n^1 | \rho | n_{A_1}^2, n_{A_2}^r \rangle \langle n^2 | \rho | n_{A_1}^3, n_{A_2}^1 \rangle \cdots \langle n^r | \rho | n_{A_1}^1, n_{A_2}^{r-1} \rangle \\
 &\quad \times (-1)^{\phi(n^1, \{n_{A_1}^2, n_{A_2}^r\})} (-1)^{\phi(n^2, \{n_{A_1}^3, n_{A_2}^1\})} \cdots (-1)^{\phi(n^r, \{n_{A_1}^1, n_{A_2}^{r-1}\})} \\
 &\quad \times (-1)^{\tau_{A_2}^r} (-1)^{\tau_{A_2}^1} \cdots (-1)^{\tau_{A_2}^{r-1}}. \tag{A1}
 \end{aligned}$$

As for the untwisted moment, simply delete the X_2 phase strings in the last line of the above equation. After doing a change of variables, $n_{A_2}^{(i-1) \bmod r} \rightarrow n_{A_2}^{(i+1) \bmod r}$, we arrive at the desired results in Eq. (5) and Eq. (7).

When ρ has a well-defined parity (denoted as P_ρ), i.e., $[\rho, \hat{P}] = 0$ with $\hat{P} = (-1)^{\sum_j c_j^\dagger c_j}$ the fermionic parity operator, there are additional constraints on the summation over dummy indices $\{n^1, n^2, \dots, n^r\}$. From the sandwich chain in the second line of Eq. (5) or (7), we deduce that, in order to have non-vanishing contribution,

$\forall i \in \{1, 2, \dots, r\}$, (i) each of n^i must be of parity P_ρ ; (ii) each of $\tilde{n}^i = n_{A_1}^i \cup n_{A_2}^{i+2}$ must also be of parity P_ρ . Formulate these constraints we obtain,

$$\begin{aligned}
 P_\rho &= (-1)^{\tau^1} = (-1)^{\tau^2} = \cdots = (-1)^{\tau^r} \\
 &= (-1)^{\tau_1^1 + \tau_2^3} = (-1)^{\tau_1^2 + \tau_2^4} = \cdots = (-1)^{\tau_1^r + \tau_2^2}. \tag{A2}
 \end{aligned}$$

Thus we further obtain the constraints on the parity of subsystems, $(-1)^{\tau_b^i} = (-1)^{\tau_b^{(i+2) \bmod r}}$ for any $b \in \{1, 2\}$ and $i \in \{1, 2, \dots, r\}$. For even-rank moments, the

dummy bit strings are naturally split into two groups, $\{n^{2\mathbb{Z}-1}\}$ and $\{n^{2\mathbb{Z}}\}$, each of which is of homogeneous subsystem parity. For odd-rank moments, all the dummy bit strings should have the same subsystem parity.

$$\text{even } k \quad \begin{cases} (-1)^{\tau_b^1} = (-1)^{\tau_b^3} = \cdots (-1)^{\tau_b^{r-1}} \\ (-1)^{\tau_b^2} = (-1)^{\tau_b^4} = \cdots (-1)^{\tau_b^r} \end{cases}, \quad (\text{A3a})$$

$$\text{odd } k \quad (-1)^{\tau_b^1} = (-1)^{\tau_b^2} = \cdots (-1)^{\tau_b^r}, b = 1, 2. \quad (\text{A3b})$$

Specifically, if ρ is even (odd), $P_\rho = 1(-1)$, then the parity of A_1 is equal (opposite) to the parity of A_2 within each group. Now we can prove the Eq. (8). Consider a slightly more general case of rank- $2\mathbb{Z}$ moments, we subtract the untwisted moment from the twisted moment,

$$\begin{aligned} & \text{Tr} \left[\left(\rho^{\tilde{T}_2^f} \right)^{2m} \right] - \text{Tr} \left[\left(\rho^{T_2^f} \right)^{2m} \right] \\ &= \sum_{n^1, \dots, n^{2m}} \langle \langle n_1^1, n_2^3 | \rho | n^2 \rangle \langle n_1^2, n_2^4 | \rho | n^3 \rangle \cdots \langle n_1^{2m}, n_2^2 | \rho | n^1 \rangle \rangle \\ & \times (-1)^{\sum_{i=1}^{2m} \phi(n^i, n^{(i+1) \bmod 2m})} \left[(-1)^{\sum_{j=1}^m \tau_2^{2j-1} + \sum_{j=1}^m \tau_2^{2j}} - 1 \right]. \end{aligned} \quad (\text{A4})$$

Here we abbreviate the subscripts of dummy bit strings, $n_b^i \equiv n_{A_b}^i$. When the total parities of the two groups (see Eq. (A3a)) are the same, then $(-1)^{\sum_j \tau_2^j} = 1$, so these kind of terms are canceled out. We may resort to the terms with even (odd) $\sum_{j=1}^m \tau_2^{2j-1}$ and odd (even) $\sum_{j=1}^m \tau_2^{2j}$. However, these terms are forbidden by the parity constraints in Eq. (A3a) when m is even. Thus we have proved the Eq. (8). Furthermore, the phase chain in the third line of Eq. (5)

$$\begin{aligned} & (-1)^{\phi(n^1, n^2)} (-1)^{\phi(n^2, n^3)} \cdots (-1)^{\phi(n^i, n^{i+1})} \cdots (-1)^{\phi(n^r, n^1)} \\ &= (-1)^{\frac{[(\tau_2^1 + \tau_2^2) \bmod 2]}{2} + \frac{[(\tau_2^2 + \tau_2^3) \bmod 2]}{2} + \cdots + \frac{[(\tau_2^r + \tau_2^1) \bmod 2]}{2}} \\ & \times (-1)^{(\tau_1^1 + \tau_1^2)(\tau_2^1 + \tau_2^2) + (\tau_1^2 + \tau_1^3)(\tau_2^2 + \tau_2^3) + \cdots + (\tau_1^r + \tau_1^1)(\tau_2^r + \tau_2^1)} \end{aligned} \quad (\text{A5})$$

can be simplified since the second line of the above equation is always unity. Indeed, when $P_\rho = 1$, τ_1^i and τ_2^i have the same parity, thus $(-1)^{\sum_i (\tau_1^i + \tau_1^{i+1})(\tau_2^i + \tau_2^{i+1})} = (-1)^{\sum_i (\tau_1^i + \tau_1^{i+1})^2} = 1$. When $P_\rho = -1$, τ_1^i and τ_2^i have opposite parities, thus $(-1)^{\sum_i (\tau_1^i + \tau_1^{i+1})(\tau_2^i + \tau_2^{i+1})} = (-1)^{\sum_i (\tau_1^i + \tau_1^{i+1})(\tau_1^{i+1} + \tau_1^{i+2})} = 1$. So we finally obtain the Eq. (9) since $(-1)^{[(\tau + \tau') \bmod 2]/2} = (-1)^{(\tau + \tau')^2/2}$.

Appendix B: Proof of Eq. (11) using the product form of Gaussian states

For physical Gaussian states of the form in Eq. (10) with Hermitian W , there exists a canonical transformation to bring ρ_0 into the product form (or standard

form) [70, 71], given by

$$\begin{aligned} \rho_0 &= \frac{1}{Z} \exp \left(\sum_j \frac{w_j}{2} i \tilde{\gamma}_{2j-1} \tilde{\gamma}_{2j} \right) \\ &= \frac{1}{Z} \prod_j \left[\cosh \frac{w_j}{2} + \sinh \frac{w_j}{2} i \tilde{\gamma}_{2j-1} \tilde{\gamma}_{2j} \right] \\ &= \frac{1}{2^N} \prod_j [1 + i \lambda_j \tilde{\gamma}_{2j-1} \tilde{\gamma}_{2j}], \end{aligned} \quad (\text{B1})$$

where $\lambda_j = \tanh \frac{w_j}{2}$ with $\{\pm w_j\}$ the eigenvalues of the W matrix, and $\{\tilde{\gamma}_j\}$ is related to the original basis via $\tilde{\gamma} = O^T \gamma$ with O a $2N \times 2N$ real orthogonal matrix satisfying $OO^T = I$. Indeed, since a real antisymmetric matrix W_0 can always be transformed to its real canonical form via a real orthogonal transformation O ,

$$O^T W_0 O = \bigoplus_{i=1}^N \begin{pmatrix} 0 & w_i \\ -w_i & 0 \end{pmatrix}, \quad (\text{B2})$$

the product form in Eq. (B1) is always available for Hermitian $W = iW_0$, and each w_j is real and positive. Each block in Eq. (B2) can be written as $iw_i \sigma_y$ and be further diagonalized to obtain W_0 's eigenvalues $\{\pm iw_i\}$, thus $\{\pm w_i\}$ are the eigenvalues of W . To be more specific, let us denote the unitary matrix that diagonalizes the Pauli matrix $\sigma_y = \begin{pmatrix} 0 & -i \\ i & 0 \end{pmatrix}$ as $V_y \equiv \frac{1}{\sqrt{2}} \begin{pmatrix} -i & -i \\ 1 & -1 \end{pmatrix}$, then $V_y^\dagger \sigma_y V_y = \sigma_z$. Therefore, W can be diagonalized by

$$U_W^\dagger W U_W = - \bigoplus_{i=1}^N \begin{pmatrix} w_i & 0 \\ 0 & -w_i \end{pmatrix} \equiv -\Lambda, \quad (\text{B3})$$

where $U_W \equiv O U_y$ and $U_y \equiv \bigoplus_{i=1}^N V_y$. Next, it is easy to evaluate the covariance matrix Γ using the product form (B1) under the new basis $\tilde{\gamma}_k = \gamma_l O_{lk}$:

$$\begin{aligned} i\Gamma_{kl} &\equiv \frac{i}{2} \langle [\gamma_k, \gamma_l] \rangle = \frac{i}{2} \langle [O_{kk'} \tilde{\gamma}_{k'}, O_{ll'} \tilde{\gamma}_{l'}] \rangle \\ &= \sum_{k', l'=1}^{2N} O_{kk'} O_{ll'} \frac{i}{2} (\langle \tilde{\gamma}_{k'} \tilde{\gamma}_{l'} \rangle - \langle \tilde{\gamma}_{l'} \tilde{\gamma}_{k'} \rangle) \\ &= \sum_{i=1}^N (O_{k, 2i-1} O_{l, 2i} - O_{k, 2i} O_{l, 2i-1}) i \langle \tilde{\gamma}_{2i-1} \tilde{\gamma}_{2i} \rangle \\ &= \left(O \left[\bigoplus_{i=1}^N \begin{pmatrix} 0 & \tanh \left(\frac{w_i}{2} \right) \\ -\tanh \left(\frac{w_i}{2} \right) & 0 \end{pmatrix} \right] O^T \right)_{kl}. \end{aligned} \quad (\text{B4})$$

We note that only the diagonal correlations have non-zero values under $\tilde{\gamma}$ -basis, with $\langle i \tilde{\gamma}_{2i-1} \tilde{\gamma}_{2i} \rangle = 2 \langle \tilde{c}_i^\dagger \tilde{c}_i \rangle - 1 = \lambda_j$. Since $i\Gamma$ has similar real canonical form as W_0 , one finds

that Γ can also be diagonalized by U_W ,

$$\begin{aligned} U_W^\dagger \Gamma U_W &= (-i) U_y^\dagger \left[\bigoplus_{i=1}^N \begin{pmatrix} 0 & \tanh \frac{w_i}{2} \\ -\tanh \frac{w_i}{2} & 0 \end{pmatrix} \right] U_y \\ &= \bigoplus_{i=1}^N \begin{pmatrix} \tanh \frac{w_i}{2} & \\ & -\tanh \frac{w_i}{2} \end{pmatrix} = \tanh \frac{\Lambda}{2}. \end{aligned} \quad (\text{B5})$$

Combine Eq. (B3) and Eq. (B5), we obtain the relation in Eq. (11). From this relation, one finds that the $\{\pm \lambda_j\}$ appeared in the product form (B1) of Gaussian states are the eigenvalues of the covariance matrix.

The essence of the above proof lies in Eq. (B2) where one finds a real orthogonal basis transformation, which is a canonical transformation preserving the anti-commutation relation between Majorana operators, $\{\gamma_i, \gamma_j\} = 2\delta_{ij}$, and the self-adjoint property of Majorana fermions, $\gamma_i^\dagger = \gamma_i$ [62, 67]. This proof procedure can be straightforwardly generalized to some special non-Hermitian W . It is easy to realize that all $W = cW_0$ with c an arbitrary complex number can be proved by the same procedure, but with complex w_j . In fact, for any complex and normal antisymmetric W satisfying $WW^\dagger = W^\dagger W$ (which includes $W = cW_0$), since its real and imaginary parts can be separately transformed to the real canonical form using the same O [102], the product form is available but with complex w_j .

For a generic non-Hermitian W , the real orthogonal transformation O and thus the product form (B1) are not always available. However, the antisymmetric property of W still provides us with some mathematically similar results. In particular, it turns out that Eq. (11) holds for arbitrary diagonalizable W [72]. Below, we outline a brief review of the proof. First of all, we note that the eigenvalues of any $2N \times 2N$ antisymmetric matrix W are in pairs of $\pm w_j$ where $j = 1, 2, \dots, N$. Denote the corresponding eigenvector to eigenvalue w as \vec{v}_w and for simplicity assume that W 's spectrum is non-degenerate⁷, there is an “orthogonal relation” between the eigenvectors, $\vec{v}_w \cdot \vec{v}_{w'} = \delta_{w+w'} \vec{v}_w \cdot \vec{v}_{-w}$. Both W and functions of W can be decomposed using W 's eigenvectors:

$$W = \sum_{j=1}^N w_j \frac{\vec{v}_{w_j} \otimes \vec{v}_{-w_j} - \vec{v}_{-w_j} \otimes \vec{v}_{w_j}}{\vec{v}_{w_j} \cdot \vec{v}_{-w_j}}, \quad (\text{B6})$$

$$f(W) = \sum_{j=1}^N \frac{f(w_j) \vec{v}_{w_j} \otimes \vec{v}_{-w_j} + f(-w_j) \vec{v}_{-w_j} \otimes \vec{v}_{w_j}}{\vec{v}_{w_j} \cdot \vec{v}_{-w_j}}. \quad (\text{B7})$$

Here, we assume the condition $\vec{v}_w \cdot \vec{v}_{-w} \neq 0$. Putting Eq. (B6) into Eq. (10), we get a similar “product form”

for Gaussian states with generic W :

$$\begin{aligned} \rho_0 &= \frac{1}{Z} \exp \left(\sum_j \frac{w_j}{2} \frac{[\vec{v}_{w_j} \cdot \gamma, \vec{v}_{-w_j} \cdot \gamma]}{2\vec{v}_{w_j} \cdot \vec{v}_{-w_j}} \right) \\ &= \frac{1}{Z} \prod_j \left[\cosh \left(\frac{w_j}{2} \right) + \sinh \left(\frac{w_j}{2} \right) \frac{[\vec{v}_{w_j} \cdot \gamma, \vec{v}_{-w_j} \cdot \gamma]}{2\vec{v}_{w_j} \cdot \vec{v}_{-w_j}} \right] \\ &= \frac{1}{2^N} \prod_j \left[1 + \tanh \left(\frac{w_j}{2} \right) \frac{[\vec{v}_{w_j} \cdot \gamma, \vec{v}_{-w_j} \cdot \gamma]}{2\vec{v}_{w_j} \cdot \vec{v}_{-w_j}} \right]. \end{aligned} \quad (\text{B8})$$

We note that the operator $[\vec{v}_{w_j} \cdot \gamma, \vec{v}_{-w_j} \cdot \gamma] / 2\vec{v}_{w_j} \cdot \vec{v}_{-w_j}$ behaves very similarly to the $i\tilde{\gamma}_{2i-1}\tilde{\gamma}_{2i}$ in Eq. (B1). Firstly, $[\vec{v}_{w_j} \cdot \gamma, \vec{v}_{-w_j} \cdot \gamma]$ with different j commutes with each other. Secondly, it satisfies $[\vec{v}_{w_j} \cdot \gamma, \vec{v}_{-w_j} \cdot \gamma]^2 = 4(\vec{v}_{w_j} \cdot \vec{v}_{-w_j})^2$. The covariance matrix Γ can be evaluated as follows,

$$\begin{aligned} \Gamma_{kl} &= \frac{1}{Z} \text{Tr} \left[\frac{[\gamma_k, \gamma_l]}{2} \exp \left(\frac{\gamma^T W \gamma}{4} \right) \right] \\ &= \frac{1}{2^N} \sum_j \tanh \left(\frac{w_j}{2} \right) \text{Tr} \left[\frac{[\gamma_k, \gamma_l]}{2} \frac{[\vec{v}_{w_j} \cdot \gamma, \vec{v}_{-w_j} \cdot \gamma]}{2\vec{v}_{w_j} \cdot \vec{v}_{-w_j}} \right] \\ &= \sum_j \frac{-\tanh \left(\frac{w_j}{2} \right) \vec{v}_{w_j, k} \vec{v}_{-w_j, l} + \tanh \left(\frac{w_j}{2} \right) \vec{v}_{w_j, l} \vec{v}_{-w_j, k}}{\vec{v}_{w_j} \cdot \vec{v}_{-w_j}} \\ &= \left[-\tanh \left(\frac{W}{2} \right) \right]_{kl}, \end{aligned} \quad (\text{B9})$$

where the last line uses the decomposition of $f(W)$ in Eq. (B7).

Appendix C: Product rule of Gaussian states

To the best of our knowledge, the terminology “product rule of Gaussian states” is first mentioned in Ref. [72]. Since many formulations and statements in Sec. II are based on the product rule, including the twisted partially transposed Gaussian state and formulation of DQMC, we review it here in both Majorana basis and (particle-number-conserving) Dirac basis.

The product rule of Gaussian states means that the product of two Gaussian states is still a Gaussian state. Let us denote the Gaussian state as $\rho_W = \frac{1}{Z_W} e^{\hat{W}}$. For the general cases in the Majorana basis, $\hat{W} \equiv \frac{1}{4} \gamma^T W \gamma$ and $Z_W = \pm \sqrt{\det(1 + e^W)}$. For the particle-number-conserving cases in the Dirac basis, $\hat{W} \equiv \mathbf{c}^\dagger W \mathbf{c}$ and $Z_W = \det(1 + e^W)$. Then we wonder whether the product of ρ_W and $\rho_{W'}$ is still a Gaussian state. The proof roots in the Baker-Campbell-Hausdorff formula,

$$\begin{aligned} e^{\hat{W}''} &\equiv e^{\hat{W}} e^{\hat{W}'} \\ &= e^{\hat{W} + \hat{W}' + \frac{1}{2} [\hat{W}, \hat{W}']} + \frac{1}{12} ([\hat{W}, [\hat{W}, \hat{W}']] + [\hat{W}', [\hat{W}, \hat{W}']]) + \dots, \end{aligned} \quad (\text{C1})$$

⁷ If W has degenerate eigenvalues, one can always redefine the eigenvectors inside this degenerate subspace to make them “orthogonal” to each other.

and the following commuting relations

$$[\gamma_l \gamma_n, \gamma_j \gamma_k] = -2\gamma_l \gamma_j \delta_{kn} + 2\gamma_l \gamma_k \delta_{jn} + 2\gamma_n \gamma_j \delta_{lk} - 2\gamma_n \gamma_k \delta_{lj}, \quad (\text{C2a})$$

$$[c_l^\dagger c_n, c_j^\dagger c_k] = c_l^\dagger c_k \delta_{nk} - c_j^\dagger c_n \delta_{lk}. \quad (\text{C2b})$$

As a result, although we do not write down a simply closed form of \hat{W}'' yet, we can assert that it is a fermionic quadratic, thus $\rho_{W''} \equiv \rho_W \rho_{W'}/\text{Tr}[\rho_W \rho_{W'}]$ is a Gaussian state.

Furthermore, using the trace formula for a product of exponential quadratic [67, 82],

$$\text{Tr} \left[e^{\hat{W}_1} e^{\hat{W}_2} \cdots e^{\hat{W}_n} \right] = (\pm) (\det [I + e^{W_1} e^{W_2} \cdots e^{W_n}])^\eta, \quad (\text{C3})$$

where $\eta = \frac{1}{2}(1)$ for Majorana (Dirac) basis and there is a sign ambiguity for Majorana cases, we can deduce more useful relations. Starting with the relation between single-particle Hamiltonians,

$$e^{W''} = e^W e^{W''}, \quad (\text{C4})$$

we obtain the relations between the covariance matrices/Green's functions,

$$\Gamma'' = (I + \Gamma') (I + \Gamma \Gamma')^{-1} (\Gamma + \Gamma') (I + \Gamma')^{-1}, \quad (\text{C5a})$$

$$G'' = [I + (G^{-1} - I) (G'^{-1} - I)]^{-1}. \quad (\text{C5b})$$

As an example, we consider the twisted PTDM $\rho^{\tilde{T}_2^f} = \rho^{T_2^f} X_2$ where $\rho^{T_2^f}$ is a Gaussian state given by the covariance matrix in Eq. (12) and $X_2 = e^{i\pi \sum_{j \in A_2} n_j} \equiv \frac{1}{Z_2} e^{\gamma^T W_2} \gamma$ with $e^{W_2} = I_1 \oplus (-I_2) \equiv U_2$. Using the product rule in Eq. (C5a), one can obtain the twisted covariance matrix in Eq. (13). By the way, we note that casting the decoupled Hamiltonian into one single Gaussian state as in Eqs. (18) and (21) also relies on the product rule. Since we only care about the covariance matrices or Green's functions about the final Gaussian state ρ_s , we do not need the relations in Eq. (C5).

Appendix D: Sign problem of the Grover determinants

In this appendix, we prove that both the untwisted and twisted Grover determinants are real and positive for two classes of sign-problem-free models. We have detailed the untwisted case in the supplementary of Ref. [51], including how to show that these two model classes are represented by the Hubbard model and the spinless t - V model respectively. Here, we focus on the mathematical structure and unify the proof for different entanglement Green's functions, including reduced, untwisted, and twisted Green's functions.

1. Sufficient condition I in the Dirac basis

Lemma 1. *If two matrices, G^\uparrow and G^\downarrow , are connected by the relation $G^\downarrow = U^\dagger (I - G^\uparrow)^\dagger U$ with U an unitary matrix satisfying $UU^\dagger = I$, then their rank- r Grover determinants defined by*

$$\det \mathbf{g}_r \equiv \det \left[\prod_{i=r}^1 G_i \left[I + \prod_{i=r}^1 (G_i^{-1} - I) \right] \right], \quad (\text{D1})$$

where $G_i = G_i^{\uparrow, \downarrow}$ and in every replica the relation $G_i^\downarrow = U^\dagger (I - G_i^\uparrow)^\dagger U$ holds, are complex conjugate to each other, i.e., $\det \mathbf{g}_r^\uparrow = (\det \mathbf{g}_r^\downarrow)^*$.

Proof. Using $G^\downarrow = U^\dagger (I - G^\uparrow)^\dagger U$ we further obtain

$$(G^\downarrow)^{-1} - I = U^\dagger \left[\left((G^\uparrow)^{-1} - I \right)^{-1} \right]^\dagger U. \quad (\text{D2})$$

Then we can prove Lemma 1 by using the fact that unitary transformation does not change determinant

$$\begin{aligned} & \det \mathbf{g}_r^\downarrow \\ &= \det \left\{ \prod_{i=r}^1 G_i^\downarrow \left[I + \prod_{i=r}^1 \left((G_i^\downarrow)^{-1} - I \right) \right] \right\} \\ &= \det \left\{ \prod_{i=r}^1 (I - G_i^\uparrow)^\dagger \left[I + \prod_{i=r}^1 \left((G_i^\uparrow)^{-1} - I \right)^{-1\dagger} \right] \right\} \\ &= \det \left\{ \left[I + \prod_{i=1}^r \left((G_i^\uparrow)^{-1} - I \right)^{-1} \right] \prod_{i=1}^r (I - G_i^\uparrow) \right\}^* \\ &= \det \left\{ \left[\prod_{i=r}^1 \left((G_i^\uparrow)^{-1} - I \right) + I \right] \prod_{i=1}^r G_i^\uparrow \right\}^* \\ &= (\det \mathbf{g}_r^\uparrow)^*. \end{aligned} \quad (\text{D3})$$

We have use $(I - G_i^\uparrow) = ((G_i^\uparrow)^{-1} - I) G_i^\uparrow$ and $\det AB = \det A \det B$ to come to the last but second line. \square

Example 1.1 The Green's function matrices of a class of sign-problem-free models, represented by the half-filled Hubbard model on bipartite lattices such as square and honeycomb lattices, can be decoupled into the two independent spin sectors under appropriate basis, such that $G = G^\uparrow \oplus G^\downarrow$, and they satisfy the relation $G_{jk}^\downarrow = (-)^{j+k} (\delta_{jk} - G_{kj}^{\uparrow*})$ [51]. Here, the superscript \uparrow and \downarrow denotes spin-up and spin-down sectors, respectively. The subscripts j and k run over the lattice sites. The matrix defined by $U_{\eta, jk} = \delta_{jk} (-)^j$ is diagonal and unitary, which gives $G^\downarrow = U_\eta^\dagger (I - G^\uparrow)^\dagger U_\eta$. Consequently, Lemma 1 applies to this case, and the Grover determinants corresponding to the total or reduced Green's functions are real and positive, i.e., $\det \mathbf{g}_r = \det \mathbf{g}_r^\uparrow \det \mathbf{g}_r^\downarrow \geq 0$ [55].

Example 1.2 Still consider the class of models in Example 1.1. Consider a continuous bipartite geometry $A = A_1 \cup A_2$ and using Eq. (15) to do untwisted partial transpose, we find that

$$G^{\downarrow, T_2^f} = V^\dagger U_\eta^\dagger \left(I - G^{\uparrow, T_2^f} \right)^\dagger U_\eta V \quad (\text{D4})$$

where $V \equiv (iI_{A_1}) \oplus (-iI_{A_2}) \equiv iU_2$ is block-diagonal, unitary and anti-Hermitian, i.e., $V^\dagger = V^{-1} = -V$. Thus the untwisted Green's function still satisfies the condition for Lemma 1 and the untwisted Grover determinant (see Eq. (30a)) is real and positive, $\det g_r = \det g_r^\uparrow \det g_r^\downarrow \geq 0$.

Example 1.3 Still consider the class of models in Example 1.1. Now we further consider twisted partial transpose given by Eq. (16). From Eq. (D4) we have

$$\left(\left(G^{\downarrow, T_2^f} \right)^{-1} - I \right) = V^\dagger U_\eta^\dagger \left(\left(G^{\uparrow, T_2^f} \right)^{-1} - I \right)^{-1\dagger} U_\eta V. \quad (\text{D5})$$

Next, using the definition of twisted partial transpose and the product rule of Gaussian state in Eq. (C5b) we have

$$\begin{aligned} \left(\left(G^{\downarrow, T_2^f} \right)^{-1} - I \right) &= \left(\left(G^{\downarrow, T_2^f} \right)^{-1} - I \right) U_2 \\ &= V^\dagger U_\eta^\dagger \left(\left(G^{\uparrow, T_2^f} \right)^{-1} - I \right)^{-1\dagger} U_\eta V U_2 \\ &= V^\dagger U_\eta^\dagger \left[\left(\left(G^{\uparrow, T_2^f} \right)^{-1} - I \right) U_2^\dagger \right]^{-1\dagger} U_\eta V U_2 \\ &= U_2^\dagger V^\dagger U_\eta^\dagger \left(\left(G^{\uparrow, T_2^f} \right)^{-1} - I \right)^{-1\dagger} U_\eta V U_2. \end{aligned} \quad (\text{D6})$$

To go to the last line, we use the fact that $U_2 \equiv I_1 \oplus (-I_2)$ commutes with any block-diagonal matrices, including V^\dagger and U_η^\dagger . Actually, due to $V U_2 = iU_2^2 = i$, the above formula can be further simplified. As a result, the twisted Green's function still satisfies the condition for Lemma 1, so the twisted Grover determinant (see Eq. (30b)) is real and positive, $\det \tilde{g}_r = \det \tilde{g}_r^\uparrow \det \tilde{g}_r^\downarrow \geq 0$.

By the way, we discuss the sign of the normalization factor $\mathcal{Z}_{\tilde{T}_2^f} \equiv \det(I_2 - 2G_{22})$ for this class of models. It turns out that $\mathcal{Z}_{\tilde{T}_2^f}$ may be negative, depending on the number of sites in subsystem A_2 (denoted as N_2):

$$\begin{aligned} \mathcal{Z}_{\tilde{T}_2^f} &= \det(I_2 - 2G_{22}) \\ &= \det(I_2^\uparrow - 2G_{22}^\uparrow) \det(I_2^\downarrow - 2G_{22}^\downarrow) \\ &= \det(-I_2^\uparrow + 2U_{\eta,2}^\dagger (G_{22}^\downarrow)^\dagger U_{\eta,2}) \det(I_2^\downarrow - 2G_{22}^\downarrow) \\ &= (-1)^{N_2} \left| \det(I_2^\downarrow - 2G_{22}^\downarrow) \right|^2. \end{aligned} \quad (\text{D7})$$

We emphasize that the final step relies on the diagonal nature of U_η , making the formula not generally applicable to all cases in Lemma 1. By combining Eq. (D7) with $\det \tilde{g}_r \geq 0$, we conclude that, for the models in Example

1.1, the modified twisted Grover determinants (namely, $\det \tilde{g}_r = (\prod_{i=1}^r \mathcal{Z}_{\tilde{T}_2^f, s(i)}) \det \tilde{g}_r$) are real and positive except when both r and N_2 are odd.

2. Sufficient condition II in the Majorana basis

The second sufficient condition for real and positive Grover determinants is proved in the Majorana basis, where the density matrix is decomposed as in Eq. (18). And we note that the W_s matrix is related to the covariance matrix Γ_s via $\Gamma_s = -\tanh(W_s/2)$.

Lemma 2. *If two matrices, $\Gamma^{(1)}$ and $\Gamma^{(2)}$, are connected by the relation $\Gamma^{(2)} = U^\dagger \Gamma^{(1)*} U$ with U an unitary matrix satisfying $UU^\dagger = I$, then their rank- r Grover determinants defined by*

$$\det \mathbf{g}_r = \left(\prod_{i=r}^1 \det [I + e^{W_i}]^{-1/2} \right) \det \left[I + \prod_{i=r}^1 e^{W_i} \right]^{1/2}, \quad (\text{D8})$$

where $\tanh(-W_i/2) = \Gamma_i = \Gamma_i^{(1),(2)}$ and in every replica the relation $\Gamma_i^{(2)} = U^\dagger \Gamma_i^{(1)*} U$ holds, are complex conjugate to each other, i.e., $\det \mathbf{g}_r^{(1)} = (\det \mathbf{g}_r^{(2)})^*$.

Proof. Since $\tanh(W_i/2) = \Gamma_i$, we know that $W_i^{(1)}$ and $W_i^{(2)}$ also fulfill the relation $W_i^{(2)} = U^\dagger W_i^{(1)*} U$. Then we can prove Lemma 2 by using the fact that unitary transformation does not change determinant

$$\begin{aligned} \det \mathbf{g}_r^{(1)} &= \left(\prod_{i=r}^1 \det [I + e^{W_i^{(1)}}]^{-1/2} \right) \det \left[I + \prod_{i=r}^1 e^{W_i^{(1)}} \right]^{1/2} \\ &= \left(\prod_{i=r}^1 \det [I + e^{W_i^{(2)}}]^{-1/2} \right)^* \left(\det \left[I + \prod_{i=r}^1 e^{W_i^{(2)}} \right]^{1/2} \right)^* \\ &= \left(\det \mathbf{g}_r^{(2)} \right)^*. \end{aligned} \quad (\text{D9})$$

□

Example 2.1 The covariance matrices of a class of sign-problem-free models, represented by the spinless t - V model on bipartite lattices such as square and honeycomb lattices, satisfy $\Gamma_{jk}^{(2)} = (-)^{j+k} \Gamma_{jk}^{(1)*}$ [51]. Here, the superscript (1) and (2) corresponds to two Majorana species, i.e., $\gamma_i^{(1)}$ and $\gamma_i^{(2)}$ in Eq. (1). The total covariance matrix in this class of models can be decoupled into the two independent species sectors under an appropriate basis where $\Gamma = \Gamma^{(1)} \oplus \Gamma^{(2)}$. The matrix defined by $U_{\eta,jk} = \delta_{jk}(-)^j$ is diagonal and unitary. Thus Lemma 2 applies to this case, and the Grover determinants corresponding to the total or reduced covariance matrices are real and positive, i.e., $\det \mathbf{g}_r = \det \mathbf{g}_r^{(1)} \det \mathbf{g}_r^{(2)} \geq 0$.

Example 2.2 Consider the class of models in Example 2.1 and the bipartition geometry in Example 1.2. Using Eq. (12) to do untwisted partial transpose, we find that

$$\Gamma^{(2),T_2^f} = U_2^\dagger U_\eta^\dagger \left(\Gamma^{(1),T_2^f} \right)^* U_\eta U_2. \quad (\text{D10})$$

Thus Lemma 2 applies to $\Gamma^{(1),T_2^f}$ and $\Gamma^{(2),T_2^f}$, and the untwisted Grover determinant is real and positive, $\det g_r = \det g_r^{(1)} \det g_r^{(2)} \geq 0$.

Example 2.3 Still consider the class of models in Example 2.1. Now we further consider twisted partial transpose given by Eq. (13). From Eq. (D10) and $\tanh(-W^{T_2^f}) = \Gamma^{T_2^f}$ we learn that

$$W^{(2),T_2^f} = U_2^\dagger U_\eta^\dagger \left(W^{(1),T_2^f} \right)^* U_\eta U_2. \quad (\text{D11})$$

Further, using the definition of twisted partial transpose and the product rule of Gaussian state in Eq. (C4) we have

$$\begin{aligned} e^{W^{(2),\tilde{T}_2^f}} &= e^{W^{(2),T_2^f}} U_2 \\ &= U_2^\dagger U_\eta^\dagger \left(e^{W^{(1),T_2^f}} \right)^* U_\eta U_2 U_2 \\ &= U_2^\dagger U_\eta^\dagger \left(e^{W^{(1),\tilde{T}_2^f}} U_2^\dagger \right)^* U_\eta U_2 U_2 \\ &= U_2^\dagger U_\eta^\dagger \left(e^{W^{(1),\tilde{T}_2^f}} \right)^* U_\eta U_2, \end{aligned} \quad (\text{D12})$$

where we have used $U_2^* = U_2 = U_2^\dagger$, $U_2^2 = I$, and the fact that U_2 commutes with U_η to go to the last line. As a result, according to Lemma 2, the twisted Grover determinant is real and positive, $\det \tilde{g}_r = \det \tilde{g}_r^{(1)} \det \tilde{g}_r^{(2)} \geq 0$.

Important Note: The proof presented in this subsection regarding the Majorana basis, while providing valuable intuitive and heuristic insights, lacks mathematical rigor. The trace of Gaussian states in the Majorana basis would involve a sign ambiguity [67], which has not been accounted for in our current proof. In our numerical investigations of the 2D t - V model, we consistently observe positive values for both untwisted and twisted Grover determinants. However, we note that the normalization factor $\mathcal{Z}_{\tilde{T}_2^f}$ does not follow Eq. (D7) and can assume negative values for even N_2 . Importantly, the rank-4 modified twisted Grover determinant $\det \tilde{g}_4$ that we consider in the main text is always real and positive.

Appendix E: Discussion on other local update schemes for untwisted Rényi negativity

In this appendix, we present two alternative local update schemes for untwisted Rényi negativity. Compared to the approach presented in the main text (hereafter referred to as "Scheme 3"), these methods offer greater conceptual simplicity and mathematical elegance, though at the cost of reduced numerical stability.

1. Scheme 1: Calculate r_2 and r_3 separately

Calculate r_2 . As a result of Eq. (47), we immediately obtain $r_2 = \det(I_m + \mathcal{V}\mathcal{U})$ by applying Sylvester's determinant identity. Considering the definition of \mathbb{B}_i , we deduce that the appropriate central matrix to be updated is the inverse of $G_{\mathbf{s}^{(i)}}^{T_2^f}$,

$$\begin{aligned} \left(G_{\mathbf{s}^{(i)}}^{T_2^f} \right)^{-1} &= (I + \mathcal{U}\mathcal{V})^{-1} \left(G_{\mathbf{s}^{(i)}}^{T_2^f} \right)^{-1} \\ &= \left(G_{\mathbf{s}^{(i)}}^{T_2^f} \right)^{-1} - \mathcal{U}(I_m + \mathcal{V}\mathcal{U})^{-1}\mathcal{V} \left(G_{\mathbf{s}^{(i)}}^{T_2^f} \right)^{-1}. \end{aligned} \quad (\text{E1})$$

In the second line, we utilize the Woodbury matrix identity, which reduces to the Sherman-Morrison formula when $m = 1$. Its numerical stabilization directly follows from the stabilization results of $G_{\mathbf{s}^{(i)}}$, followed by performing the FPT and taking the inverse.

Calculate r_3 . Since r_3 shares a mathematical structure similar to the DQMC ratio r_1 , with \mathbb{B}_i corresponding to B_l , it can be evaluated using formulas analogous to those employed in DQMC. When an update occurs in replica- i , the modification of \mathbb{B}_i is described by:

$$\begin{aligned} \mathbb{B}'_i &= (I - \mathcal{U}\mathcal{V}^a)\mathbb{B}_i, \\ \mathcal{V}^a &= (I_m + \mathcal{V}\mathcal{U})^{-1}\mathcal{V} \left(G_{\mathbf{s}^{(i)}}^{T_2^f} \right)^{-1} \mathbb{B}_i^{-1}. \end{aligned} \quad (\text{E2})$$

Here, the term $(I - \mathcal{U}\mathcal{V}^a)$ is analogous to the matrix Δ in DQMC. The calculation of r_3 then closely follows the DQMC ratio:

$$\begin{aligned} r_3 &= \frac{\det [I + \mathbb{B}(r, i)(I - \mathcal{U}\mathcal{V}^a)\mathbb{B}(i, 0)]}{\det [I + \mathbb{B}(r, 0)]} \\ &= \det [I - \mathcal{U}\mathcal{V}^a(I - \mathbb{G}(i, i))] = \det [I_m - \mathbb{V}\mathcal{U}], \end{aligned} \quad (\text{E3})$$

where $\mathbb{V} \equiv \mathcal{V}^a(I - \mathbb{G}(i, i))$. We define an equal-replica "Green's function" analogous to $G(\tau, \tau)$,

$$\mathbb{G}(i, i) \equiv (I + \mathbb{B}(i, 0)\mathbb{B}(r, i))^{-1}, \quad (\text{E4})$$

which generalize $\mathbb{G}(0, 0) = \mathbb{G}(r, r)$ as previously defined in Eq. (36). The central matrices to be updated are \mathbb{B}_i^{-1} and \mathbb{G} , with update formulas given by:

$$(\mathbb{B}_i^{-1})' = \mathbb{B}_i^{-1} (I + \mathcal{U}(I_m - \mathcal{V}^a\mathcal{U})^{-1}\mathcal{V}^a), \quad (\text{E5})$$

$$\mathbb{G}'(i, i) = \mathbb{G} [I + \mathcal{U}(I_m - \mathbb{V}\mathcal{U})^{-1}\mathbb{V}]. \quad (\text{E6})$$

The stabilization of \mathbb{B}_i and \mathbb{B}_i^{-1} directly derives from $G_{\mathbf{s}^{(i)}}$, while the stabilization routines for $\mathbb{G}(i, i)$ are similar to those for $G_{\mathbf{s}^{(i)}}$, with all instances of $B(\tau, \tau') \rightarrow \mathbb{B}(i, i')$ (see Eq. (36) and similar formulas in Appendix F). When the local updates in one replica are completed and we need to move to the next replica, $\mathbb{G}(i, i)$ also follows a propagation formula similar to $G(\tau, \tau)$, for example:

$$\begin{aligned} \mathbb{G}(i+1, i+1) &= \mathbb{B}_{i+1}\mathbb{G}(i, i)\mathbb{B}_{i+1}^{-1}, \\ \mathbb{G}(i-1, i-1) &= \mathbb{B}_i^{-1}\mathbb{G}(i, i)\mathbb{B}_i. \end{aligned} \quad (\text{E7})$$

Measure $\det g_{r,\bar{s}}$. The measurement of the Grover determinant, and consequently its N_{inc} -th root, can be conducted after numerical stabilization, where $\ln \det G_{\mathbf{s}^{(i)}}^{T_2^f}$ and $\ln \det \mathbb{G}(i, i)$ have been calculated stably. By retrieving $\ln \det G_{\mathbf{s}^{(j)}}^{T_2^f}$ from other replicas ($j \neq i$), which remain unchanged during updates in replica- i , we can calculate $\det g_{r,\bar{s}}$ as follows:

$$\ln \det g_{r,\bar{s}} = \sum_{j=1}^r \ln \det G_{\mathbf{s}^{(j)}}^{T_2^f} - \ln \det \mathbb{G}(i, i). \quad (\text{E8})$$

2. Scheme 2: Calculate $r_2 r_3$ together

In this approach, we focus on a more stable update object that combines $G_{\mathbf{s}^{(i)}}^{T_2^f}$ and $(I + \mathbb{B}(i, 0)\mathbb{B}(r, i))$:

$$\mathbb{F}_i = \left[G_{\mathbf{s}^{(i)}}^{T_2^f} (I + \mathbb{B}(i, 0)\mathbb{B}(r, i)) \right]^{-1} = \mathbb{G}(i, i) \left(G_{\mathbf{s}^{(i)}}^{T_2^f} \right)^{-1}. \quad (\text{E9})$$

This is because $G_{\mathbf{s}^{(i)}}^{T_2^f} \mathbb{B}(i, 0)$ inside the square bracket results in the cancellation of one inverse of $G_{\mathbf{s}^{(i)}}^{T_2^f}$ (note that $G_{\mathbf{s}^{(i)}}^{T_2^f} \mathbb{B}_i = I - G_{\mathbf{s}^{(i)}}^{T_2^f}$). The update formula for \mathbb{F}_i can be derived from the update of $G_{\mathbf{s}^{(i)}}^{T_2^f}$ in Eq. (47)

$$\mathbb{F}'_i = \mathbb{F}_i \left(I - \mathcal{U} (I_m + \mathcal{V}^b \mathcal{U})^{-1} \mathcal{V}^b \right), \quad (\text{E10})$$

where we define

$$\mathcal{V}^b \equiv \mathcal{V} \mathbb{G}_{\mathbb{F}}^{-1} \mathbb{F}_i \text{ with } \mathbb{G}_{\mathbb{F}}^{-1} \equiv I - \mathbb{B}(i-1, 0)\mathbb{B}(r, i). \quad (\text{E11})$$

Thus, the ratio $r_2 r_3$ is given by

$$r_2 r_3 = \frac{\det g_{r,\bar{s}'}}{\det g_{r,\bar{s}}} = \frac{\det \mathbb{F}_i}{\det \mathbb{F}'_i} = \det (I_m + \mathcal{V}^b \mathcal{U}). \quad (\text{E12})$$

Here, the subscript \mathbb{F} of $\mathbb{G}_{\mathbb{F}}$ indicates that it does not depend on the auxiliary fields in replica- i . This choice of updating object (i.e., \mathbb{F}_i) was also recommended by a former work on high-rank REE calculations [55]. The stabilization of \mathbb{F}_i directly follows from $\mathbb{G}(i, i)$ and $G_{\mathbf{s}^{(i)}}^{T_2^f}$. The measurement of $\det g_{r,\bar{s}}$ is similar to Scheme 1, given by

$$\ln \det g_r = \sum_{j \neq i}^r \ln \det G_{\mathbf{s}^{(j)}}^{T_2^f} - \ln \det \mathbb{F}_i. \quad (\text{E13})$$

3. Practical experience and discussion

We have tested Schemes 1 and 2 on the 1D/2D half-filled Hubbard model, and the high-rank RN behaves well at moderate temperatures (not shown). However, for the spinless t - V model (see Sec. VIB for details), updating

$\left(G_{\mathbf{s}^{(i)}}^{T_2^f} \right)^{-1}$, \mathbb{B}_i^{-1} , and \mathbb{F}_i is unstable for a generic bipartition⁸. Specifically, the total phase of $W_{\mathbf{s}^{(1)} \dots \mathbf{s}^{(r)}}^{(k)}$ may deviate from unity during updates. This issue motivates us to update a more complex and stable object (see Eq. (48)), which is a variant of the total Grover matrix in Eq. (30a), maintaining the same determinant ratio. Compared to Eq. (E9), Eq. (48) cancels one additional inverse of $G^{T_2^f}$, as shown in the first term of the second line of Eq. (49).

Appendix F: Numerical stabilization routines in DQMC

In this appendix, we briefly review the numerical stabilization routines used in DQMC. They aim at stably dealing with matrices with exponentially large conditional numbers, including the $B(\tau, \tau')$ matrices defined below Eq. (25) and also the $\mathbb{B}(i, j)$ matrices defined in Eq. (35). For numerical stable matrix operations, these matrices are decomposed into UDV forms [83, 84]. The real diagonal matrix D stores scale information of $B(\tau, \tau')$ or $\mathbb{B}(i, j)$, and for matrices with large conditional numbers, there are both exponentially large and small number among the entries of D . In most numerically stable routines, we further factorize it to become $D = D_+ D_-$ with $D_+ = \max(D, 1)$ and $D_- = \min(D, 1)$, and avoid adding or subtracting these different scales during computation as much as possible. In practice, there are two kinds of UDV decomposition, one is singular value decomposition (SVD) and the other is a QR decomposition followed by extracting the absolute value of diagonal elements of R as D . One can see a detailed comparison and benchmark of them in Ref. [84]. In both choices, U is a unitary matrix that will be used to simplify some formulas.

In this and the next appendices, we use A (and other variant fonts like \mathbb{A}) to represent the matrix decomposition form of some matrix B , and their relation is denoted as $A := B = UDV$. Since we store $B(\beta, \tau)^\dagger = U_L D_L V_L =: A_L$ and $B(\tau, 0) = U_R D_R V_R =: A_R$ in practice, the following stable inverse routines are used for calculating Green's functions stably. For equal-time Green's functions, we need:

$$\begin{aligned} G(\tau, \tau) &= \left[1 + A_R A_L^\dagger \right]^{-1} \\ &= U_L D_{L+}^{-1} M^{-1} D_{R+}^{-1} U_R^\dagger \\ \text{with } M &\equiv D_{R+}^{-1} U_R^\dagger U_L D_{L+}^{-1} + D_{R-} V_R V_L^\dagger D_{L-}. \end{aligned} \quad (\text{F1})$$

⁸ An exception occurs in the special case of an equal bipartition, where the Green's functions exhibit much weaker singularities (see the discussion in Sec. IV); in this scenario, Schemes 1 and 2 can be effective.

In particular, we have simplified forms at $\tau = 0$ and β

$$\begin{aligned} G(0,0) &= \left[I + A_L^\dagger \right]^{-1} \\ &= U_L D_{L+}^{-1} \left[U_L^\dagger D_{L+}^{-1} + T_L^\dagger D_{L-} \right]^{-1}, \end{aligned} \quad (\text{F2})$$

$$\begin{aligned} G(\beta, \beta) &= \left[I + A_R \right]^{-1} \\ &= \left[D_{R+}^{-1} U_R^\dagger + D_{R-} V_R \right]^{-1} D_{R+}^{-1} U_R^\dagger. \end{aligned} \quad (\text{F3})$$

For time-displaced Green's functions we need:

$$\begin{aligned} G(\tau, 0) &= \left[A_R^{-1} + A_L^\dagger \right]^{-1} \\ &= U_L D_{L+}^{-1} M^{-1} D_{R-} V_R, \end{aligned} \quad (\text{F4})$$

with $M \equiv D_{R+}^{-1} U_R^\dagger U_L D_{L+}^{-1} + D_{R-} V_R V_L^\dagger D_{L-}$,

$$\begin{aligned} -G(0, \tau) &= \left[A_L^{\dagger-1} + A_R \right]^{-1} \\ &= V_R^{-1} D_{R+}^{-1} M^{-1} D_{L-} U_L^\dagger \\ \text{with } M &\equiv D_{L+}^{-1} \left(V_L^\dagger \right)^{-1} V_R^{-1} D_{R+}^{-1} + D_{L-} U_L^\dagger U_R D_{R-}, \end{aligned} \quad (\text{F5})$$

and we can also evaluate $G(0, 0)$ at time τ

$$\begin{aligned} G(0, 0) &= \left[1 + A_L^\dagger A_R \right]^{-1} \\ &= V_R^{-1} D_{R+}^{-1} M^{-1} D_{L+}^{-1} \left(V_L^\dagger \right)^{-1} \\ \text{with } M &\equiv D_{L+}^{-1} \left(V_L^\dagger \right)^{-1} V_R^{-1} D_{R+}^{-1} + D_{L-} U_L^\dagger U_R D_{R-}. \end{aligned} \quad (\text{F6})$$

Similarly, to calculate $\mathbb{G}(i, i)$ defined in Eq. (E4), just let $A_L := \mathbb{B}(r, i)^\dagger$ and $A_R := \mathbb{B}(i, 0)$ in Eq. (F1).

Appendix G: Numerical stabilization in the Scheme 3 of incremental algorithm

In this appendix, we detailed the numerical stabilization of the update object \mathbb{F}_i defined in Eq. (48),

$$\mathbb{F}_i = \left[G_{\mathbf{s}^{(i)}}^{T_2^f} \mathbb{F}_{\mathbb{A}}^{-1} + I - G_{\mathbf{s}^{(i-1)}}^{T_2^f} \right]^{-1}, \quad (\text{G1})$$

where $\mathbb{F}_{\mathbb{A}}^{-1}$ is given by Eq. (49)

$$\mathbb{F}_{\mathbb{A}}^{-1} \equiv \underbrace{\mathbb{B}_{i+1}^{-1} \cdots \mathbb{B}_r^{-1}}_{\mathbb{A}_L(i)} \underbrace{\mathbb{B}_1^{-1} \cdots \mathbb{B}_{i-2}^{-1}}_{\mathbb{A}_R(i-2)} G_{\mathbf{s}^{(i-1)}}^{T_2^f} - \left(I - G_{\mathbf{s}^{(i-1)}}^{T_2^f} \right). \quad (\text{G2})$$

Here we defined two matrix decompositions, namely, $\mathbb{A}_L(i) := (\mathbb{B}(r, i))^{-1}$, $\mathbb{A}_R(i) := (\mathbb{B}(i, 0))^{-1}$, where $0 \leq i \leq r$. It reduces to simpler formulas in special replicas close to the boundary:

$$\begin{aligned} \mathbb{F}_{\mathbb{A}}^{-1} &\equiv \underbrace{\mathbb{B}_2^{-1} \cdots \mathbb{B}_{r-1}^{-1}}_{\mathbb{A}_L(1)} G_{\mathbf{s}^{(r)}}^{T_2^f} - \left(I - G_{\mathbf{s}^{(r)}}^{T_2^f} \right) \\ &= \underbrace{\mathbb{B}_2^{-1} \cdots \mathbb{B}_r^{-1}}_{\mathbb{A}_L(1)} \left(I - G_{\mathbf{s}^{(r)}}^{T_2^f} \right) - \left(I - G_{\mathbf{s}^{(r)}}^{T_2^f} \right), \end{aligned} \quad (\text{G3a})$$

$$\mathbb{F}_{\mathbb{A}}^{-1} \equiv \underbrace{\mathbb{B}_3^{-1} \cdots \mathbb{B}_r^{-1}}_{\mathbb{A}_L(2)} G_{\mathbf{s}^{(1)}}^{T_2^f} - \left(I - G_{\mathbf{s}^{(1)}}^{T_2^f} \right), \quad (\text{G3b})$$

$$\mathbb{F}_{\mathbb{A}}^{-1} \equiv \underbrace{\mathbb{B}_1^{-1} \cdots \mathbb{B}_{r-2}^{-1}}_{\mathbb{A}_R(r-2)} G_{\mathbf{s}^{(r-1)}}^{T_2^f} - \left(I - G_{\mathbf{s}^{(r-1)}}^{T_2^f} \right) \quad (\text{G3c})$$

Both $\mathbb{F}_{\mathbb{A}}^{-1}$ and $G_{\mathbf{s}^{(i-1)}}^{T_2^f}$ are unchanged during sweeping inside replica- i . When going from one replica to the next, we need to update these two matrices. For the best stability, all the $G_{\mathbf{s}^{(i)}}^{T_2^f}$ and \mathbb{B}_i^{-1} are decomposed into UDV form,

$$G_{\mathbf{s}^{(i)}}^{T_2^f} = U_i D_i V_i =: A_i, \quad (\text{G4})$$

$$I - G_{\mathbf{s}^{(i)}}^{T_2^f} = \bar{U}_i \bar{D}_i \bar{V}_i =: \bar{A}_i, \quad (\text{G5})$$

$$\begin{aligned} \mathbb{B}_i^{-1} &= (A_i^{-1} - I)^{-1} \\ &= U_i D_{i-} \left(\underbrace{V_i^{-1} D_{i+}^{-1} - U_i D_{i-}}_{U' D' V'} \right)^{-1} \\ &= U_i \underbrace{D_{i-} V'^{-1} D'^{-1} U'}_{U'' D'' V''} \\ &= \underbrace{U_i U''}_{\mathbb{U}_i} \underbrace{D''}_{\mathbb{D}_i} \underbrace{V'' U'}_{\mathbb{V}_i} =: \mathbb{A}_i. \end{aligned} \quad (\text{G6})$$

Thus we also have $\mathbb{A}_L(i) = \prod_{j=i+1}^r \mathbb{A}_j$ and $\mathbb{A}_R(i) = \prod_{j=1}^i \mathbb{A}_j$. Next, all the matrix multiplications in the first term of Eq. (G2) are done in decomposition form, i.e.,

$$\begin{aligned} A_1 A_2 &= U_1 \underbrace{D_1 V_1 U_2 D_2 V_2}_{U' D' V'} \\ &= \underbrace{U_1 U'}_{U_{12}} \underbrace{D'}_{D_{12}} \underbrace{V' V_2}_{V_{12}} = A_{12}. \end{aligned} \quad (\text{G7})$$

After added with $(I - G_{\mathbf{s}^{(i)}}^{T_2^f})$, we obtain an accurate $\mathbb{F}_{\mathbb{A}}^{-1}$. Finally, the evaluation of Eq. (G1) is done using normal matrix operations.⁹

For the twisted case, the numerical stabilization requires only minor adjustments. First, store $\tilde{\mathbb{B}}_i^{-1} = U_2 \mathbb{B}_i^{-1} = (U_2 \mathbb{U}_i) \mathbb{D}_i \mathbb{V}_i =: \tilde{\mathbb{A}}_i$ instead of \mathbb{A}_i . Second, the

⁹ One could have tried an even more stable approach: keep the $G_{\mathbf{s}^{(i)}}^{T_2^f} \mathbb{F}_{\mathbb{A}}^{-1}$ and $(I - G_{\mathbf{s}^{(i-1)}}^{T_2^f})$ in Eq. (G1) stay in UDV decomposition forms, and then use a stable inverse routine (which is similar to Eq. (F4) but without any inverse or Hermitian conjugate) to calculate \mathbb{F}_i . We find that normal matrix operations are stable enough.

stable calculation of $\tilde{\mathbb{B}}_i^{-1}$ (see Eq. (61)) involves additional U_2 matrices during UDV multiplication:

$$\tilde{\mathbb{B}}_i^{-1} \equiv \underbrace{\tilde{\mathbb{B}}_{i+1}^{-1} \cdots \tilde{\mathbb{B}}_r^{-1}}_{\tilde{\mathbb{A}}_L(i)} \underbrace{\tilde{\mathbb{B}}_1^{-1} \cdots \tilde{\mathbb{B}}_{i-2}^{-1}}_{\tilde{\mathbb{A}}_R(i-2)} U_2 G_{\mathbf{s}^{(i-1)}}^{T_2^f} U_2 - U_2 \left(I - G_{\mathbf{s}^{(i-1)}}^{T_2^f} \right) U_2. \quad (\text{G8})$$

The pseudo codes in Algorithms 1 and 2 detail the forward (from replica-1, time-0 to replica- n , time- β , see Fig. 5 for illustration) and backward procedures. We maintain two arrays consisting of UDV decompositions for conducting numerical stabilization for $G_{\mathbf{s}^{(i)}}$ and \mathbb{F}_i , namely, the A_{stab} of shape $(r, N_{\text{stab}} + 1)$ and \mathbb{A}_{stab} of shape $(r + 1)$, respectively. The workflow with A_{stab} is the same as normal DQMC implementation [82] but now there are r replicas. Within each replica, we conduct stable calculations of $G_{\mathbf{s}^{(i)}}$ at regular intervals of τ_{stab} , where $\tau_{\text{stab}} N_{\text{stab}} = \beta$. The workflow with \mathbb{A}_{stab} is also similar: every time before going from replica- i to replica- $(i + 1)$ (replica- $(i - 1)$), we calculate $\mathbb{A}_R(i)$ ($\mathbb{A}_L(i - 1)$) by right (left) multiplying \mathbb{A}_i to it according to Eq. (G7), and then set it to become $\mathbb{A}_{\text{stab}}[i]$ ($\mathbb{A}_{\text{stab}}[i - 1]$).

Below we list other routines we need. The first one is the update routines for Green's functions:

$$\begin{aligned} G_{\mathbf{s}'}(\tau, \tau) &= G_{\mathbf{s}} - G_{\mathbf{s}} U (I_m + VU)^{-1} V, \\ G_{\mathbf{s}'}(\tau, 0) &= G_{\mathbf{s}}(\tau, 0) - G_{\mathbf{s}} U (I_m + VU)^{-1} P_{k \times N} G_{\mathbf{s}}(\tau, 0), \\ G_{\mathbf{s}'}(0, \tau) &= G_{\mathbf{s}}(0, \tau) - G_{\mathbf{s}}(0, \tau) U (I_m + VU)^{-1} V, \\ G_{\mathbf{s}'}(0, 0) &= G_{\mathbf{s}}(0, 0) + G_{\mathbf{s}}(0, \tau) U (I_m + VU)^{-1} P_{k \times N} G_{\mathbf{s}}(\tau, 0). \end{aligned} \quad (\text{G9})$$

Again, we note that if the symmetric Trotter decomposition is utilized, one should apply the above update formula to partially propagated Green's function (see the footnote before Eq. (46)) instead of the true Green's functions. Secondly, two routines for multiplying a normal matrix with a UDV decomposition are needed:

$$BA = \underbrace{BUD}_{U_0 D_0 V_0} V = \underbrace{U_0}_{U'} \underbrace{D_0}_{D'} \underbrace{V_0 V}_{V'} = A', \quad (\text{G10a})$$

$$AB = U \underbrace{DVB}_{U_0 D_0 V_0} = \underbrace{UU_0}_{U'} \underbrace{D_0}_{D'} \underbrace{V_0}_{V'} = A'. \quad (\text{G10b})$$

Algorithm 1: Forward propagation framework for Scheme 3 of incremental algorithm

Input: $\{G_{\mathbf{s}^{(i)}}(0, 0) \mid i = 1, 2, \dots, r\}, \{G_{\mathbf{s}^{(i)}}^{T_2^f} \mid i = 1, 2, \dots, r\}$

Input: $\{A_i := G_{\mathbf{s}^{(i)}}^{T_2^f} \mid i = 1, 2, \dots, r\}, \{\bar{A}_i := I - G_{\mathbf{s}^{(i)}}^{T_2^f} \mid i = 1, 2, \dots, r\}$

Input: $A_{\text{stab}}[1 : r, 0 : N_{\text{stab}}] = \{A_L(i, l_{\text{stab}}) := B_{\mathbf{s}^{(i)}}(\beta, l_{\text{stab}}\tau_{\text{stab}})^\dagger \mid i = 1, 2, \dots, r; l_{\text{stab}} = 0, 1, 2, \dots, N_{\text{stab}}\}$

Input: $\mathbb{A}_{\text{stab}}[0 : r] = \{\mathbb{A}_L(i) := \mathbb{B}(r, i)^{-1} \mid i = 0, 1, 2, \dots, r\}$

1 Set $\mathbb{A}_{\text{stab}}[0] = \mathbb{A}_R(0) := I$;

2 **for** $i \in 1, 2, \dots, r$ **do**

3 **if** $i == 1$ **then**

4 Retrieve $\mathbb{A}_L(1) = \mathbb{A}_{\text{stab}}[1]$ and \bar{A}_r ;

5 Calculate \mathbb{F}_1^{-1} using Eq. (G3a);

6 **else if** $i == 2$ **then**

7 Retrieve $\mathbb{A}_L(2) = \mathbb{A}_{\text{stab}}[2]$ and A_1 ;

8 Calculate \mathbb{F}_2^{-1} using Eq. (G3b);

9 **else if** $i == r$ **then**

10 Retrieve $\mathbb{A}_R(r-2) = \mathbb{A}_{\text{stab}}[r-2]$ and A_{r-1} ;

11 Calculate \mathbb{F}_{r-1}^{-1} using Eq. (G3c);

12 **else**

13 Retrieve $\mathbb{A}_L(i) = \mathbb{A}_{\text{stab}}[i]$, $\mathbb{A}_R(i-2) = \mathbb{A}_{\text{stab}}[i-2]$ and A_{i-1} ;

14 Calculate \mathbb{F}_{i-1}^{-1} using Eq. (G2);

15 **end if**

16 Calculate \mathbb{F}_i using Eq. (G1);

17 Set $A_{\text{stab}}[i, 0] = A_R(i, 0) := I$;

18 **for** $l \in 1, 2, \dots, L_\tau$ **do**

19 Propagate to $G_{\mathbf{s}^{(i)}}(\tau, \tau), G_{\mathbf{s}^{(i)}}(\tau, 0), G_{\mathbf{s}^{(i)}}(0, \tau)$;

20 Update $G_{\mathbf{s}^{(i)}}(\tau, \tau), G_{\mathbf{s}^{(i)}}(\tau, 0), G_{\mathbf{s}^{(i)}}(0, \tau), G_{\mathbf{s}^{(i)}}(0, 0)$ using Eq. (G9) and update \mathbb{F}_i using Eq. (52);

21 **if** $\tau == l_{\text{stab}}\tau_{\text{stab}}$ **then**

22 Retrieve $A_L(i, l_{\text{stab}}) = A_{\text{stab}}[i, l_{\text{stab}}]$;

23 Calculate $B_{\mathbf{s}^{(i)}}(\tau, \tau - \tau_{\text{stab}})$;

24 **if** $l_{\text{stab}} == 1$ **then**

25 Calculate $A_R(i, 1) := B_{\mathbf{s}^{(i)}}(\tau, \tau - \tau_{\text{stab}})$;

26 **else**

27 Retrieve $A_R(i, l_{\text{stab}} - 1) = A_{\text{stab}}[i, l_{\text{stab}} - 1]$;

28 Calculate $A_R(i, l_{\text{stab}}) = B_{\mathbf{s}^{(i)}}(\tau, \tau - \tau_{\text{stab}})A_R(i, l_{\text{stab}} - 1)$ using Eq. (G10a);

29 **end if**

30 Set $A_{\text{stab}}[i, l_{\text{stab}}] = A_R(i, l_{\text{stab}})$;

31 **if** $l == L_\tau$ **then**

32 Calculate $G_{\mathbf{s}^{(i)}}(\beta, \beta) = [I + A_R(i, N_{\text{stab}})]^{-1}$ using Eq. (F3);

33 Calculate $G_{\mathbf{s}^{(i)}}(\beta, 0) = I - G_{\mathbf{s}^{(i)}}(\beta, \beta)$;

34 Calculate $G_{\mathbf{s}^{(i)}}(0, \beta) = -G_{\mathbf{s}^{(i)}}(\beta, \beta)$;

35 Calculate $G_{\mathbf{s}^{(i)}}(0, 0) = G_{\mathbf{s}^{(i)}}(\beta, \beta)$;

36 **else**

37 Calculate $G_{\mathbf{s}^{(i)}}(\tau, \tau) = [I + A_R(i, l_{\text{stab}})A_L^\dagger(i, l_{\text{stab}})]^{-1}$ using Eq. (F1);

38 Calculate $G_{\mathbf{s}^{(i)}}(\tau, 0) = [A_R^{-1}(i, l_{\text{stab}}) + A_L^\dagger(i, l_{\text{stab}})]^{-1}$ using Eq. (F4);

39 Calculate $G_{\mathbf{s}^{(i)}}(0, \tau) = -[A_L^\dagger(i, l_{\text{stab}}) + A_R(i, l_{\text{stab}})]^{-1}$ using Eq. (F5);

40 Calculate $G_{\mathbf{s}^{(i)}}(0, 0) = [I + A_L^\dagger(i, l_{\text{stab}})A_R(i, l_{\text{stab}})]^{-1}$ using Eq. (F6);

41 **end if**

42 Calculate $G_{\mathbf{s}^{(i)}}^{T_2^f} = (G_{\mathbf{s}^{(i)}}(0, 0))^{T_2^f}$ using Eq. (15);

43 Calculate \mathbb{F}_i using Eq. (G1);

44 Measure $\det g_r$;

45 **end if**

46 **end for**

47 Calculate $A_i := G_{\mathbf{s}^{(i)}}^{T_2^f}$, $\bar{A}_i := I - G_{\mathbf{s}^{(i)}}^{T_2^f}$, and $\mathbb{A}_i := \mathbb{B}_i^{-1}$;

48 **if** $i == 1$ **then**

49 Set $\mathbb{A}_R(i) = \mathbb{A}_i$;

50 **else**

51 Retrieve $\mathbb{A}_R(i-1)$;

52 Calculate $\mathbb{A}_R(i) = \mathbb{A}_R(i-1)\mathbb{A}_i$ using Eq. (G7);

53 **end if**

54 Set $\mathbb{A}_{\text{stab}}[i] = \mathbb{A}_R(i)$;

55 **end for**

Output: $A_{\text{stab}}[1 : r, 0 : N_{\text{stab}}] = \{A_R(i, l_{\text{stab}}) := B_{\mathbf{s}^{(i)}}(l_{\text{stab}}\tau_{\text{stab}}, 0) \mid i = 1, 2, \dots, r; l_{\text{stab}} = 0, 1, 2, \dots, N_{\text{stab}}\}$

Output: $\mathbb{A}_{\text{stab}}[0 : r] = \{\mathbb{A}_R(i) := \mathbb{B}(i, 0)^{-1} \mid i = 0, 1, 2, \dots, r\}$

Algorithm 2: Backward propagation framework for Scheme 3 of incremental algorithm

Input: $\{G_{s^{(i)}}(\beta, \beta) \mid i = 1, 2, \dots, r\}, \{G_{s^{(i)}}^{T_2^f} \mid i = 1, 2, \dots, r\}$
Input: $\{A_i := G_{s^{(i)}}^{T_2^f} \mid i = 1, 2, \dots, r\}, \{\bar{A}_i := I - G_{s^{(i)}}^{T_2^f} \mid i = 1, 2, \dots, r\}$
Input: $A_{\text{stab}}[1 : r, 0 : N_{\text{stab}}] = \{A_R(i, l_{\text{stab}}) := B_{s^{(i)}}(l_{\text{stab}}\tau_{\text{stab}}, 0) \mid i = 1, 2, \dots, r; l_{\text{stab}} = 0, 1, 2, \dots, N_{\text{stab}}\}$
Input: $\mathbb{A}_{\text{stab}}[0 : r] = \{\mathbb{A}_R(i) := \mathbb{B}(i, 0)^{-1} \mid i = 0, 1, 2, \dots, r\}$

1 Set $\mathbb{A}_{\text{stab}}[r] = \mathbb{A}_L(r) := I$;
2 **for** $i \in r, r-1, \dots, 1$ **do**
3 **if** $i == 1$ **then**
4 Retrieve $\mathbb{A}_L(1) = \mathbb{A}_{\text{stab}}[1]$ and \bar{A}_r ;
5 Calculate \mathbb{F}_1^{-1} using Eq. (G3a);
6 **else if** $i == 2$ **then**
7 Retrieve $\mathbb{A}_L(2) = \mathbb{A}_{\text{stab}}[2]$ and A_1 ;
8 Calculate \mathbb{F}_2^{-1} using Eq. (G3b);
9 **else if** $i == r$ **then**
10 Retrieve $\mathbb{A}_R(r-2) = \mathbb{A}_{\text{stab}}[r-2]$ and A_{r-1} ;
11 Calculate \mathbb{F}_r^{-1} using Eq. (G3c);
12 **else**
13 Retrieve $\mathbb{A}_L(i) = \mathbb{A}_{\text{stab}}[i]$, $\mathbb{A}_R(i-2) = \mathbb{A}_{\text{stab}}[i-2]$ and A_{i-1} ;
14 Calculate \mathbb{F}_i^{-1} using Eq. (G2);
15 **end if**
16 Calculate \mathbb{F}_i using Eq. (G1);
17 Set $\mathbb{A}_{\text{stab}}[N_{\text{stab}}] = \mathbb{A}_L(N_{\text{stab}}) := I$;
18 **for** $l \in L_\tau, L_\tau-1, \dots, 1$ **do**
19 Update $G_{s^{(i)}}(\tau, \tau), G_{s^{(i)}}(\tau, 0), G_{s^{(i)}}(0, \tau), G_{s^{(i)}}(0, 0)$ using Eq. (G9) and update \mathbb{F}_i using Eq. (52);
20 Propagate to $G_{s^{(i)}}(\tau - \Delta_\tau, \tau - \Delta_\tau), G_{s^{(i)}}(\tau - \Delta_\tau, 0), G_{s^{(i)}}(0, \tau - \Delta_\tau)$;
21 **if** $\tau - \Delta_\tau == l_{\text{stab}}\tau_{\text{stab}}$ **then**
22 Retrieve $A_R(i, l_{\text{stab}}) = A_{\text{stab}}[i, l_{\text{stab}}]$;
23 Calculate $B_{s^{(i)}}(\tau - \Delta_\tau + \tau_{\text{stab}}, \tau - \Delta_\tau)$;
24 **if** $l_{\text{stab}} + 1 == N_{\text{stab}}$ **then**
25 Calculate $A_L(i, l_{\text{stab}}) := B_{s^{(i)}}(\tau - \Delta_\tau + \tau_{\text{stab}}, \tau - \Delta_\tau)$;
26 **else**
27 Retrieve $A_L(i, l_{\text{stab}} + 1) = A_{\text{stab}}[i, l_{\text{stab}} + 1]$;
28 Calculate $A_L(i, l_{\text{stab}}) = A_L(i, l_{\text{stab}} + 1)B_{s^{(i)}}(\tau - \Delta_\tau + \tau_{\text{stab}}, \tau - \Delta_\tau)$ using Eq. (G10b);
29 **end if**
30 Set $A_{\text{stab}}[i, l_{\text{stab}}] = A_L(i, l_{\text{stab}})$;
31 **if** $l == 1$ **then**
32 Calculate $G_{s^{(i)}}(0, 0) = [I + A_L^\dagger(i, 0)]^{-1}$ using Eq. (F2);
33 Calculate $G_{s^{(i)}}(0, 0^+) = G_{s^{(i)}}(0, 0) - I$;
34 **else**
35 Calculate $G_{s^{(i)}}(\tau - \Delta_\tau, \tau - \Delta_\tau) = [I + A_R(i, l_{\text{stab}})A_L^\dagger(i, l_{\text{stab}})]^{-1}$ using Eq. (F1);
36 Calculate $G_{s^{(i)}}(\tau - \Delta_\tau, 0) = [A_R^{-1}(i, l_{\text{stab}}) + A_L^\dagger(i, l_{\text{stab}})]^{-1}$ using Eq. (F4);
37 Calculate $G_{s^{(i)}}(0, \tau - \Delta_\tau) = -[A_L^{\dagger-1}(i, l_{\text{stab}}) + A_R(i, l_{\text{stab}})]^{-1}$ using Eq. (F5);
38 Calculate $G_{s^{(i)}}(0, 0) = [I + A_L^\dagger(i, l_{\text{stab}})A_R(i, l_{\text{stab}})]^{-1}$ using Eq. (F6);
39 **end if**
40 Calculate $G_{s^{(i)}}^{T_2^f} = (G_{s^{(i)}}(0, 0))^{T_2^f}$ using Eq. (15);
41 Calculate \mathbb{F}_i using Eq. (G1);
42 **end if**
43 **end for**
44 Calculate $A_i := G_{s^{(i)}}^{T_2^f}$, $\bar{A}_i := I - G_{s^{(i)}}^{T_2^f}$, and $\mathbb{A}_i := \mathbb{B}_i^{-1}$;
45 **if** $i == r$ **then**
46 Set $\mathbb{A}_L(i-1) = \mathbb{A}_i$;
47 **else**
48 Retrieve $\mathbb{A}_L(i)$;
49 Calculate $\mathbb{A}_L(i-1) = \mathbb{A}_i \mathbb{A}_L(i)$ using Eq. (G7);
50 **end if**
51 Set $\mathbb{A}_{\text{stab}}[i-1] = \mathbb{A}_L(i-1)$;
52 **end for**
Output: $A_{\text{stab}}[1 : r, 0 : N_{\text{stab}}] = \{A_L(i, l_{\text{stab}}) := B_{s^{(i)}}(\beta, l_{\text{stab}}\tau_{\text{stab}})^\dagger \mid i = 1, 2, \dots, r; l_{\text{stab}} = 0, 1, 2, \dots, N_{\text{stab}}\}$
Output: $\mathbb{A}_{\text{stab}}[0 : r] := \{\mathbb{A}_L(i) = \mathbb{B}(r, i)^{-1} \mid i = 0, 1, 2, \dots, r\}$
